The role of yolk syncytial layer and blastoderm movements during gastrulation in zebrafish

Dissertation

zur Erlangung des akademischen Grades

Doctor rerum naturalium

(Dr. rer. nat.)

vorgelegt der

Fakultät Mathematik und Naturwissenschaften

der Technischen Universität Dresden

von

Lara Cristina de Jesus Carvalho

geboren am 18. Mai 1979 in Santa Iria de Azóia, Portugal

Gutachter: Prof. Dr. Michael Brand, Technische Universität Dresden

Dr. Carl-Philipp Heisenberg, Max Planck Institute of Molecular Cell Biology and Genetics, Dresden

Prof. Dr. António Jacinto, Universidade de Lisboa, Portugal

Eingereicht am: 13. August 2007

Tag der Verteidigung: 30. November 2007

Summary

During gastrulation, a set of highly coordinated morphogenetic movements creates the shape and internal organization of the embryo. In teleostean fishes, these morphogenetic movements involve not only the embryonic progenitor cells (deep cells) but also two extra-embryonic tissues: an outer sheet of epithelial cells (EVL) and a yolk syncytial layer (YSL). Epiboly is characterized by the spreading of the blastoderm (deep cells and EVL) to cover the large yolk cell, whereas convergence and extension leads, respectively, to mediolateral narrowing and anteroposterior elongation of the embryo.

Recent studies have shown that the nuclei of the YSL undergo epiboly and convergence and extension movements similarly to the overlying deep cells, suggesting that these tissues interact during gastrulation. However, it is so far not clear whether and how the movements of YSL nuclei and deep cells influence each other.

In the first part of this thesis, the convergence and extension movement of YSL nuclei was quantitatively compared to the movement of the overlying mesendodermal progenitor (or "hypoblast)" cells. This revealed that, besides the similarity in the overall direction of movement, YSL nuclei and hypoblast cell movements display differences in speed and directionality.

Next, the interaction between YSL and hypoblast was addressed. The movement of the blastoderm was analyzed when YSL nuclei movement was impaired by interfering with the YSL microtubule cytoskeleton. We found that YSL and blastoderm epiboly were strongly reduced, while convergence and extension were only mildly affected, suggesting that YSL microtubules and YSL nuclei movement are required for epiboly, but not essential for convergence and extension of the blastoderm. We also addressed whether blastodermal cells can influence YSL nuclei movement. In maternal-zygotic *one-eyed pinhead* (MZ*oep*) mutant embryos, which lack hypoblast cells, YSL nuclei do not undergo proper convergence movement. Moreover, transplantation of wild type hypoblast cells into these mutants locally rescued the YSL nuclei convergence phenotype, indicating that hypoblast cells can control the movement of YSL nuclei.

Finally, we propose that the hypoblast influences YSL nuclei movement as a result of shape changes caused by the collective movement of cells, and that this process requires the adhesion molecule E-cadherin.

TABLE OF CONTENTS

Index of figures

Abbreviations

SI units and symbols of standard multiples and symbols of chemical elements are not listed here; gene names and protein/gene family names are explained in the text.

2D	Two-dimensional
3D	Three-dimensional
AVE	Anterior visceral endoderm
BSA	Bovine serum albumin
cDNA	Complementary DNA
DAB	3'-3'-Diaminobenzidine
DEL	Deep cell layer
DIC	Differential interference contrast (Nomarski) optics
DIG	Digoxygenin
DMSO	Dimethylsulfoxide
DNase	Desoxyribonuclease
dpf	Days post-fertilization
ECM	Extracellular matrix
e. g.	exemplu gratii (Latin): for example
EGFP	Enhanced green fluorescent protein
EMT	Epithelial to mesenchymal transition
ER	Endoplasmic reticulum
EVL	Enveloping layer
E-YSL	External yolk syncytial layer
GFP	Green fluorescent protein
h	Hours
HEPES	4-(2-hydroxyethyl)-1-piperazineethanesulfonic acid
hpf	Hours post-fertilization
IgG	Immnoglobulin G
I-YSL	Internal yolk syncytial layer
kDa	kilo Dalton; protein weight
LMP	Low melting point agarose
min	Minutes
mo	Morpholino oligonucleotide
mRNA	messenger RNA
MAB	Maleic acid buffer
MW	Molar weight
MTOC	Microtubule organizing center
MZ	Maternal and zygotic mutant
n	Number
NA	Numerical aperture
NGS	Normal goat serum

NMJ	Neuromuscular junction
p	Probability value (Student's t test)
PBS	Phosphate buffered saline
PCP	Planar cell polarity
PCR	Polymerase chain reaction
PFA	Paraformaldheyde
RNase	Ribonuclease
SSC	Sodium chloride solution supplemented with citrate
SDS	Sodium dodecyl sulfate
TEM	Transmission electron microscopy
UTR	Untranslated region of messenger RNA
UV	Ultraviolet light
YCL	Yolk cytoplasmic layer
YSL	Yolk syncytial layer

1. Introduction

1.1 The zebrafish as a model system

Teleosts, such as the killifish (*Fundulus heteroclitus*), the medaka (*Oryzias latipes*) and the zebrafish (*Danio rerio*), have been used since the late 1800s for biological studies. More recently, the zebrafish embryo has come into focus to answer developmental and physiological questions. This was initiated mainly by George Streisinger and colleagues, who began genetic analysis in the zebrafish and established the methodological foundation allowing its use as a vertebrate model organism (Streisinger et al., 1981; Westerfield, 2000).

Indeed, the zebrafish embryo offers many advantages to study embryonic development compared to other organisms. It is very easy to handle; it develops externally and it is relatively large, which facilitates the execution of experimental manipulations such as microinjection and cell transplantations. Its transparency allows the use of live microscopy. In addition, the adult zebrafish can be readily bred, embryonic development takes place within only two days, and the fish are sexually mature after three months of development. Furthermore, following a particular light-dark cycle, adult female fish generate large, synchronized clutches of eggs.

Very importantly, the zebrafish is amenable to genetic analysis and has therefore been subject of two large-scale genetic screens that identified essential genes controlling a wide range of biological processes (Driever et al., 1996; Haffter et al., 1996). The vast and rapid expansion of new tools and resources in the last decades has also motivated the increasing use of zebrafish to study cell biology *in vivo*. Important advances include the analysis of gene expression and protein localization in the live embryo with fluorescently tagged proteins and transgenes, and the use of confocal time-lapse microscopy (Amsterdam et al., 1995; Cooper et al., 1999; Peters et al., 1995).

In summary, the unique combination of embryological, genetic and cell biological approaches make zebrafish a perfect model system for developmental cell biology.

1.2 Overview of zebrafish development

The zebrafish embryo develops in a typical teleost manner and morphological aspects of its development, as well as defined stages, have already been described in detail (Kimmel et al., 1995; see Fig. 1.1). Still, we will briefly describe the main features of the early zebrafish embryonic development.

When the teleolecithal eggs are laid, yolk and cytoplasm are mixed and the zygote is surrounded by a transparent chorion. External fertilization occurs by the entrance of the sperm into the oocyte at the future animal pole side. At this stage ("one-cell stage"), contractile forces cause yolk-free cytoplasm to accumulate at the animal pole of the zygote, segregating it from the large yolk mass. About 30 minutes after fertilization, the blastodisc has formed at the animal pole, while a big yolk mass constitutes the vegetal portion of the egg. During early cleavage stages, the zygote starts to divide in a discoidal-meroblastic manner, with marginal vegetal blastomeres maintaining large cytoplasmic bridges with the yolk cell (Kimmel and Law, 1985a; Wilson, 1889). Cell divisions at this stage are rapid and synchronous.

During early blastula stages, when the embryo consists of 512 cells, a series of cellular changes occur, collectively called the "mid-blastula transition" (MBT). The timing of MBT is controlled by the ratio of nuclei to cytoplasm, similar to the case of frogs and flies (Edgar et al., 1986; Kane and Kimmel, 1993; Newport and Kirschner, 1982). At MBT, zygotic transcription starts and the cell cycles become longer and asynchronous. This coincides with the generation of the first three separate lineages of the embryo. The first one is the enveloping layer (EVL), which arises by asymmetric cell divisions of outermost blastomeres and is composed by a single sheet of epithelial cells at the surface of the blastoderm that will eventually cover the entire embryo (Kane et al., 1992; Kimmel et al., 1995). The yolk syncytial layer (YSL), an extraembryonic structure derived from the collapse of vegetal marginal blastomeres into the yolk cell, forms a multinucleate layer at the interface between the yolk and the blastoderm (Kimmel and Law, 1985b; Trinkaus, 1993; see below). Between EVL and YSL, the deep cell layer (DEL) will give rise to the embryo proper (Kimmel et al., 1995). At this stage, it is also possible to distinguish the yolk cytoplasmic layer (YCL), a thin, anucleate layer of cytoplasm that surrounds the entire yolk cell (Long, 1984; Solnica-Krezel and Driever, 1994; Trinkaus, 1992).

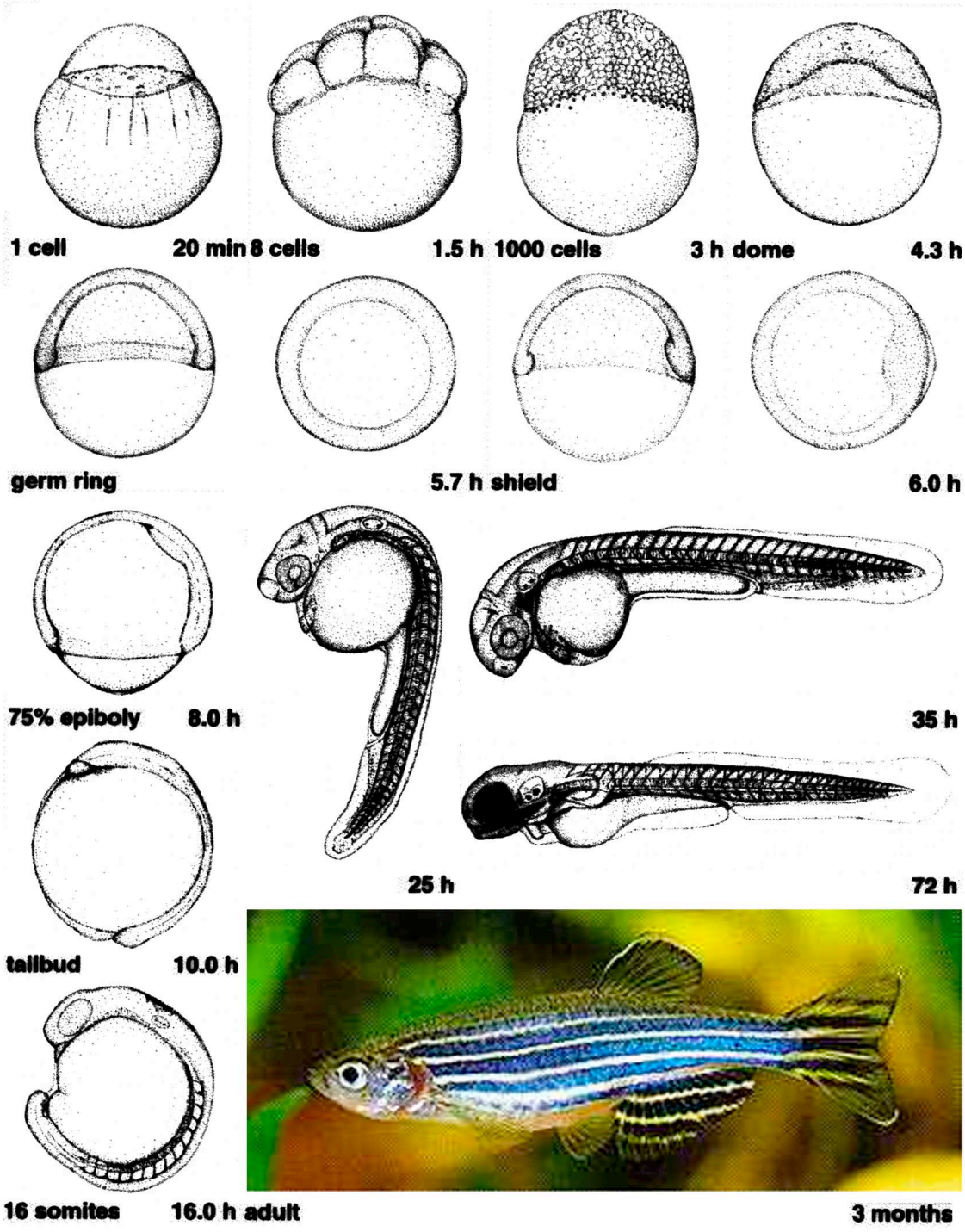

Figure 1.1 Development of the zebrafish. Stages are named after anatomical features and developmental age at 28ºC. The percentage of epiboly describes the degree of coverage of the yolk cell by the blastoderm. The embryos are illustrated in lateral views; germ ring and shield stage embryos are also shown from the top. Until 25h, the dorsal side of the embryo is on the right. This figure is modified after camera lucida drawings of Kimmel et al. (1995).

At late blastula stages, the first cellular rearrangements begin to reshape the blastoderm into a characteristic vertebrate body plan. In the process of epiboly, radial cell intercalation leads to the thinning of the blastoderm as it spreads over the entire yolk. The extent of yolk cell coverage ("percent epiboly") provides a convenient measure of the embryo's developmental stage. At 50% epiboly, additional morphogenetic cell movements start, hallmarking the onset of gastrulation. During gastrulation, a combination of patterning events and tissue movements specifies the three germs layers (ecto-, meso- and endoderm), and establish the embryonic body axes. The marginal-most DEL cells internalize and form the so-called "hypoblast", which contains the precursors of mesoderm and endoderm, while the "epiblast layer" on the outside of the embryo will give rise to the ectoderm. At the same time, lateral and ventral cells converge to the prospective dorsal side of the embryo, leading to the formation of a localized thickening termed "embryonic shield". The shield is the functional equivalent to the dorsal blastopore lip of amphibians and the node in mammals and birds, since it can organize a secondary embryonic axis when transplanted into a host embryo (Ho, 1992; Oppenheimer, 1936). In addition to convergence movements along the dorsal-ventral axis, extension occurs along the anterior-posterior axis, and acts in concert with epiboly to elongate the embryo. At the end of gastrulation, the yolk is completely covered by the blastoderm and dorsal-ventral and anterior-posterior axes are established.

After gastrulation, the embryo is being further patterned and extended during the "segmentation period", characterized by the progressive formation of the somites, the precursors of the body musculature. During these stages, the organ rudiments become visible, and the tailbud extends away from the yolk cell to generate the embryonic tail. After one day post-fertilization (1 dpf), the "pharyngula stage" starts, during which the embryo undergoes organogenesis. Between 2 and 3 dpf, the larva hatches from the chorion, and begins to swim and eat at 5 dpf, when morphogenesis is largely complete.

1.3 The YSL

1.3.1 Formation of the YSL

A unique and fascinating feature of early teleost development is the formation of a syncytium at the surface of the yolk cell during cleavage stages. This syncytium, originally known as "periblast", is now called "yolk syncytial layer" (YSL; Betchaku and Trinkaus, 1978). The formation of the YSL was first discovered by Agassiz and Whitman (1884) in *Ctenolabrus* and described in more detail by Wilson (1889) in *Serranus*. More recently, its has been carefully studied in *Fundulus heteroclitus* (Trinkaus, 1993) and in zebrafish (Kimmel and Law, 1985b).

During late cleavage stages, the cytoplasm of some marginal blastomeres is confluent with the yolk cell cytoplasm, as a result of the incomplete, meroblastic, pattern of cleavage typical of teleosts. These cytoplasmic bridges have already been pointed out by Wilson (1889), and were later confirmed by electron microscopy in *Fundulus* (Lentz and Trinkaus, 1967) and by intracellular dye injection in zebrafish (Kimmel and Law, 1985a,b). In zebrafish, Kimmel and Law (1985a,b) have described in detail how the YSL is formed. Between the ninth and the tenth cleavage (512- to 1024-cell stages), some of these marginal blastomeres collapse and contribute their nuclei and cytoplasm into the cytoplasmic cortex of the yolk cell (Fig. 1.2). The nuclei are then detected within the newly formed YSL, lined up in a single row along the blastoderm margin. After that, no further contributions of blastomeres to the YSL are observed and the cytoplasmic connections between blastoderm and YSL are lost, as revealed by the restriction of injected tracer dyes to the YSL (Kimmel and Law, 1985b). These authors have also demonstrated that the marginal blastomeres that form the YSL do not constitute a restricted lineage. Rather, only a subset of the progeny of early marginal cells contributes to the YSL. Conversely, non-marginal blastomeres never participate in the formation of the YSL. Therefore, the marginal position and the cytoplasmic connection with the yolk cell seem to be important factors determining which cells will form the YSL.

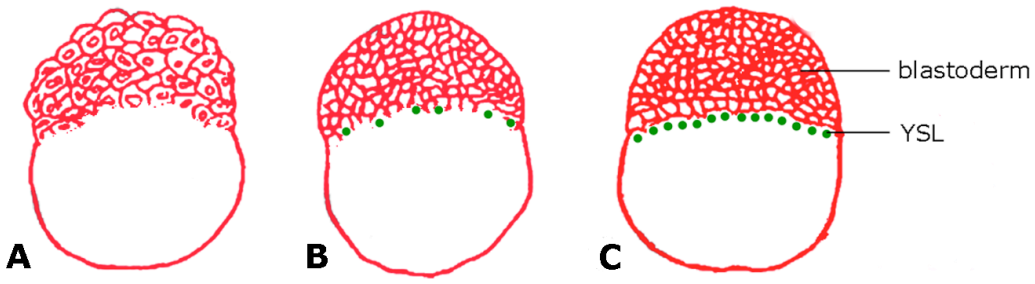

Figure 1.2 – Formation of the YSL. (A) 216-cell stage. The blastodisc has the form of a half ball sitting on top of the yolk cell. At this stage, blastomeres are still connected to the yolk by cytoplasmic bridges. (B) 512-cell stage, the beginning of the midblastula transition. Upon entering the tenth mitosis, marginal blastomeres begin to lose their lower borders where they join the yolk cell. This event marks the beginning of YSL formation. (C) High stage. The blastoderm has lost its cytoplasmic connections to the yolk cell and the YSL forms a thin ring at the margin. Adapted from Zalik et al., 1999.

After the YSL is formed, its nuclei typically divide three to five more times without cytokinesis and in a metachronous manner (Kane et al., 1992; Kimmel et al., 1995; Trinkaus, 1993). When epiboly starts, the nuclei become strictly post-mitotic and increase in size, which may indicate that they are actively transcribing RNA. Indeed, it has been suggested that the YSL nuclei possess high transcriptional activity, as based on elevated transgene activities in this compartment of the embryo (Williams et al., 1996). During the nuclear divisions, nuclei spread underneath the blastoderm, forming the so-called "internal YSL" (I-YSL) already visible at sphere stage (D'Amico and Cooper, 2001). Nuclei remaining at the margin become part of the "external YSL" (E-YSL; Trinkaus, 1993).

An interesting aspect of YSL formation is its variability. As mentioned before, both the lineage and number of blastomeres that contribute to the YSL vary significantly between embryos, as does timing of YSL formation. This leads to a considerable variation in the total number of nuclei in the definitive YSL. Yet, this variation does not seem to interfere with the development of the embryo, suggesting that the precise mode of YSL formation is not crucial (Kimmel and Law, 1985b; Trinkaus, 1993).

1.3.2 YSL functions during development

The YSL has many important functions for embryonic development. One of them is related to nutrient transport: since the YSL separates the yolk from the embryo, all nutrients must pass through this layer in order to reach the embryo, and later the larva. It has been shown for many teleost species that the YSL is necessary for the hydrolysis of

yolk material and for transfer of nutrients to the embryonic blastoderm and larval tissues (Lentz and Trinkaus, 1967; Mani-Ponset et al., 1996; Sire et al., 1994; Trinkaus and Drake, 1956; Van der Ghinst, 1935; Walzer and Schönenberger, 1979). In zebrafish, a more recent study has demonstrated that Ferroportin1, a vertebrate-conserved transmembrane iron exporter, is specifically expressed in the YSL and plays a crucial role in the transport of iron from the yolk to the embryo (Donovan et al., 2000).

The YSL has also a role in regulating the migration of the heart precursor cells to the midline of the embryo. A recent study has shown that the homeobox transcription factor *mtx1*, which is expressed exclusively in the YSL during gastrulation, regulates fibronectin expression in the embryonic tissue. Fibronectin expression is then necessary for the assembly of a proper extracellular matrix, which is used by the heart precursor cells as a substrate for migration (Sakaguchi et al., 2006).

Furthermore, the YSL serves critical inductive and patterning functions (illustrated in Fig. 1.3). Transplantation experiments support the idea that the dorsal YSL in teleosts is equivalent to the amphibian Nieuwkoop center present in the dorsovegetal region of the endoderm, and is responsible for the induction of the Spemann-Mangold organizer (Mizuno et al., 1999). When an isolated yolk cell was transplanted onto the animal pole of a host embryo, it induced the expression of dorsal specific genes such as *goosecoid* (*gsc*) in the surrounding cells. In addition, the *dharma*/*bozozok* gene, a transcription factor necessary for the organizer function, is expressed in the dorsal YSL before gastrulation (Koos and Ho, 1998; Yamanaka et al., 1998). *dharma* mutants can be rescued by injection of *dharma* mRNA into the YSL, showing that YSL expression of this gene is sufficient to induce the organizer (Fekany et al., 1999). However, the dorsal blastoderm can also autonomously develop dorsal fates, since abolishing all endogenous mRNA activity in the YSL via injection of RNase does not inhibit *dharma* or *gsc* expression in dorsal blastomeres (Chen and Kimelman, 2000). On the other hand, the same experiments showed that *dharma* expression is altered in the absence of YSL mRNAs, such that it remains expressed in dorsal blastomeres at a stage when it is normally restricted in the dorsal YSL. Therefore, the authors propose that the dorsal determinants are present in both the dorsal YSL and dorsal blastomeres, and that both cooperate to regulate dorsal organizer gene expression.

Furthermore, similar yolk cell transplantation experiments have demonstrated that the YSL can induce mesoderm and endoderm in the surrounding blastomeres, as evidenced by the ectopic expression of mesodermal (*no tail*) and endodermal (*gata5*) in host embryos (Mizuno et al., 1996; Mizuno et al., 1999; Ober and Schulte-Merker, 1999; Rodaway et al., 1999). As in the case of the organizer function, the requirement of the YSL for mesodermal and endodermal induction was also analyzed by RNase treatment of the YSL. Interestingly, RNase injected embryos do not develop ventrolateral mesoderm and endoderm, while dorsal regions are unaffected (Chen and Kimelman, 2000). This indicates that the YSL is necessary and sufficient to induce at least ventrolateral mesoderm and endoderm in zebrafish.

Another interesting aspect of YSL function involves the homeobox gene *hhex*, which is expressed in the dorsal half of the YSL during gastrulation (Bischof and Driever, 2004; Ho et al., 1999; Liao et al., 2000). Over-expression experiments have demonstrated that Hhex antagonizes ventralizing and posteriorizing factors such as Bmp2b and Wnt8 in the overlying blastoderm (Ho et al., 1999). Homologues of *hhex* in mouse and *Xenopus* are expressed in tissues responsible for organizing anterior structures, namely the anterior visceral endoderm (AVE) and anterior endomesoderm (Jones et al., 1999; Thomas et al., 1998). Since the mouse AVE and the amphibian anterior endomesoderm express homologous genes and are both implicated in head and heart induction, it has been proposed that they are functionally equivalent structures (Beddington and Robertson, 1998; Bouwmeester and Leyns, 1997; Jones et al., 1999; Martinez-Barbera et al., 2000). Following this rationale, the dorsal YSL of the zebrafish gastrula has been proposed to be the teleost equivalent of the mouse AVE (Beddington and Robertson, 1998; Bouwmeester and Leyns, 1997; Ho et al., 1999; Viebahn, 1999), and might thus be important for inducing and/or patterning anterior neural tissues.

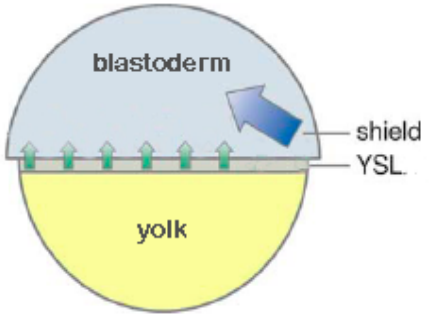

Figure 1.3 – Patterning roles of the YSL. Lateral view of an embryo at the onset of gastrulation, with dorsal to the right and animal pole on top. The YSL is necessary to induce ventral and lateral mesendodermal fates (green arrows) and participates in dorsal organizer function together with the dorsal blastoderm margin (blue arrow). Modified from Schier and Talbot (2005).

In addition, the E-YSL has been suggested to be essential for epibolic movement of the blastoderm (Chen and Kimelman, 2000; Cheng et al., 2004; Solnica-Krezel and Driever, 1994; Strähle and Jesuthasan, 1993; Trinkaus, 1951). This will be discussed in more detail in section 1.4.1 of this Introduction.

1.4 Gastrulation movements

Gastrulation entails a set of morphogenetic processes that create the internal organization and the external shape of developing animals (Leptin, 2005; Solnica-Krezel. 2005). In the course of gastrulation, the precursors of the three germ layers are repositioned from the surface of the blastula, placing the mesoderm between the internal endoderm and the superficial ectoderm. Moreover, the embryo is molded into a body rudiment with anteroposterior and dorsoventral asymmetries. Vertebrate gastrulation involves four evolutionarily conserved types of morphogenetic movements (Fig. 1.4): "epiboly", which leads to spreading and typically thinning of the tissue; "internalization", which occurs at the blastopore and directs mesendodermal precursor cells from the blastula surface to the interior, while prospective ectoderm remains on the exterior of the embryo; "convergence", which narrows embryonic tissues mediolateraly; and "extension", which elongates the them anteroposteriorly. These movements require a variety of cellular behaviors, such as directed cell migration, intercalation and cell shape changes. These morphogenetic movements will be discussed in detail in this section.

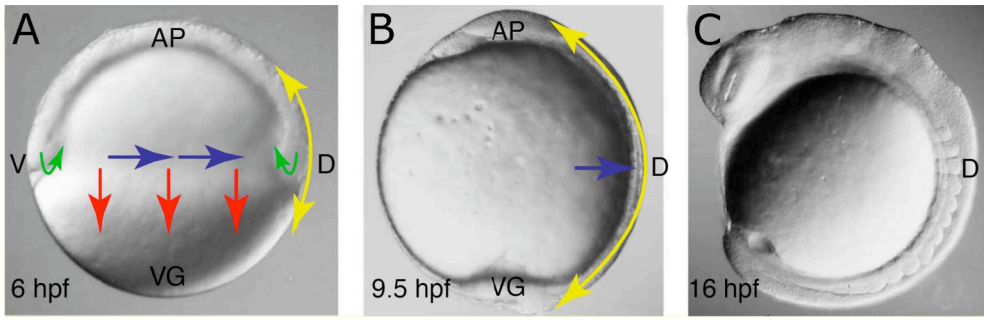

Figure 1.4 – Gastrulation movements in the zebrafish embryo. Lateral view of embryos during gastrulation. Dorsal (D) is to the right; ventral (V) to the left; animal pole (AP) on top; and vegetal pole (VG) at the bottom. Epiboly (red arrows) spreads and thins the blastoderm vegetally until it covers the yolk. Internalization (green arrows) forms the germ layers, the outer epiblast and the inner hypoblast. Convergence (blue arrows) narrows the tissue medio-laterally, while extension (yellow arrow) lengthens the embryonic axis. (A) Shield stage embryo (6 hpf) at the onset of gastrulation. (B) Tailbud stage embryo (9.5 hpf; end of gastrulation) has distinct anteroposterior and dorsoventral axes, with head and tail rudiments clearly visible. (C) Embryo during segmentation period (16 hpf) continues to narrow and elongate. Adapted from Myers et al., 2002b.

1.4.1 Epiboly

Epiboly is the first morphogenetic movement occurring in the embryo, characterized by the spreading of the blastoderm and YSL over the yolk cell. This process is analogous to that of many organisms that produce teleolecithal eggs, where smaller animal pole-derived cells internalize large, vegetally derived yolky cells (Kane and Adams, 2002; Solnica-Krezel, 2005).

Description of epiboly movements

Epiboly begins at late-blastula stage and completes at tailbud stage, when the entire yolk cell is engulfed by the blastoderm. Before the beginning of these morphogenetic movements, the blastoderm sits on top of a spherical yolk cell as a mound of cells of about six to eight cells thick. At dome stage the blastodisc thins considerably by radial intercalation of cells (Kimmel and Warga, 1987; Warga and Kimmel, 1990; Wilson et al., 1993; Wilson et al., 1995; Fig. 1.5), and at the same time, the yolk cell bulges or "domes" toward the animal pole. Subsequently, EVL, YSL, and deep cells begin to move toward the vegetal pole until the yolk cell is entirely covered.

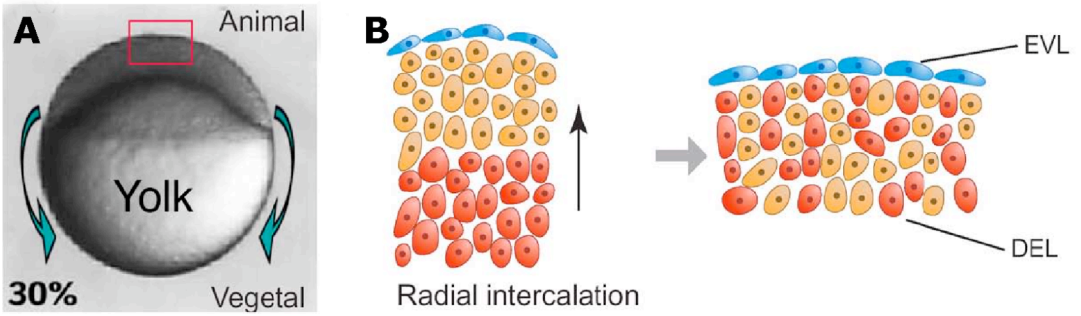

Figure 1.5 – Epiboly movements in the zebrafish embryo. (A) Lateral view of an embryo at 30% epiboly (5 hpf). Epiboly movements are defined by the spreading of the blastoderm over the yolk cell toward the vegetal pole (green arrows). These movements continue until the entire yolk cell is covered by the blastoderm. The red box outlines the embryonic region at the animal pole schematized in (B). (B) Schematic representation of radial intercalation movements. Deepest cells (red) intercalate among more superficial cells (orange). These movements contribute to the flattening of the tissue during epiboly. EVL, Enveloping layer; DEL, deep cell layer. Animal pole is on top; vegetal pole is at the bottom. Adapted from Montero and Heisenberg (2004).

The mechanism of epiboly seems to require an interplay among all three tissue types, EVL, YSL and DEL, although the contribution of each is not completely understood. In *Fundulus*, where this process has been studied more thoroughly, the YSL has been considered as the major driving force for epiboly. Brilliant work by John

Philip Trinkaus has shown that epiboly of the YSL is completely autonomous and independent of the EVL and DEL. Surprisingly, when the blastoderm of an embryo was removed before the onset of epiboly, the YSL proceeded normally towards the vegetal pole; indeed, the first phase of YSL epiboly was even faster than in a normal embryo, suggesting that EVL and/or DEL actually inhibit the onset of YSL epiboly (Trinkaus, 1951; Trinkaus, 1984). Moreover, it has been demonstrated that tight junctions develop between the E-YSL and the EVL (Betchaku and Trinkaus, 1978) and suggested that epiboly starts when the E-YSL contracts and narrows, pulling the I-YSL and the attached EVL vegetally (Trinkaus, 1984). Endocytosis might also be part of the epiboly motor. YSL plasma membrane is endocytosed near the advancing margin of the blastoderm, leading to the disappearance of the YCL (Betchaku and Trinkaus, 1978; Betchaku and Trinkaus, 1986; Trinkaus, 1984). Localized endocytosis at the margin of the E-YSL has also been observed in zebrafish (Solnica-Krezel and Driever, 1994). To account for I-YSL expansion, Betchaku and Trinkaus (1978) have postulated that it comes from the membrane of the numerous, long microvilli present in the I-YSL at the onset of epiboly, which gradually disappear. Furthermore, the EVL undergoes active cell rearrangements during epiboly. Some of the leading edge cells leave the margin and intercalate amongst more animal cells, and other cells constrict while others become wider (Keller and Trinkaus, 1987; Köppen et al., 2006; Zalik et al., 1999). This indicates that the EVL is not a totally passive component of epiboly.

Role of the cytoskeleton in epiboly movements

In zebrafish, studies suggest that YSL epiboly is at least in part microtubule dependent (Solnica-Krezel and Driever, 1994; Strähle and Jesuthasan, 1993). The yolk cell exhibits a set of microtubules that radiate from organizing centers associated with the E-YSL nuclei, which are aligned along the animal-vegetal axis, suggesting that microtubules are involved in regulating nuclear movements (Fig. 1.6). Supporting this notion, interfering with microtubule organization severely impairs epibolic movement of the E-YSL, but only partially blocks DEL and EVL epiboly. However, these observations were carried out either by incubating the embryos in microtubule depolymerizing (nocodazole) or stabilizing (paclitaxel) drugs, or by disrupting the microtubule network with UV light or cold treatment. As these treatments affect all

tissues of the embryo, the role of microtubules in the YSL has not been specifically addressed. However, a recent study has shown that a high level of polymerized microtubules in the YSL is essential for proper epiboly movements. Specifically blocking the function of the steroidogenic enzyme Cyp11a1 in the YSL, which catalyzes the conversion of colesterol to pregnenolone, decreases the level of polymerized microtubules in the YSL and consequently blocks epiboly movements without affecting early embryonic patterning (Hsu et al., 2006).

In addition to microtubules, the actin cytoskeleton likely serves a critical function during zebrafish epiboly movements (Cheng et al., 2004; Köppen et al., 2006; Zalik et al., 1999). These studies show that the leading edge of the E-YSL contains a punctate band of actin and myosin (Fig. 1.6), which might function as a contractile ring that pulls the YSL, and consequently EVL and DEL, towards the vegetal pole, as proposed for *Fundulus* (Trinkaus, 1984).

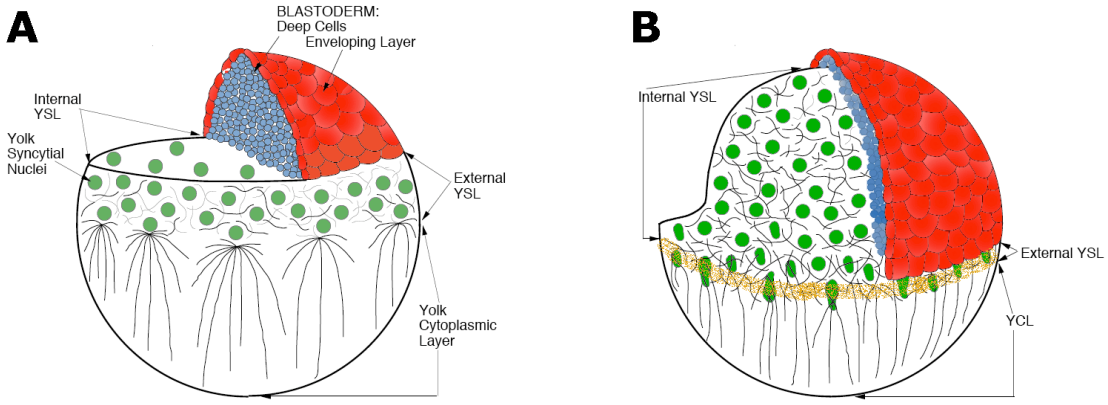

Fig. 1.6 – Morphogenesis and organization of the cytoskeleton in the YSL. Schematic view of the organization of the YSL and blastoderm at late blastula stage (A) and early gastrula (B). Animal pole is on top, vegetal pole is at the bottom. Only part of the blastoderm is shown to reveal the morphology of the yolk cell. (A) Sphere stage (4 hpf), just before the onset of epiboly. The blastoderm, composed of the internal deep cells (DEL, blue) and the superficial enveloping layer (EVL, red), is positioned on top of the syncytial yolk cell. The animal surface of the yolk cell underlying the blastoderm is flat. At this stage, two domains of YSL nuclei (green circles) can be distinguished: the external YSL (E-YSL), a thin layer of nuclei at the margin of the blastoderm, and the internal YSL (I-YSL), which contains most of the syncytial nuclei, located in the central region of the yolk under the blastoderm. At this stage, YSL nuclei undergo their last division and microtubules (thin black lines) start to irradiate from the marginal E-YSL nuclei, toward the vegetal pole, aligned along the animal-vegetal axis, through the anuclear yolk cytoplasmic layer (YCL). (B) 60% epiboly stage (6.5 hpf), the onset of gastrulation. Deep cells cover 60% of the yolk cell. The E-YSL nuclei are now visible in front of the blastoderm and lead the epibolic movement. The EVL is more advanced in epiboly than the deep cells. An actin ring (orange) starts to form at the leading edge of the E-YSL/EVL. The YCL, as well as the animal-vegetal parallel arrays of microtubules, is diminished. The I-YSL contains a dense network of microtubules. Modified from Solnica-Krezel and Driever (1994).

Role of E-cadherin in epiboly

To date, no experiment has demonstrated the role of the DEL in epiboly. At the onset of epiboly movements, the deep cells undergo considerable cell mixing, which can be explained as driven both by the doming of the yolk or by intrinsic behaviors of the cells (Wilson et al., 1995). Despite this, mutants for zebrafish *e-cadherin* (*cadherin1/half-baked*, *cdh1/hab*), as well as morpholino antisense inhibition of *cdh1* translation, demonstrate that at least some aspects of epiboly of the deep cells are under a separate genetic control from the EVL and YSL (Babb and Marrs, 2004; Kane et al., 1996; Kane et al., 2005; McFarland et al., 2005; Montero et al., 2005; Shimizu et al., 2005). These mutants/morphants show an arrest in epiboly movement of the DEL at about 70%-80% epiboly, while EVL and YSL are unaffected.

More careful analysis of *cdh1/hab* mutants has revealed that radial intercalation of epiblast cells is impaired, suggesting that these cell movements are important for epiboly of the DEL (Kane et al., 2005). Electron microscopy analysis of mutants for the *cdh1/hab*^{rk3} allele show adhesion defects between deep cells and EVL, which is indicative of a role of EVL/DEL adhesion in epiboly (Shimizu et al., 2005).

Another interesting aspect is that impairment of E-cadherin function does not seem to significantly affect the actin bands present at the leading edge of the epibolizing EVL and DEL, indicating that the function of E-cadherin in epiboly might be independent of these structures (Köppen et al., 2006; Shimizu et al., 2005).

Transcriptional and translational control of epiboly

A number of transcription factors are also involved in epiboly. The T-box *eomesodermin* (*eomes*) and the homeobox *mtx2* transcription factors are some of the already characterized genes. Eomes function is necessary from the early stages of epiboly, at least partially by promoting the expression of the *mtx2* gene, which is only expressed in the YSL (Bruce et al., 2005; Hirato et al., 2000). Epibolic movements are also reduced in maternal-zygotic *spiel ohne grenzen* (*spg*)/*pou5f1* mutants (Reim et al., 2004; Reim and Brand, 2006). In contrast to Eomes and Mtx2 loss-of-function, *spg/pou5f1* mutants show a block in epiboly of the deep cells while EVL and YSL epiboly occur normally, reminiscent to the phenotype of *cdh1/hab* mutants (Kane et al., 1996; Kane et al., 2005; McFarland et al., 2005; Shimizu et al., 2005). However,

spg/pou5f1 mutants do not show any effect on *cdh1* transcription, and thus it is not clear by which mechanism this transcription factor regulates epiboly (Reim and Brand, 2006).

A recent study has shown that embryos deficient in maternal and zygotic function of the Dicer enzyme, which produces microRNAs, exhibit slow epiboly with respect to mesendodermal cell internalization (Giraldez et al., 2005). This suggests that regulation of translation is required for normal epiboly.

Further insight into the molecular control of epiboly awaits the molecular analysis of recently isolated maternal-effect mutants showing epiboly defects (Wagner et al., 2004).

1.4.2 Hypoblast formation and migration

When epiboly has progressed to cover about 50% of the yolk cell, the first mesendodermal progenitors are induced at the margin of the blastoderm, forming a thickening around the circumference of the blastoderm, known as the "germ ring" (Warga and Kimmel, 1990). Germ ring formation starts when cells close to the margin of the blastoderm slow down their epibolic movement. These cells then move as a continuous stream over the margin towards the yolk cell and become the hypoblast layer. This shares similarities with the involution movement of the mesodermal and endodermal germ layers at the onset of *Xenopus* gastrulation (for a review see Winklbauer et al., 1996). Simultaneously, convergence of blastodermal cells leads to a compaction of cells at the dorsal side of the germ ring, where the embryonic organizer (the "shield") forms (Fig. 1.7).

The exact mode of hypoblast formation has been a question of debate for many years (Kane and Adams, 2002). Two main mechanisms have been proposed: "involution", which describes the inward movement of the hypoblast as a cohesive sheet of cells (D'Amico and Cooper, 2001; Warga and Kimmel, 1990; Wood and Timmermans, 1988); and "ingression", the internalization of single cells from the epiblast into the hypoblast (Trinkaus, 1996). A recent study by Montero and colleagues (Montero et al., 2005) seems to have clarified this. Using high-resolution two-photon confocal time-lapse microscopy, these authors have shown that single hypoblast cells delaminate at the margin of the germ ring, close to the yolk cell, supporting the "ingression" model. Interestingly, ingression was not detected at a distance from the

margin, suggesting that ingression of hypoblast cells is restricted to the marginal region of the germ ring. Further evidence supporting this model comes from transplantation experiments, revealing that single hypoblast cells transplanted into mutant embryos that do not form hypoblast (maternal-zygotic *one-eyed pinhead* mutants) ingress in a cell-autonomous manner (Carmany-Rampey and Schier, 2001).

In conclusion, it seems that hypoblast cells ingress as single cells in a locally coordinated way, which might give the impression of a flow of cells, the previously alleged involution-like movement (Fig. 1.7B). It has thus been proposed that we call this internalization process by "synchronized ingression" (Solnica-Krezel, 2006).

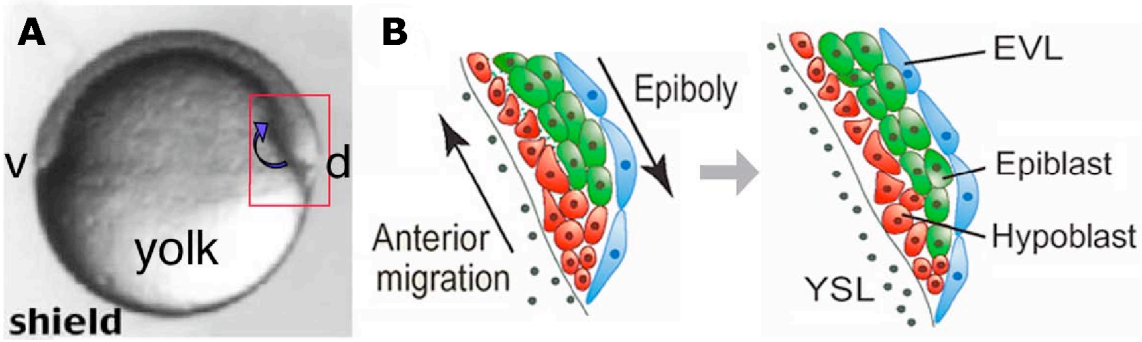

Figure 1.7 – Internalization and anterior migration of mesendodermal progenitor cells at the onset of gastrulation. (A) Lateral view of an embryo at shield stage (6 hpf). Animal pole is on top; vegetal pole at the bottom; ventral (v) to the left; and dorsal (d) to the right. Internalization of hypoblast cells occurs at the germ ring margin by synchronized ingression (blue arrow). The red box outlines the dorsal marginal region schematized in (B). (B) Schematic representation of internalization and anterior migration of hypoblast cells at the dorsal margin. Ingressing hypoblast cells (red) move toward the animal pole by active migration, forming the hypoblast layer. Overlying epiblast cells (green) do not internalize and continue epiboly movement toward the vegetal pole. EVL, enveloping layer; YSL, yolk syncytial layer. Adapted from Montero and Heisenberg (2004).

1.4.3 Convergence and extension

During gastrulation, convergence and extension movements lead to the mediolateral narrowing (convergence) and anteroposterior elongation (extension) of tissues or cell populations, and occur in many instances of metazoan development (for a review see Keller et al., 2000). Examples include archenteron elongation in echinoderms (Ettensohn, 1985), germ band extension in *Drosophila* (Irvine and Wieschaus 1994), and elongation of dorsal axial embryonic tissues of ascidians (Miyamoto and Crowther, 1985), fishes (Warga and Kimmel, 1990), amphibians (Burnside and Jacobson, 1968; Keller, 1984), birds (Schoenwolf and Alvarez 1989) and mammals (Sausedo and Schoenwolf, 1994).

Different modes of convergence and extension movements have been observed in various organisms. In the frog gastrula, convergence and extension are simultaneous and interdependent processes, thus leading to the use of the term "convergent extension". However, in the zebrafish gastrula, convergence can lead to tissue thickening without extension. Alternatively, a tissue might extend and at the same time decrease its thickness (Solnica-Krezel and Cooper, 2002). In zebrafish, convergence and extension seem to be genetically separable processes (Myers et al., 2000b). For example, in *no tail* and *somitabun* mutants, in which convergence is impaired, extension continues relatively normally (Glickman et al., 2003).

Distinct domains of convergence and extension

In the zebrafish, the majority of convergence and extension movements occur at gastrula stages and in all the three germ layers of the embryo (Myers et al., 2002a; Myers et al., 2002b; Warga and Nüsslein-Volhard, 1999). However, these movements differ according to the observed germ layer. In the dorsal region, extension of mesendoderm exceeds that of ectoderm and, eventually, most of the mesendodermal cells gather dorsally, leaving a zone depleted of cells in the ventral region. In contrast, convergence and extension of prospective neuroectoderm is accompanied by mediolateral expansion of non-neural ectoderm, which in the end occupies the ventral side of the gastrula (Concha and Adams, 1998; Woo and Fraser, 1995). Another aspect that varies is the cellular organization. Prospective ectodermal cells migrate as a sheet at the beginning of gastrulation, forming pronounced cell-cell contacts (Concha and Adams, 1998). On the contrary, mesodermal cells move individually or as small groups, while endodermal cells move exclusively as individuals (Trinkaus et al., 1992; Warga and Nüsslein-Volhard, 1999).

Speed and degree of convergence and extension of the different cell populations is also temporally and spatially controlled. While movement is slow at the beginning of gastrulation, the rate increases toward the end (Concha and Adams, 1998; Heisenberg et al., 2000; Kimmel et al., 1994; Sepich et al., 2000; Sepich et al., 2005). In addition, the degree of convergence and extension varies according to the dorsoventral position (Fig. 1.8). Trinkaus's pioneering investigations had already revealed regional differences in convergence and extension movements within the *Fundulus* gastrula (Trinkaus et al.,

1992; Trinkaus, 1998). More dorsally, both hypoblast and epiblast undergo strong extension movements and only limited convergence. In lateral regions, cells initially converge and extend slowly, but the speed increases as they approach the dorsal side. On the other hand, convergence and extension of mesodermal cells is almost absent in the ventral side (Sepich et al., 2000).

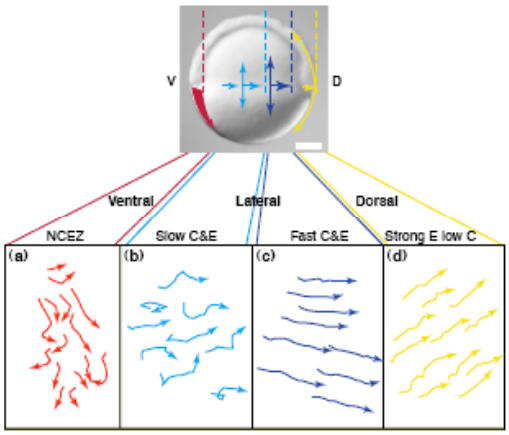

Figure 1.8 - Cell movement trajectories in ventral, lateral and dorsal convergence and extension (C&E) domains. (a) Cells in the ventral side of the embryo show zig-zaging movements towards the future tailbud, with no net dorsal speed. (b) Lateral cells far away from the dorsal side undergo slow C&E and meander significantly with slow net dorsal speed. (c) Lateral cells closer to the dorsal side undergo fast C&E, displaying straighter trajectories. (d) The paths of dorsal cells are oriented dorsally and biased towards anterior or posterior, depending on their position along the animal-vegetal axis. Their net dorsal speed is reduced compared to lateral cells participating in fast C&E movements. Scale bar, 100 µm. D, dorsal; V, ventral. Adapted from Myers et al. (2002b).

Migration of prechordal plate mesoderm cells

As outlined above, dorsal hypoblast formation is initiated when prospective prechordal plate mesoderm cells (prospective head mesoderm) internalize at the dorsal germ ring margin by synchronized ingression. These cells then migrate as a cohesive group toward the animal pole using the epiblast as a substrate (Montero et al., 2005). Therefore, prechordal plate progenitor cells have to move in a highly dynamic manner to obtain some net movement in the opposite direction of the epiblast.

Coordinated migration of these cells seems to be highly dependent on adhesive cell properties. It has been suggested that internalizing mesendodermal cells undergo an epithelial to mesenchymal transition (EMT), triggered by the nuclear localization of Snail, a transcriptional repressor of *e-cadherin/cdh1* (Yamashita et al., 2004). However, a more recent study has shown that prechordal plate progenitors express very high levels of E-cadherin, which is required for normal directed migration of these cells (Montero et al., 2005). These data lead the authors to propose that internalization of prechordal plate cells is not triggered by a classical EMT but rather by a change in cell adhesiveness.

In addition, anterior migration of prechordal plate progenitors is regulated by the non-canonical Wnt signaling (Ulrich et al., 2003; Ulrich et al., 2005). Wnt11 was shown to function non-autonomously in orienting filopodial-like protrusions and movement direction of hypoblast cells at the onset of gastrulation by regulating E-cadherin mediated-adhesion. Witzel and colleagues have recently proposed that Wnt11 locally functions at the plasma membrane by accumulating its receptor Frizzled 7 and the intracellular mediator Dishevelled, thereby modulating local cell contact persistence during gastrulation (Witzel et al., 2006).

Despite these insights into the coordination of prechordal plate movement, it remains a mystery what determines the global direction of this tissue in the embryo. One of the hypotheses is that attractive guidance cues are involved, since the behavior of these cells resembles chemotatic cell movements. Supporting this notion, activation of Stat3-dependent signaling on the dorsal side of the embryo is cell-autonomously required for anterior migration of these cells (Yamashita et al., 2002). This signaling pathway is typically activated in response to cytokines and growth factors (Kisseleva et al., 2002). Alternatively, anterior migration could be a more passive process, generated by continuous ingression of cells at the germ ring margin. Evidence that a community effect directs anterior migration of mesendodermal cells resulted from the transplantation of single wild type cells into the margin of maternal-zygotic *one-eyed pinhead* embryos (which essentially lack all mesendodermal cells): while able to internalize, the single cells failed to move to the animal pole as in normal wild-type embryos (Carmany-Rampey and Schier, 2001).

Mediolateral cell intercalation in axial mesodermal cells

After mid-gastrulation, the strong extension movement of the dorsal hypoblast, which becomes the notochord, has been believed to be driven mainly by mediolateral cell intercalation (Concha and Adams, 1998; Heisenberg et al., 2000; Kimmel et al., 1994; Myers et al., 2002a; Myers et al., 2002b; Solnica-Krezel et al., 1996; Warga and Kimmel, 1990; Fig. 1.9). In the *Xenopus* gastrula, this cell behavior is thought to be the main motor for convergent extension of mesodermal tissues (Keller et al., 2000). Similarly to what occurs in the frog, in zebrafish, dorsal mesodermal cells become highly elongated and align their bodies parallel to the mediolateral embryonic axis

(Concha and Adams, 1998). However, it has recently been shown that mutants for the T-box gene *no tail* have defects in convergence and mediolateral intercalation but not in extension of axial mesodermal cells (Glickman et al., 2003). These observations suggested that besides mediolateral intercalation, epiboly movements are also important for the extension of the notochord.

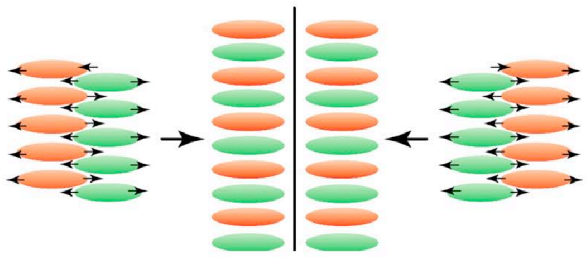

Figure 1.9 – Scheme of mediolateral intercalation of axial cells at late stages of of gastrulation. Convergence and extension movements of axial cells are mainly driven by mediolateral intercalation, where bipolar protrusive activity of mediolaterally-elongated cells results in their intercalation between their medial (dorsal) and lateral neighbors. Adapted from Myers et al., 2002b.

Migration of lateral mesendodermal cells

Lateral mesendodermal cells undergo simultaneous convergence and extension movements. Upon internalization, these cells extend but do not converge, and only around 70% epiboly a dorsal movement bias is observed (Sepich et al., 2005). Furthermore, detailed analysis using Nomarski optics has revealed that as lateral mesendodermal cells move dorsally, their direction is biased animally or vegetally depending on the animal-vegetal position. Cells in the equatorial region of the gastrula migrate dorsally, while cells closer to the animal pole move dorsoanimally, and cells closer to the vegetal pole show a vegetal bias in their paths (Sepich et al., 2005). These migratory behaviors are reminiscent of cells undergoing chemotaxis, as proposed for migrating prechordal plate progenitor cells. In fact, mathematical models suggest that the dorsal midline is a source of guidance cues; however, experimental evidence is still missing. As the lateral mesendodermal cells move closer to the dorsal side, they become tightly packed and highly mediolaterally elongated. They display straighter movement trajectories, thereby increasing their net dorsal speed (Jessen et al, 2002; Trinkaus, 1998). These cellular behaviors require both non-canonical Wnt and Stat3-dependent signaling (Miyagi et al., 2004; Myers et al., 2002b; Tada et al., 2002).

Convergence and extension movements of nuclei within the YSL

A study by D'Amico and Cooper (2001) has recently revealed that besides the three germ layers, the extra-embryonic YSL nuclei also undergo long-range convergence and extension movements during gastrulation and early segmentation (Fig. 1.10). Already at the onset of gastrulation, two spatially distinct domains of YSL nuclei with different morphogenetic behaviors become apparent. Nuclei located more animally start to move to the animal pole, while nuclei underneath the margin move to the vegetal pole. At mid-gastrulation, I-YSL nuclei from ventral and lateral regions of the gastrula start to converge to the dorsal side and then extend along the animal-vegetal axis. Nuclei underlying the dorsal midline at the beginning of gastrulation undergo extension movements, either toward the animal or vegetal pole, depending on their latitudinal positions. At the same time, I-YSL nuclei located close to the animal pole become displaced and move ventrally and laterally. Altogether, these movements generate a swirling flow pattern within the YSL. These patterns globally resemble those of the morphogenetic movements undertaken by the overlying hypoblast cells (D'Amico and Cooper, 2001; Solnica-Krezel and Cooper; 2002).

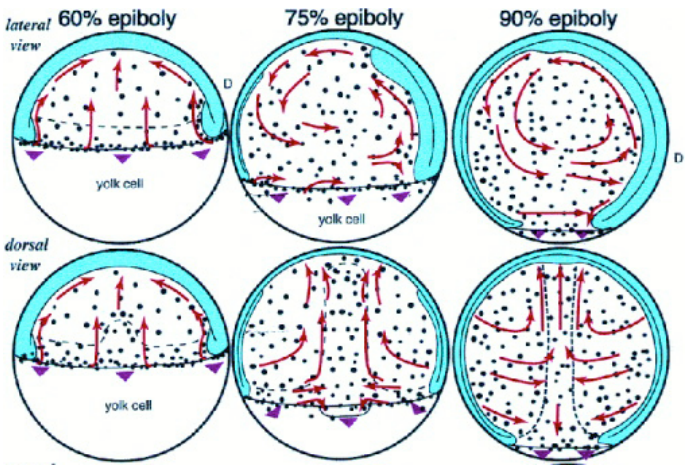

Figure 1.10 - Detailed diagram of YSL nuclei movement during gastrulation. Lateral and dorsal views are shown, from the onset of gastrulation (60% epiboly) until late mid-gastrulation (90% epiboly). Arrows summarize the regional trajectories of YSL nuclei. Dotted lines denote the location of the axial hypoblast and germ ring. Arrowheads represent epibolic progression. Nuclei start converging toward the dorsal midline (D) during mid-gastrulation (75% epiboly). Concurrently, nuclei located in the axial YSL domain extend along the anterior-posterior axis. As the axial YSL domain extends toward the animal pole, it displaces anteriorly located nuclei toward more ventral and lateral positions underlying the future hatching gland and forebrain. Adapted from D'Amico and Cooper (2001).

These observations led the authors to propose that the movement of the YSL nuclei and overlying deep cells are interdependent (Cooper and Virta, 2007; D'Amico and Cooper, 2001). YSL nuclei might influence the direction of hypoblast cell migration, which seem to move using the YSL membrane as a substrate (Warga and Nüsslein-

Volhard, 1999). However, no direct evidence for this model was provided.

Molecular control of convergence and extension

Several signaling pathways have been implicated in the regulation of convergence and extension movements in the zebrafish, such as Eph-ephrin, Slit, calcium, Prostaglandin and cell adhesion molecules (for reviews see Solnica-Krezel and Cooper, 2002; Solnica-Krezel, 2006). However, non-canonical Wnt signaling is clearly the major mediator of convergence and extension movements in zebrafish as well as in *Xenopus* (Kuhl, 2002; Tada et al., 2002). This pathway shares many components with the planar cell polarity (PCP) pathway in *Drosophila*, which regulates cell polarity in an epithelium (for reviews see Adler and Lee, 2001; Seifert and Mlozik, 2007), although in vertebrates it features members not identified on flies, such as the ligands Wnt11 and Wnt5 (Heisenberg et al., 2000; Kilian et al., 2003; Rauch et al., 1997). In both frogs and zebrafish, reduction as well as over-expression of Wnt11 and Wnt5 disrupts convergence and extension typically resulting in a shorter and broader body axis. This indicates that a balance of Wnt signaling is necessary for normal gastrulation movements (Heisenberg et al., 2000; Makita et al., 1998; Moon et al., 1993; Rauch et al., 1997). Other components of this signaling pathway critical for gastrulation movements include the intracellular mediator Dishevelled, the transmembrane protein Strabismus/Vang-like2, the Formin-homology protein Daam1, the small GTPase RhoA, the Rho kinase Rok2, the glypican Knypek, and several others (for more detailed reviews see Myers et al., 2002b; Tada et al., 2002).

Impairment of the non-canonical Wnt pathway leads to defects in gastrulation movements without affecting cell fate specification (Hammerschmidt et al., 1996; Solnica-Krezel et al., 1996). Therefore, an interesting question in the field is how cell fate specification is coordinated with cell movements. Two recent studies have proposed that BMP signaling might coordinate gastrulation movements with cell fate specification (Myers et al., 2002a; von der Hardt et al., 2007). In particular, a BMP gradient seems to be required for proper dorsal convergence of mesodermal cells independently of its role in dorsoventral patterning and of non-canonical Wnt signaling, by negatively regulating cadherin-mediated cell-cell adhesion (von der Hardt et al., 2007). In addition, Stat3-dependent signaling appears to act downstream of Wnt/β-

catenin activation (Yamashita et al., 2002), and upstream or parallel to the Wnt/PCP pathway (Miyagi et al., 2004), supporting the idea that control of cell movement occurs in parallel to cell specification.

In *Drosophila*, cell polarity is characterized by the asymmetric distribution of PCP components and by cytoskeletal remodeling. In vertebrates, the mechanisms by which Wnt/PCP pathway polarizes cells and promotes convergence and extension movements at the cellular level have only started to be unraveled. So far, the known localization of a few PCP factors indicates that the molecular mechanisms might be more complex in the vertebrate case than for the better characterized *Drosophila* PCP pathway, hence further studies are required to clarify this question (for a review see Seifert and Mlodzik, 2007).

1.5 Aims and approaches of this thesis

The central aim of this thesis was to understand whether and how YSL nuclei interact with the overlying blastoderm during gastrulation movements in the zebrafish embryo. Our major focus was to study the proposed interaction between the nuclei of the I-YSL and the overlying hypoblast cell layer during their analogous convergence and extension movements, which has not been directly addressed in previous studies. In parallel, we tried to clarify some aspects related to the epiboly movement of E-YSL nuclei and blastoderm.

To gain insight into the internal structure of the YSL syncytium, we started by analyzing its subcellular organization, specially focusing on the microtubule cytoskeleton, by transmission electron microscopy and single-photon confocal microscopy

To address I-YSL nuclei movement in detail, we developed an assay that allowed us to quantify and compare nuclei movement between wild type and different loss-of-function conditions. YSL nuclei were fluorescently labeled and their movement followed over time by two-photon confocal time-lapse microscopy. We analyzed the obtained data by a custom-built software that allowed us to automatically track and quantify the movement of the syncytial nuclei. The quantitative analysis was done in collaboration with Prof. Yannis Kalaidzidis (MPI-CBG, Dresden). To directly compare I-YSL nuclei movement with hypoblast cell movement, we performed time-lapses using

Nomarski interference optics.

To study the influence of the I-YSL nuclei on blastoderm movement, we interfered with the YSL microtubule cytoskeleton. Conversely, to understand how the blastoderm affects I-YSL nuclei movement, we analyzed different mutants that do not develop a proper hypoblast cell layer.

Finally, we investigated the function of a candidate molecule in mediating the interaction between I-YSL and hypoblast during convergence and extension movements, the adhesion protein E-cadherin. For that we analyzed I-YSL nuclei and hypoblast movements in mutant embryos for *cdh1/hab* as well as in embryos where we specifically knocked-down E-cadherin function in the YSL.

2. Materials and methods

2.1 Materials

2.1.1 Technical equipment

Ball-joint-holder	WPI
Glass capillaries:	Harward GC100F-15 (injection); Harward GC120-10 (transplantation)
Magnet holder:	MB-B (Kanetec)
Microbeveler	48000 (WPI)
Microinjectors:	PV820 and Pico-Pump with foot pedal (WPI)
Micromanipulators:	Narishige MN-151; Narishige MO-155 (transplantation)
Needle puller	Flaming/Brown P87 Sutter
Pipette holders:	MN-151 (injection); MPH3 (transplantation)
Glass rings:	MNK-145-030K (Fisher Scientific)
Microtome:	Ultracut microtome (Leica)
Vibratome	Leica VT1000S
Stereomicroscopes:	Leica MZ 125
	Olympus SZX12
DIC Microscope:	Zeiss Axioplan 2
Confocal microscopes:	Leica TCS-SP2
	Biorad Radiance 2000 with Nikon Eclipse TE300 microscope
Electron microscope:	Morgagni (FEI, Eindhoven)

2.1.2 Chemicals

All chemicals, if not noted otherwise, where purchased from Applichem, Merck, Roth and Sigma. Agarose was purchased from Pharmacia.

2.1.3 Reagents and buffers

E3 medium:	5 mM NaCl, 0.17 mM KCl, 0.33 mM $CaCl_2$ x 2 H_2O, 0.33 mM $MgSO_4$ x 7 H_2O, 0.2‰ methylene blue, pH 6.5
Danieau's buffer	58 mM, 0.7 mM KCl, 0.4 mM $MgSO_4$, 0.6 mM $Ca(NO_3)_2$, 5 mM HEPES, pH 7.6
Penicillin and streptomycin:	10000 units penicillin/ml and 10000 µg/ml streptomycin (Invitrogen)
Mounting medium:	1% (m/v) LMP agarose (Invitrogen) in E3 medium
Hybridization solution (Hyb+):	50% deionized formamide, 5x SSC, 0.1% Tween-20, 0.5 mg/ml torula (yeast) RNA, 50 µg/ml heparin, pH 6.0 (adjusted by adding 92 µl 1M citric acid per 10 ml Hyb+)
MABT:	150 mM NaCl, 100 mM maleic acid, pH 7.5
SSC (20x):	300 mM NaCl, 300 mM Na-Citrate, pH 7.0
PBS:	1.7 mM KH_2PO_4; 5.2 mM Na_2HPO_4; 150 mM NaCl
PBST:	PBS, 0.1% Tween-20
PBSTT:	PBS, 0.1% Tween-20, 0.1% Triton X-100
PFA 4%:	4% (w/v) paraformaldehyde, 81 mM Na_2HPO_4 19 mM, NaH_2PO_4
Bodipy ceramide	Bodipy® FL C_5-ceramide, stock at 1mM in DMSO (D3521, Invitrogen)
ER tracker	ER-tracker™ Blue-White DPX dye, stock at 1mM in DMSO (D12353, Invitrogen)
Histone:	Histone H1 Alexa Fluor® 488 conjugate; Stock at 10 mg/ml (H13188, Invitrogen)
Mini-ruby	Dextran, tetramethylrhodamine and biotin, 10000 MW, lysine fixable, stock at 50 mg/ml (D3312, Invitrogen)
Paclitaxel	Stock at 10 mM in DMSO (Sigma)

2.1.4 Molecular biological reagents

All restriction enzymes used were purchased from New England Biolabs. DNA and RNA ladders were purchased from MBI-Fermentas.

2.1.5 Molecular biological kits used

Name	*Company*	*Application*
BD advantage PCR kit	Clontech	PCR amplification of DNA
DIG labeling kit	Roche	Synthesis of in situ hybridization probes
Gel extraction kit	Qiagen	Purification of DNA from agarose gels
Message Machine kit	Ambion	Synthesis of mRNA for injection
Mini/Midi-prep Kit	Qiagen	small/big scale purification of plasmid DNA from bacteria cultures
PCR purification kit	Qiagen	purification of PCR and digestion products
TOPO-Cloning Kit	Invitrogen	Sub-cloning of DNA fragments
Vectastain Elite ABC Kit	Vector Laboratories	Detection of biotin in fixed embryos

2.1.6 Plasmids and constructs

Several DNA constructs were used for generation of in situ hybridization probes and mRNA for injection. In general, constructs used for probes were based on pBluescript II SK+ vector (Stratagene), while constructs used for mRNA for injection were based on pCS2+ vector (provided by D. Turner, Washington).

Antisense riboprobes:

Name	*Vector backbone*	*Source/Reference*
cathepsin L,1b (ctsl1b/ hgg1)	pBluescript SK+	Thisse et al., 1994
chordin (chd)	pCR2.1	M. Hammerschmidt, MPI-Freiburg
distal-less 3 (dlx3)	pBluescript SK+	Akimenko et al., 1994
forkhead box A2 (fkdA2)	pBluescript SK+	Strähle et al., 1993
hhex	pCS2+	Ho et al., 1999
nkx2.5	pBluescript SK+	Chen et al., 1997
no tail (ntl)	pBluescript SK+	Schulte-Merker et al., 1994
one-eyed pinhead (oep)	pBluescript SK+	Zhang et al., 1998
sox17	pCRII	M. Rhinn, MPI-CBG Dresden

mRNA for injection:

Plasmid name	*Gene*	*Vector backbone*	*Source*
cyc	*cyclops (ndr2)*	pCS2+	Rebagliati et al., 1998
EB3-GFP	*end-binding protein 3*	pCS2+	D. Gilmour, EMBL Heidelberg
GAP43-GFP	*gap43* (mammalian)	pCS2+	Okada et al., 1999
oep	*one-eyed pinhead*	pSP64T	F. Rosa, ENS Paris
tarA*	Constitutive active form of *taramA*	pCS2+	Y. Kikuchi, Nagoya University, Japan
Tau-EGFP	*tau* (bovine)	pCS2+	Geldmacher-Voss et al., 2003

2.1.7 Antibodies

Name	*Antigen*	*Species*	*Source*	*Dilution*
α-tubulin	Hybridoma DM1A	Mouse monoclonal	Sigma, T6199	1:500
γ-tubulin	synthetic peptide, N-terminal region human γ-tubulin	Rabbit polyclonal	Sigma, T3559	1:10000
E-cadherin	Zebrafish E-cadherin peptide	Rabbit polyclonal	MPI-CBG antibody facility	1:200
Pan-cadherin	C-terminus of chicken N-cadherin	Rabbit polyclonal	Sigma, C3678	1:1000
Alexa Fluor 568-conjugated anti-mouse IgG	Mouse IgGs	Goat polyclonal	Invitrogen, A11004	1:1000
Alexa Fluor 488-conjugated anti-rabbit IgG	Rabbit IgGs	Goat polyclonal	Invitrogen, A11008	1:1000
Alexa Fluor 546-conjugated anti-rabbit IgG	Rabbit IgGs	Goat polyclonal	Invitrogen, A11010	1:1000
Cy5-conjugated anti-rabbit IgG	Rabbit IgGs	Goat polyclonal	Jackson, 111-175-003	1:1000

2.1.8 Morpholino oligonucleotides

Morpholino oligonucleotides were used to specifically knock-down the translation of speficic mRNAs. All morpholinos used in this study were obtained from Gene Tools (USA) and used according the provided instructions. *e-cadherin1/cadherin1* (*cdh1*) morpholino was described previously (Babb and Marrs, 2004), as well as *wnt5/pipetail* (*ppt*) morpholino (Lele et al., 2001).

Name	*Target site*	*Sequence*	*Injected amount*
cdh1-ATG	From ATG translational start codon	5'-ATCCCACAGTTGTTACACAAGCCAT-3'	4-16 ng
wnt5/ppt	From ATG translational start codon	5'-GTCCTTGGTTCATTCTCACATCCAT-3'	2 ng

2.2 Methods

2.2.1 Embryo staging and maintenance

Fish maintenance and embryo collection was carried out as described (Westerfield, 2000). Embryos were raised in E3 medium when kept inside their chorion or in Danieau's buffer 1X with 0.5% of a mixture of penicillin and streptomycin after dechorionation. Embryos were kept at 31˚C and staged according to morphological criteria (Kimmel et al., 1995). Wild-type embryos were taken from TL (Tupfel long fin) and AB backgrounds. *silberblick/wnt11*^{tx226} (*slb/wnt11*^{tx226}; Heisenberg et al., 1996), and *half-baked/cadherin1*^{tx230} (*hab/cdh1*^{tx230}; Kane et al., 1996) carriers were maintained in a TL background, while maternal zygotic *one-eyed pinhead* (*oep*^{z1}; Zhang et al., 1998) mutants were maintained in a WIK background. To reduce background variability, *slb* and *hab* mutants were only compared to wild-type TL embryos.

2.2.2 Injection of mRNA, morpholinos and dyes into embryos

Preparation of the injection needle

The injection needles were prepared from glass capillaries containing an internal filament, which allowed back-filling. The desired shape of the needle was obtained using a needle puller (Flaming/Brown, P87 Sutter Instruments). The injection needle was placed on a micropipette holder and mounted on a micromanipulator. The micropipette holder was connected to a pneumatic pico pump PV820 that allowed the

injection of a drop of approximately 0.5 nl by regulating the pulse duration of the pressure.

Injection into one-cell stage embryos

To prepare the mRNA dilution for injection, stock mRNA was thawed and diluted on ice using RNAse-free water. Morpholinos were incubated for 10 minutes at 65˚C to dissolve precipitations, followed by 5 minutes of centrifugation. Embryos were injected into the yolk just underneath the first cell through the chorion.

Injection into the YSL

Blastula stage embryos were dechorionated in 2 mg/ml of pronase for 10 minutes, washed and maintained in Danieau's buffer 1X with 0.5% (v/v) of a mixture of penicillin and streptomycin, in 2% agarose-coated Petri dishes. For the injection procedure, a special agarose chamber containing vertical furrows was prepared as described (Westerfield, 1995). The embryos were aligned in the furrows and oriented in a lateral position. One or two drops with a volume of 0.5 nl were injected in the centre of the YSL by inserting the needle through the yolk, in embryos between high and sphere stage.

To label YSL nuclei, 1 mg/ml of Histone H1 conjugated to Alexa Fluor® 488 (Invitrogen) was injected into the YSL. Whenever morpholinos against *chd1* were injected into the YSL, histone was mixed in the injection solution to give a final concentration of 1 mg/ml. To look at YSL microtubules and microtubule plus-ends, 100 pg of *tau-GFP* or 100 pg *EB3-GFP* mRNA respectively were injected into the YSL. In these cases, no histone was added to the solution. When fluorescent beads were used, histone was diluted in the solution containing the beads and 0.5 nl were injected into the YSL.

2.2.3 Cell transplantation

Preparation of the transplantation setup

Transplantation needles were prepared from thin wall borosilicate glass capillaries without internal filament using the needle puller. The tip of the needles was broken with a watchmaker forcep and beveled with a MicroBeveler System (WPI), creating a 45º

angle to facilitate penetration into the embryo. The diameter of the tip was slightly larger than the size of a cell (approximately 60 µm). The needle was placed on a micropipette holder attached to a syringe with an airtight tube. The holder was mounted on a micromanipulator and by varying the air pressure with the syringe, cells could be sucked in and transferred from donor to host embryos. To immobilize the embryos, a special agarose chamber was used. The lid of a Petri dish was coated with 2% agarose and a plexiglass mould was used to create squared shaped depressions beveled on one side, where one embryo could fit.

For transplantation experiments, MZ*oep* mutants were used as host embryos. To be able to later follow YSL nuclei movements in these embryos, histone was injected into the YSL at high stage (see above for detailed procedure). As donors of the cells to be transplanted, one-cell stage wild-type embryos were injected with a mixture of 100 pg of *cyclops/ndr2 (cyc/ndr2)* mRNA, 100 pg of *GAP43-GFP* mRNA and 5 mg/ml of dextran conjugated to tetramethylrhodamine and biotin (mini-ruby, Invitrogen). Cyc/ndr2 over-expression was used to induce mesendodermal cell fates ubiquitously; *GAP43-GFP* was injected to label the plasma membrane, thus allowing the distinction between transplanted cells and YSL nuclei of the host embryo; mini-ruby was used as a lineage tracer to follow the transplanted cells in the host embryo with low magnification and for their detection after fixation. At high stage, both host and donor embryos were dechorionated with pronase and maintained in Danieau's buffer with 0.5% (v/v) penicillin and streptomycin (see above). At sphere stage, the embryos were transferred into the depressions in a previously prepared agarose chamber. About 20-30 cells from a donor embryo were transferred into the blastoderm margin of a host MZ*oep* embryo. After transplantation, the embryos were transferred to new agarose-coated Petri dishes and incubated at 31°C until the desired stage.

2.2.4 Implantation of polystyrene beads in the YSL

Polystyrene beads were used to study cytoplasmic flows within the YSL. About 20 µl of Polybead® Microspheres with a diameter of 20 µm, or Fluoresbrite® Yellow-Green Carboxylate Microspheres with a diameter of 0.5 µm were pipeted into an Eppendorf tube and washed twice in PBS by brief centrifugation and removal of the supernatant.

Beads were re-suspended in 0.1 µg/µl of bovine serum albumin to block unspecific binding.

For implantation of 20-µm beads, high stage wild-type embryos were dechorionated with pronase, injected with histone into the YSL and transferred to agarose-coated dishes with small depressions (same procedure as described for transplantation experiments). A few beads were pipeted onto the plate and a small hole was done close to the blastoderm margin of the embryo, with a tungsten needle. A bead was taken with the tip of a fine watchmaker forcep and pushed into the hole until reaching the YSL cytoplasm. The embryos were then transferred to a new agarose-coated dish and incubated at 31ºC until the stage desired for time-lapse imaging. To insert 0.5-µm fluorescent beads, a normal YSL injection procedure was performed (see above).

2.2.5 Incubation of embryos in bodipy ceramide and ER-tracker

To detect the Golgi apparatus and the endoplasmic reticulum (ER), embryos were incubated in specific vital dyes. For the Golgi, sphere stage embryos were incubated in medium containing 1% (v/v) Bodipy® FL C_5-ceramide (Invitrogen) for one hour at 22ºC, followed by two hours in medium only at 31ºC. For the ER, sphere stage embryos were incubated in medium containing ER-tracker™ Blue-White DPX dye (Invitrogen) at 0.1% (v/v) for one hour at 31ºC followed by one hour in medium only, at 31ºC. For both experiments, embryos were mounted in 1% agarose and imaged by two-photon confocal microscopy.

2.2.6 Incubation of embryos in paclitaxel

To disrupt microtubules, embryos were incubated in the microtubule-stabilizing agent paclitaxel. Embryos were first dechorionated with pronase and histone was injected into the YSL. Embryos were incubated in Danieau's buffer containing 10 µM paclitaxel (0.05%, v/v; Sigma), and in the dark, since this compound is light-sensitive. Control embryos were incubated in Danieau's buffer containing 0.05% (v/v) DMSO. When these embryos were mounted for two-photon confocal microscopy, paclitaxel was added to the agarose-mounting medium at an identical concentration.

2.2.7 Generation of plasmids for mRNA injections and antisense riboprobes

The cloning of DNA fragments was performed according to standard protocols described in Sambrook and Russell (2001). The commercial kits used are listed in the material section and used according to manufacturer's instructions. All plasmids used in this study are listed in section 2.1.6.

2.2.8 Synthesis of mRNA for injection

Before synthesis of mRNA, DNA from a pCS2+ expression vector containing the desired insert was linearized by digestion with Not1 restriction enzyme for 3 hours at 37ºC. The pCS2+ plasmid contains a Not1 restriction site after the poly (A) signal, which, after mRNA injection into the embryo, mediates the generation of a poly (A) tail at the end of synthetic mRNA, making it more stable. The linearized DNA was purified using PCR purification kit (Qiagen) according to manufacturer's instructions. The DNA was eluted in RNAse free water, checked for complete linearization by agarose gel electrophoresis and the concentration determined using a UV spectrometer. The DNA was stored at -20ºC.

Linearized plasmid DNA was then taken as a template to synthesize mRNA in vitro using SP6 polymerase reaction. This was performed using the mMessage mMachine kit (Ambion, UK) following the manufacturer's instructions.

2.2.9 Synthesis of DIG labeled probes for in situ hybridization

DIG labeled antisense riboprobes were synthesized from cDNA inserted in pBluescript vector (Stratagene, USA). The plasmid DNA was first linearized with the appropriate restriction enzyme and then used as a template for RNA synthesis, using DIG labeling kit (Roche Diagnostics, Germany). After synthesis, the DIG labeled RNA was precipitated by incubation with LiCl, overnight at -20°C. The RNA was then pelleted by a 30-minute centrifugation at 14000 rpm at 4°C, washed with 70% ethanol and re-suspended in 100 µl of RNase-free water. This solution was further diluted to 500 µl with hybridization solution. Routinely, a dilution of 1:100 of this stock was used for in situ hybridization protocols. A detailed description of all the probes used, including corresponding references, can be found in section 2.1.6.

2.2.10 Whole mount in situ hybridization

In order to detect gene expression in the embryo, whole mount in situ hybridization was performed as previously described (Barth and Wilson, 1995). Briefly, embryos were fixed in 4% PFA overnight at 4ºC. They were then washed in PBST, transferred into 100% methanol and stored at -20ºC. Before hydridization, embryos were re-hydrated and rinsed in PBST. They were then transferred into hybridization solution and incubated for 3-6 houts at 70ºC followed by hydridization with the desired DIG-labeled probe, overnight at 70ºC. Then they were washed in decreasing concentrations of SSC, transferred to MABT, followed by incubation with 2% blocking solution (Roche Diagnostics, Germany) for 5 hours at room temperature. The embryos were then incubated in an α-DIG antibody coupled to alkaline phosphatase (Roche Diagnostics, Germany) overnight at 4ºC. the antibody was washed away with MABT followed by a 5-minute incubation in 0.1 M Tris buffer pH 9.5 to adjust the pH. The probes were then detected with BM Purple solution (Roche Diagnostics, Germany). After detection, the embryos were washed with PBST and re-fixed in 4% PFA. To reduce background, embryos were incubated in a series of glycerol solutions with increasing concentrations. For sections, stained embryos were not incubated in glycerol, but instead equilibrated in gelatine/albumen solution (0.49% gelatine, 30% egg albumen, 20% sucrose in PBS). They were then transferred into an embedding form coated with fresh polymerisation solution (albumen, 25% gluteraldehyde, 10:1) and kept 15 minutes at room temperature to allow polymerization. 20-µm serial sections were taken using a Leica Vibratome VT1000S. Images of whole-mount embryos were taken on an Olympus SZX12 stereomicroscope attached to an Olympus camera using Spot software. Images of sections were taken on a Zeiss Axioplan 2 microscope using Spot software. Final processing of the images was done with Adobe Photoshop software.

2.2.11 Biotin detection of transplanted cells

To detect the transplanted mini-ruby labeled donor cells in a host embryo, Vectastain Elite ABC kit (Vector Laboratories, USA) was used. First, solution A (streptavidin) was diluted and well mixed in the provided blocking solution (1:100) and then solution B was added (biotin-peroxidase, 1:100). After in situ hibridization, embryos were washed with PBST and then incubated in the previously prepared AB solution for 1 hour at

room temperature. Then they were washed with PBST and transferred to a DAB solution (1 mg/ml, Sigma). After a 5-minute incubation, 1 μl of 0.3% H_2O_2 was added. The reaction was stopped by several washes in PBST.

2.2.12 Whole mount antibody staining

To detect YSL microtubules, immunohistochemistry was performed essentially as described previously for *Xenopus* oocytes (Gard, 1993). Briefly, embryos were fixed in 3.7% formaldehyde and 0.25% gluteraldehyde in microtubule buffer for 2 hours at room temperature, followed by overnight incubation at 4ºC. The embryos were washed in PBSTT and blocked in PBST with 0.5% Triton X-100 and 10% normal goat serum (NGS) for 4 hours at room temperature. They were then incubated in a mixture of two primary antibodies diluted in PBST with 0.5% Triton X-100 and 5% NGS: mouse α-tubulin antibody and rabbit γ-tubulin (both from Sigma), overnight at 4ºC. After washing with PBSTT, the embryos were incubated in anti-mouse Alexa Fluor® 568 (Invitrogen) and anti-rabbit Cy5 (Jackson Laboratories) secondary antibodies diluted in PBST with 0.5% Triton X-100 and 5% NGS, overnight at 4ºC. The embryos were then rinsed and mounted on agarose-coated dishes with depressions (see cell transplantation section) in PBST with the region of interest facing up. Images were acquired with a 63x water immersion objective (NA 0.9), using 488, 543 and 633 nm laser lines on a Leica TCS-SP2 confocal microscope.

2.2.13 Immunohistochemistry on paraffin sections

In order to detect E-cadherin localization, embryos were sectioned and immunohistochemistry performed according to Montero et al. (2005). Briefly, embryos at gastrulation stages were fixed in 4% PFA overnight at 4°C, dehydrated in ethanol and embedded in paraffin wax (Sigma). 10-μm serial sections were taken on a microtome, collected on Superfrost/Plus slides (Fisher Scientific) floating on water to avoid wrinkling and dried overnight at 37°C. Sections were deparaffinized in xylene and then re-hydrated. Blocking was done in PBST with 10% NGS for 4 hours at room temperature and then incubated in rabbit anti-E-cadherin (MPI-CBG, Dresden) or anti-pan-cadherin (Sigma) primary antibody overnight at 4°C, in a humidified chamber. The next day, sections were washed in PBST, incubated with anti-rabbit Alexa Fluor® 488

or Alexa Fluor® 546 (Invitrogen) secondary antibodies for 2 hours at room temperature and mounted in Vectashield medium (Vector Laboratories, USA). Images were acquired on a Leica TCS-SP2 confocal microscope with a Plan Apo 40x objective (NA 0.75).

2.2.14 Electron microscopy

For analysis of the YSL ultrastructure, transmission electron microscopy was performed essentially as described in Montero et al. (2005), and in collaboration with Dr. Michaela Wilsch-Bräuninger (MPI-CBG, Dresden). Dechorionated embryos of different stages were fixed in 2% gluteraldehyde and 0.5% PFA in 0.1 M phosphate buffer overnight at 4°C. They then were post-fixed in 1% osmium tetroxide (Science Services, Munich) for 1 hour, dehydrated through a graded series of ethanol and infiltrated in Embed-812 resin (Science Services, Munich) overnight. The samples were cured for 48 hours at 65°C. Ultrathin sections (70-nm thick) were cut on an Ultracut microtome (Leica Microsystems, Vienna). The samples were viewed in a Morgagni Electron Microscope (FEI, Eindhoven). Micrographs were taken with a charge-coupled device camera (MegaviewII, Soft Imaging System) and AnalySis software (Soft Imaging System).

For immunogold labeling experiments, the procedure was similar except that embryos were fixed in 4% PFA and 0.01% gluteraldehyde in 0.1 M phosphate buffer overnight at 4°C and Lowieryl HM20 resin was used for embedding. Embryos were processed for cryosectioning and subsequent immunolabeling. Sections were incubated in mouse anti-actin antibody (Linaris, Wertheim) dilluted 1:75, 3 hours at room temperature. Secondary antibody used was goat anti-mouse IgG/M coupled to 12 nm gold (Dianova, Hamburg) diluted 1:30.

2.2.15 Mounting of live embryos in agarose for time-lapse microscopy

For time-lapse microscopy, embryos were mounted in 1% low melting point agarose in E3 medium. The mounting device used for inverted microscopes consisted a self-assembled imaging chamber similar to what has been described by Concha and Adams (1998). Briefly, a glass ring was glued onto a cover-slip using silicon grease (Beckmann); a few drops of 1% LMP agarose (previously melted at 70ºC) were placed on the cover-slip where one dechorionated embryo was then transferred to and carefully

oriented with a hair-loop; after the agarose was solidified, a few drops of E3 medium were added and silicon grease used to seal a glass slide to the glass ring. For upright microscopes, the procedure was similar, except that the mounting chamber consisted only of a glass slide and a glass ring, and a dipping objective was used to image the embryo from the top.

2.2.16 DIC live imaging

For analysis of cell and I-YSL nuclei movements, time-lapse imaging was performed using a 20x water immersion lens on a Zeiss Axioplan 2 microscope equipped with Nomarski optics. Time-lapses were acquired with Openlab 3.1 software (Improvision, UK). 20 Z-stacks (5-7 µm steps) were acquired with 2 minutes between time points, over approximately 5 hours (from 65% epiboly until tailbud stage). Importantly, these time-lapses were performed at room temperature, therefore embryonic development was slower in DIC time-lapses in comparison to two-photon confocal time-lapses. The image sequences were analyzed using NIH Image software or ImageJ (NIH, USA). Cells and I-YSL nuclei were manually tracked by following the centre of each nucleus and recording the (*x,y*) coordinates of every fifth frame (every 10 minutes). The tracks were further processed with Microsoft Excel software.

For statistical analysis, time lapses with 110 frames were analyzed, that, in developmental stages, corresponded approximately to 65%-70% until 90% epiboly. Between 2 to 6 embryos for each condition were analyzed and about 10 I-YSL nuclei and hypoblast cells were tracked. Several parameters, such as total speed, net dorsal speed, and directionality, were calculated using Microsoft Excel software. Directionality was calculated by dividing the net displacement by the total displacement. To analyze the significance between two mean values, unpaired Student's *t* test with a two-tailed distribution was used. To test for the difference between the values of one I-YSL nucleus and those of the hypoblast cells migrating directly above it, a paired Student's *t* test with a two-tailed distribution was used. For all the analysis, a normal distribution of values was assumed.

2.2.17 Two-photon confocal time-lapse imaging

Single channel live time-lapse imaging was performed with a Bio-Rad Radiance 2000 multiphoton confocal microscope setup. A mode-locked, 890-900 nm, infra-red laser with an average power of 500 mW, originated from a Coherent Mira 900 Ti::Sapphire laser, was used to achieve two photon-excitation of the sample. For time-lapses of YSL nuclei movements, imaging was obtained with a Plan Fluor 20x water-immersion objective (NA 0.75) typically connected to a Bioptechs objective heater in order to maintain a stable temperature of 28-29ºC; in time-lapses of paclitaxel, *chd1* YSL-morpholino, and respective control embryos, no objective heater was used, and thus experiments were performed at room temperature (22-24ºC). Z-stacks were acquired by scanning an area of 621.6 µm x 621.6 µm (1.214 µm/pixel) with a spacing of 5 µm over a total vertical distance of 150-200 µm. Time lapses were acquired over a period of 150-300 minutes with 150 or 300 seconds between each time point. For time lapses of microtubule dynamics, imaging was obtained with a Plan Apo 60x water-immersion objective (NA 1.2) also connected to a Bioptechs objective heater (28-29ºC). For Tau-GFP, bodipy ceramide and ER tracker time-lapses, Z-stacks were acquired by scanning an area of 102.4 µm x 102.4 µm (0.2 µm/pixel) with a spacing of 1 µm over a total vertical distance of 10-25 µm. Time-lapses were acquired over a period of 5-60 minutes with 3-150 seconds between each time point. For EB3-GFP movies, only one stack was acquired, every 3 seconds, maximum of 5 minutes; all the other settings were the same as for Tau-GFP. Laser Sharp 2000 software was used for time-lapse recording.

2.2.18 Analysis and quantification of YSL nuclei movement obtained with two-photon confocal time-lapse imaging

To analyze and compare the dynamics of YSL nuclei movement between wild-type and mutant embryos, a software that allows the automated tracking of particles in two dimensions was used. For that, maximum projections of the two-photon acquired Z-slices were obtained for every time point using ImageJ software (NIH, USA) and exported as 8-bit TIFF files. These image sequences were analyzed using Motion Tracking software, designed by Prof. Yannis Kalaidzidis (MPI-CBG, Dresden), and with his collaboration. The concept of this program has been previously described in detail (Helenius et al., 2006; Rink et al., 2005). Briefly, the program starts by

identifying peaks in the pixel intensity values for a single frame of the movie. Following background subtraction by windowed floating mean, fluorescent structures in the images were modeled by a sum of squared Lorentzian functions. Fitted structures were subtracted from the image, and the procedure was repeated iteratively to capture all structures above noise values. Image fitting produced a particle set with known position, cross sectional area, and total fluorescence, serving as basis for all further calculations. Next, the program examines subsequent frames, and links the positions of individual nuclei together into tracks. Track assignments were made on basis of the weighted sum of scores for position, speed, cross sectional area, maximum intensity, total vesicle fluorescence, and termination penalty. Occasionally, the program makes errors when constructing the trajectories, therefore all the tracks were manually inspected and the ones that were not correct were excluded.

For statistical analysis of wild-type, and MZ*oep*, *slb/ppt*, and *hab* mutant embryos, time lapses with 60 frames (2.5 hours), which, in developmental stages, corresponded to 70-80% epiboly until 1-2 somites, were analyzed. For *cdh1* YSL-morphants and respective controls, time-lapses with 60 frames (5 hours), which corresponded to 65%-70% epiboly until 1-2 somites, were analyzed. Between 2 to 5 embryos for each condition were analyzed and about 30-50 nuclei tracked. The total speed of movement was calculated and the mean values for each embryo obtained automatically with Motion Tracking software. To calculate net speed values for *x* and *y* axes in separate, the track coordinates were exported to Microsoft Excel and the parameters calculated manually. Net speeds were calculated by dividing the net displacement (difference between the final and initial position in the *x* or *y* axis) by the total time. To analyze the significance between two mean values, unpaired Student's t-test with a two-tailed distribution was used (Microsoft Excel). For all the analysis, a normal distribution of values was assumed.

3. Results

3.1 YSL nuclei movement during gastrulation

3.1.1 I-YSL nuclei undergo convergence and extension movement similar to hypoblast cells during gastrulation

D'Amico and Cooper (2001) have shown that, during zebrafish gastrulation, I-YSL nuclei undergo convergence and extension movements similar to the overlying hypoblast cells. These findings inspired the work of this thesis, which was set out to learn how I-YSL and hypoblast influence each other during gastrulation movements. We decided to first carry out a more detailed and quantitative comparison of the movements of I-YSL nuclei and hypoblast cells.

To achieve this, we performed a series of time-lapse recordings of paraxial regions of the embryo during gastrulation (60%-65% epiboly until 90%-100% epiboly; Fig. 3.1A). The use of Nomarski interference contrast optics (DIC) allowed us to simultaneously follow the trajectories of I-YSL nuclei and hypoblast cells (Fig. 3.1B; Movie 1). Figure 3.1C illustrates plots of representative tracks showing that the animal-most hypoblast cells (the first cells that involute at margin) underwent highly directed movement toward the animal pole, while the cells located closer to the germ ring margin (the cells involuting after the beginning of the time-lapse) showed a stronger tendency to converge to the dorsal side of the embryo (Fig. 3.1C, red tracks). These observations are consistent with the results obtained by Sepich and co-workers, who showed that hypoblast cells mainly move to the animal pole in the beginning of gastrulation, and start to converge dorsally from mid-gastrulation stages onwards (Sepich et al., 2005). In addition, we noticed that cells within the deeper layer of the hypoblast (closer to the YSL) showed more directed convergence movement than more superficial hypoblast cells, and also moved faster (data not shown).

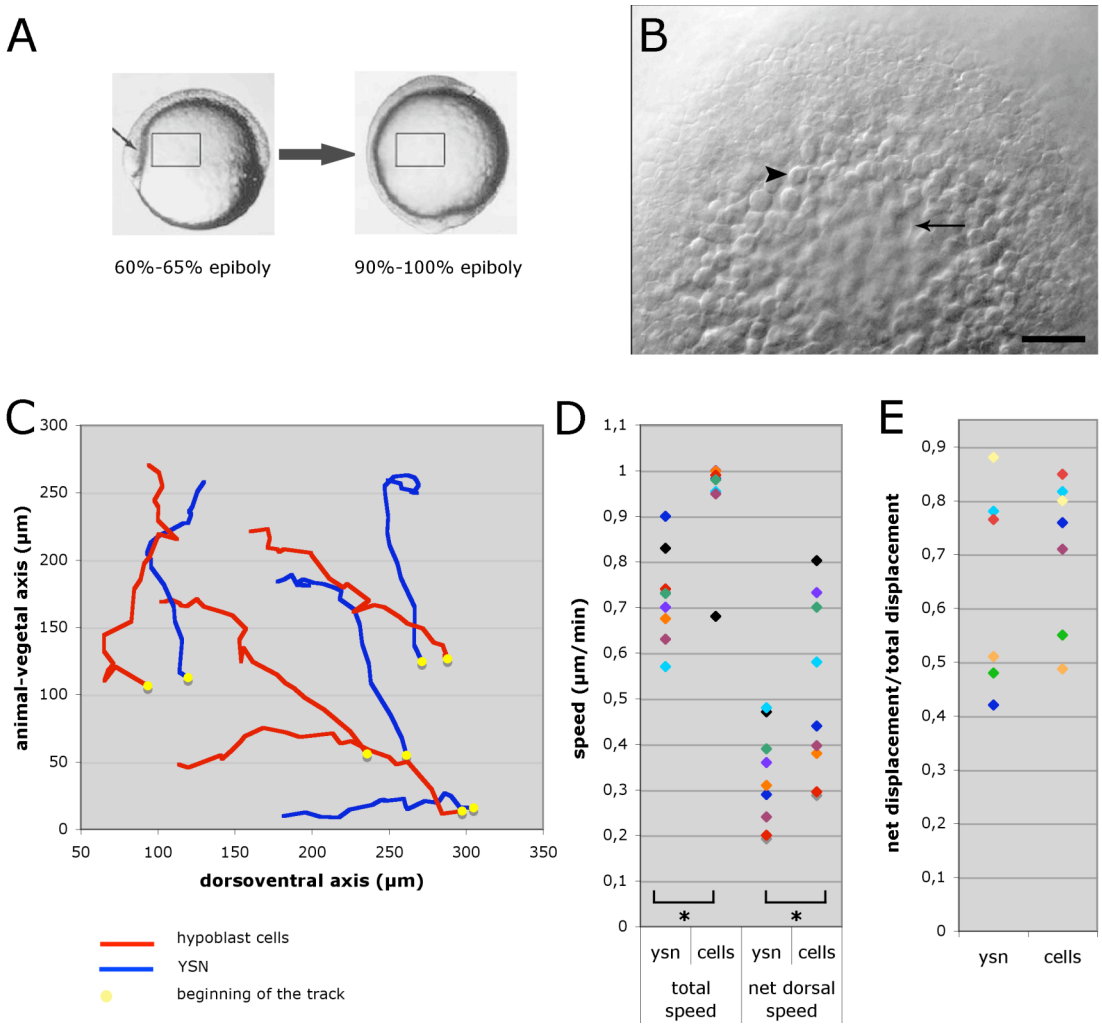

Figure 3.1 – Comparison between the movements of hypoblast cells and I-YSL nuclei during wild type gastrulation by time-lapse imaging using Nomarski optics. (A) Representation of the region of the embryo and time period used during live imaging. The squared box indicates approximately the imaged region shown in (B). Time-lapses were taken from 60%-65% epiboly until 90%-100% epiboly; dorsal side was always on the left, and animal pole on top. Small arrow points out the embryonic shield. (B) Nomarski image of the paraxial region of a wild-type embryo as depicted in (A). Both hypoblast cells (arrowhead) and I-YSL nuclei (arrow) are visible by Nomarski optics. Scale bar, 50 µm. (C) Graphical representation of typical trajectories of paraxial hypoblast cells and I-YSL nuclei during gastrulation. Red tracks, hypoblast cells; blue tracks, I-YSL nuclei; yellow circles, beginning of each track. Approximately ten tracks of cells and nuclei from each embryo (n=6) were obtained manually by recording their (*x,y*) coordinates every 10 minutes. Animal pole is on top, dorsal side is on the left. Hypoblast cells and I-YSL nuclei located closer to the dorsal midline moved mainly to the animal pole; hypoblast cells and I-YSL nuclei close to the margin mainly moved to the dorsal side; laterally located hypoblast cells and I-YSL nuclei, farther from the margin, moved dorso-animally. Note that the trajectories of hypoblast cells and I-YSL nuclei are not identical even though they show a similar tendency. (D) Quantification of total and net dorsal speed of hypoblast cells and I-YSL nuclei. Both total and net dorsal speed of hypoblast cells was significantly higher than that of I-YSL nuclei ($p<0.01$; n=8 pairs). (E) Quantification of directionality of movement of hypoblast cells and I-YSL nuclei. Directionality was calculated by dividing net by total displacement. Directionality of cells was similar to that of I-YSL nuclei ($p>0.05$; n=8 pairs). A paired Student's *t* test was performed to test the differences between speed and directionality of a cell and that of the nucleus directly underlying it. Each square represents the value of one cell or nucleus. ysn, internal yolk syncytial nuclei.

Trajectories of I-YSL nuclei were similar to those of hypoblast cells: more anteriorly located I-YSL nuclei moved directly toward the animal pole, whereas I-YSL nuclei underlying the later involuting hypoblast cells showed strong convergence movement (Fig. 3.1C, blue tracks). However, taking a closer look at the individual tracks and comparing each nucleus with the hypoblast cells directly above it, revealed distinct differences between the respective movement patterns. I-YSL nuclei started to converge to the dorsal side slightly after the hypoblast cells (65-70% epiboly for hypoblast cells *versus* 70-75% epiboly for I-YSL nuclei; data not shown) and in a less dorsally-directed way (Fig. 3.1C). We therefore compared their precise speed and directionality. We found that the speed of lateral hypoblast cells was markedly higher than that of the I-YSL nuclei located approximately in the same position (Fig. 3.1D). To analyze how dorsally-oriented and directional was the movement, we calculated two additional parameters: "net dorsal speed", which reflects the net displacement taking place only in the dorsal (*x*) axis over time; and "directionality" or "meandering rate", which represents the ratio between the net displacement and the total displacement, considering both *x* and *y* axes. The net dorsal speed of hypoblast cells was higher than that of I-YSL nuclei, indicating that hypoblast cells are more dorsally-oriented than the underlying nuclei (Fig. 3.1D). In what respects directionality, I-YSL nuclei and hypoblast cells showed similar values, suggesting that they undergo the same degree of meandering (Fig. 3.1E).

3.1.2 Quantitative analysis of YSL nuclei movement

To obtain a clearer and more quantitative overview of I-YSL nuclei movement during gastrulation, we developed a more precise imaging method, based on two-photon confocal time-lapse microscopy; this allowed us to: a) precisely detect and follow more nuclei in the YSL; b) follow I-YSL nuclei within a larger area/volume of the embryo; and c) track nuclei during a longer period of time.

We specifically labeled YSL nuclei by injecting a fluorescent-tagged version of the protein Histone H1 into the YSL. To restrict labeling to the YSL, injection was performed at sphere stage, when cytoplasmic connections between the yolk membrane and blastoderm have closed (Kimmel and Law, 1985a,b; Kimmel et al., 1995). This method had already been used by D'Amico and Cooper (2001) to successfully label the

YSL nuclei without exerting secondary effects on the development of the embryo. Similar observations were also obtained when injecting other impermeant nuclear dyes such as Sytox Green into the YSL (data not shown; D'Amico and Cooper, 2001). We then imaged the YSL nuclei by two-photon confocal time-lapse microscopy, which allowed us to perform long-term imaging without major photobleaching and phototoxicity, and to image very deeply within the embryo (ca. 200 µm; Helmchen and Denk, 2005; Oheim et al., 2006). Embryos were always imaged on the dorsal side, from 70% of epiboly until the 1 or 2-somite stage (Fig. 3.2A), to detect all the I-YSL nuclei of dorsal and lateral regions of the embryo. This imaging technique also allowed us to use an in-house tracking software (Motion Tracking, Y. Kalaidzidis; see more details in methods section), which automatically detects, follows and quantitatively analyzes the trajectories of the YSL nuclei. Nevertheless, we have to state two main disadvantages of this method. First, we could only follow YSL nuclei in two-dimensions (*x,y*). Taking into account that YSL nuclei undergo long-range movements in the dorsoventral and animal-vegetal axis of the embryo, our measurements can only be considered for comparative analysis. Second, we could not simultaneously track YSL nuclei and blastodermal cells.

In summary, we observed that, in wild-type embryos: *1)* animal-most I-YSL nuclei move directly to the animal pole of the embryo with little convergence; *2)* I-YSL nuclei located around the margin in lateral regions move toward the dorsal side and show strong convergence and less extension; *3)* YSL nuclei initially located on the dorsal side of the embryo move to the animal or vegetal pole, depending roughly on their initial animal-vegetal position; *4)* E-YSL nuclei initially located more vegetally move in a highly directed way to the vegetal pole of the embryo (Figs. 3.2B-E, Movie 2).

Together, our observations are in agreement with the previous study of D'Amico and Cooper (2001): I-YSL nuclei undergo long-range convergence and extension movements that roughly resemble overlying hypoblast movements. However, we noticed distinct differences between I-YSL nuclei and hypoblast movements. I-YSL nuclei start to converge dorsally shortly after the overlying hypoblast cells, and move in a slower and less dorsally-directed way. Furthermore, the trajectories of I-YSL nuclei and overlying hypoblast cells, although displaying a similar tendency in terms of direction of movement, do not show a one-to-one association.

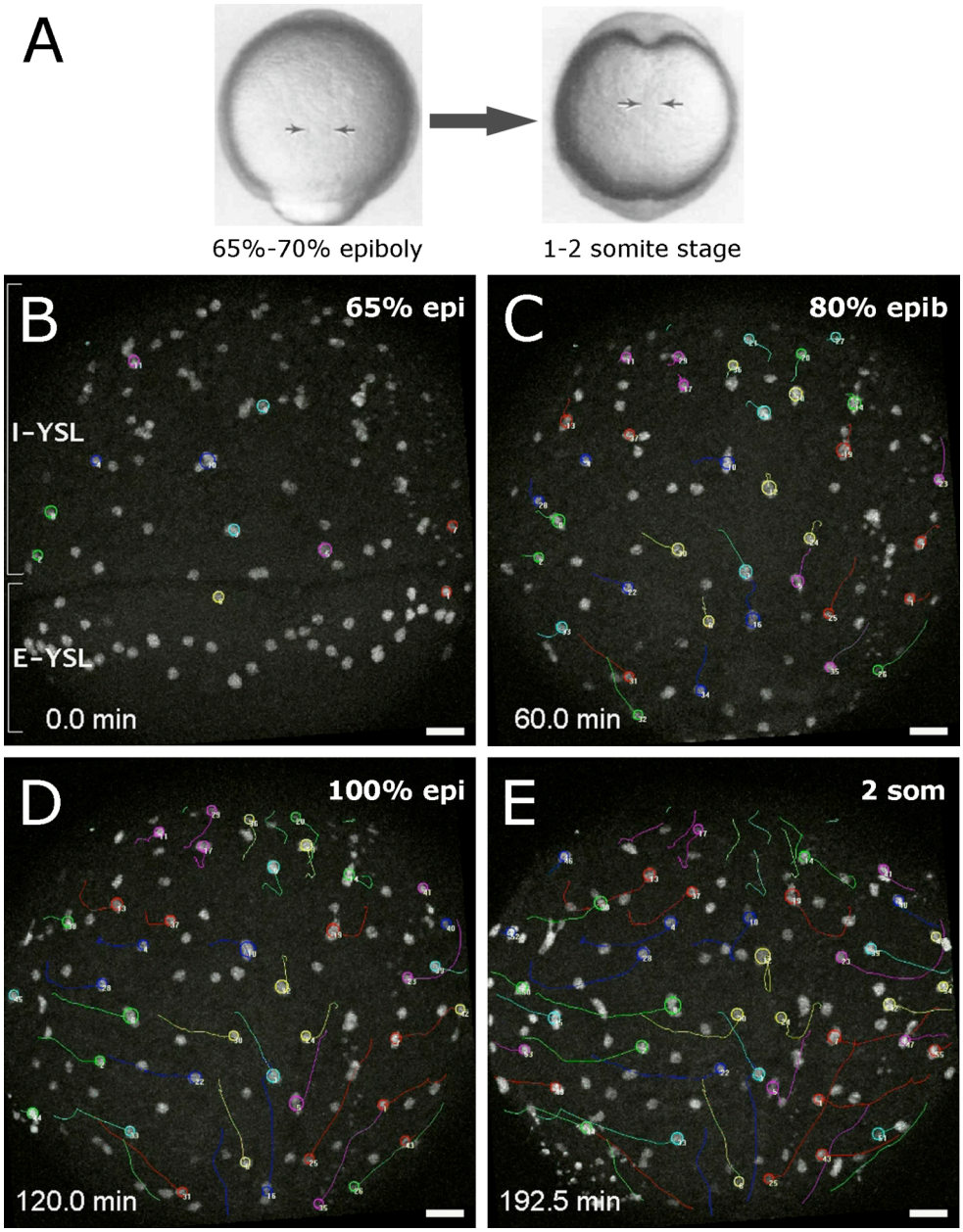

Figure 3.2 – Two-photon confocal time-lapse imaging of YSL nuclei during gastrulation in a wild-type embryo. (A) Schematic view of the embryo orientation and time scale used for time-lapse (n=17). The dorsal side of the embryo was imaged from 65%-70% epiboly until 1-2 somite stage. Animal pole is on top. Arrows delimit the dorsal axis. (B-E) Still images of a histone-injected wild-type embryo from 65% epiboly until 2-somite stage. Images are projections of 35 Z-slices. Some of the nuclear trajectories obtained with the Motion Tracking Software are shown. The circles indicate the end-point of each track. (B) Embryo at 65% of epiboly. The white lines delimit I-YSL and E-YSL. (C) Embryo at 80% epiboly. Most of the I-YSL nuclei did not show major convergence movement, while E-YSL nuclei underwent epiboly, further than blastoderm cells. (D) At 100% epiboly, the animal-most I-YSL nuclei moved to the animal pole, presumably together with prechordal plate cells, and some are not visible anymore. Vegetal-most I-YSL and E-YSL nuclei moved toward the vegetal pole. Lateral I-YSL nuclei converged to the dorsal side. (E) Embryo at 2-somite stage. Lateral I-YSL nuclei continued to converge to the dorsal side. Abbreviations: epi, epiboly; som, somite. Scale bars, 50 µm.

3.2 Subcellular organization of the YSL

In order to better understand the dynamics of the YSL, we investigated how this compartment is organized at the subcellular level. The central questions were: is the YSL polarized in a similar way to normal migrating cells? Does its organization change during gastrulation? Do other organelles move in a similar fashion to the nuclei?

Early studies in the teleost *Fundulus heteroclitus* have examined the YSL structure during gastrulation, using transmission and scanning electron microscopy (Betschaku and Trinkaus, 1978). However, equivalent studies have never been conducted in the zebrafish embryo. Since the YSL originates from the cytoplasmic and nuclear content of early marginal blastomeres, it is possible that each of the YSL nuclei possesses its own secretory apparatus associated with it. This secretory machinery could be important for the localized secretion of signaling molecules into the overlying blastoderm, with a role during gastrulation. Another structure we focused on was the YSL membrane, which is composed of distinct specializations probably required for YSL movement.

3.2.1 Secretory machinery

We started by studying the distribution of the secretory machinery, specifically the Golgi apparatus and endoplasmic reticulum (ER). To observe their distribution within the YSL, we used two different approaches: transmission electron microscopy (TEM), to obtain insight into the ultrastructure, and live imaging, to investigate how these organelles distribute during gastrulation movements. For the TEM analysis, wild-type embryos fixed at 60% epiboly were sectioned. We observed that in both I-YSL and E-YSL, the Golgi apparatus was well differentiated, composed of several stacks and many associated vesicles (Figs. 3.3A,B). The number and degree of complexity of the Golgi units in the YSL appeared to be higher than that of embryonic cells (Fig. 3.3D). No preferential localization relative to the nuclei or to specific regions of the YSL was observed. When we analyzed the distribution of the ER, we observed that the YSL contained less visible ER structures than the embryonic cells (Figs. 3.3C,D; data not shown), while the yolk cytoplasmic layer (YCL) contained abundant ER (Figs. 3.3E,F). The ER was not as closely associated with the nuclei as it is in typical eukaryotic cells, and no preferential localization within the YSL was detected. In contrast to what was

observed before in *Fundulus* embryos (Lentz and Trinkaus, 1967), the density of ribosomes and vesicular structures in the zebrafish YSL cytoplasm appeared to be higher than in the cytosplasm of the embryonic cells.

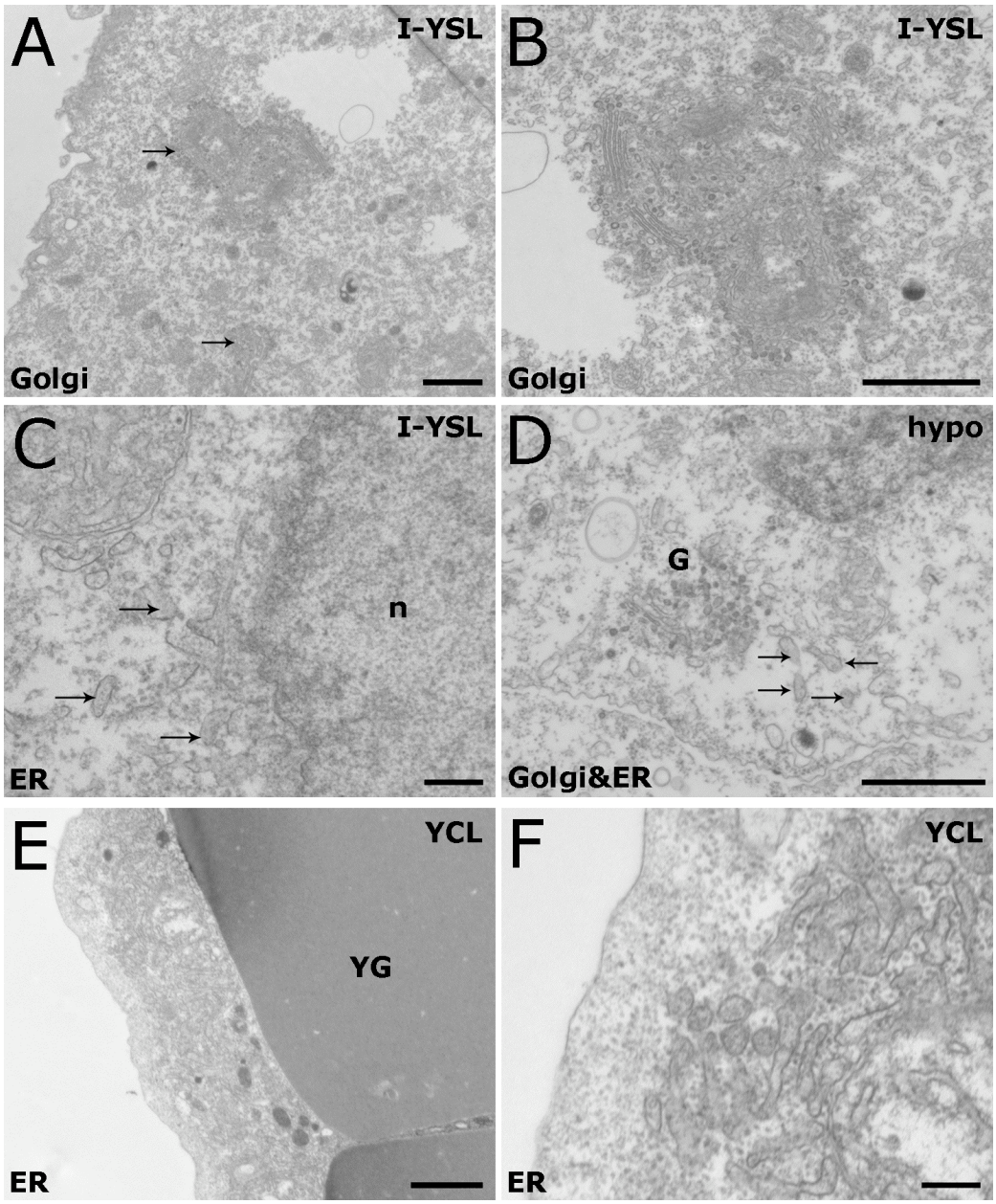

Figure 3.3 –Organization of the Golgi apparatus and ER in the YSL of shield stage embryos visualized by TEM. Longitudinal sections of shield stage wild-type embryos were taken. (A) Highly differentiated Golgi stacks in the I-YSL cytoplasm (arrows). (B) High magnification of image shown in (A) depicting highly differentiated Golgi apparatus. (C) Some ER stacks were visible in the I-YSL cytoplasm (arrows). (D) Golgi (G) and ER (arrows) distribution in a hypoblast cell, showing a less differentiated appearance than in the (A-C). (E) Many ER stacks are visible in the cytoplasm of the YCL. (F) High magnification of image shown in (E). Abbreviations: ER, endoplasmic reticulum; G, Golgi apparatus; hypo, hypoblast cell; I-YSL, internal yolk syncytial layer; n, nucleus; YCL, yolk cytoplasmic layer; YG, yolk granule. Scale bars: (A,B,D,E) 1 µm; (C,F) 200 nm.

For live imaging of organelles, we incubated embryos in various vital dyes: bodipy ceramide to label the Golgi apparatus (Lipsky and Pagano, 1985; Pagano et al., 1991) and "ER-tracker" to label the ER (Cole et al., 2000). We then analyzed their distribution by two-photon confocal time-lapse microscopy. In general, we obtained similar results as with TEM analysis. The Golgi apparati were very abundant within the YSL, whereas the ER stacks were less numerous, and neither organelle showed a preferential localization within the YSL (Figs. 3.4A,B). Unfortunately, it was not possible to follow the movements of these organelles during gastrulation movements, due to resolution limitations and strong photobleaching of the fluorophores.

We can conclude that the YSL presents a highly differentiated secretory apparatus during gastrulation stages, which is indicative of very active and specialized synthesis and transport of molecules within this tissue.

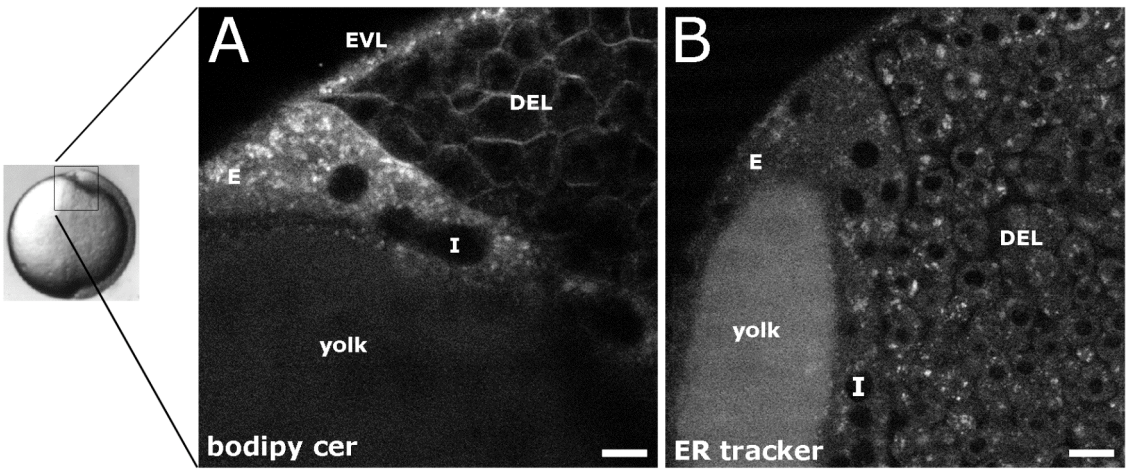

Figure 3.4 – Organization of the Golgi apparatus and ER in the YSL of live shield stage embryos. Live wild-type embryos were incubated in bodipy ceramide to label the Golgi (A) or in ER-tracker to label the ER (B) and then imaged by two-photon confocal microscopy. Both images represent single longitudinal focal planes from the margin of the embryo, as on the left. Animal pole is on the right. (A) The Golgi apparatus of the YSL and EVL are clearly visible, while in the blastoderm the dye is mainly localized at the plasma membrane (B) ER-tracker vital dye showing distribution of the ER in YSL and blastoderm. Abbreviations: blast, blastoderm; bodipy cer, bodipy ceramide; E, external yolk syncytial layer; EVL, enveloping layer; I, internal yolk syncytial layer. Scale bars, 10 µm.

3.2.2 YSL membrane organization

A very interesting feature that we found during the TEM analysis was the presence of numerous protrusions in the YSL membrane. Similar structures were also described in the YSL of *Fundulus heteroclitus* and proposed to be important for YSL epiboly

movements (Betchaku and Trinkaus, 1978; see also introduction). We observed that the shape of these protrusions varied depending on the region of the YSL, as well as on the embryonic stage. At the beginning of gastrulation, protrusions in the I-YSL were thin and long, similar to microvilli (Figs. 3.5A,C), while those in the E-YSL were wider and shorter, resembling membrane ruffles or folds (Figs. 3.5D-F). Both types were actin-based, since they were immunoreactive to actin-gold particles (Figs. 3.5C,F). In the I-YSL, the thin, microvilli-like protrusions were often closely associated with hypoblast cells. In addition, we observed a different type of protrusions of the I-YSL membrane, also typically in regions close to hypoblast cells and positive for actin, but smaller and more electron-dense (Fig 3.5B; data not shown). Their ultrastructure resembled that of anchoring-like cadherin junctions, however they were never observed in the contacting hypoblast cell membrane.

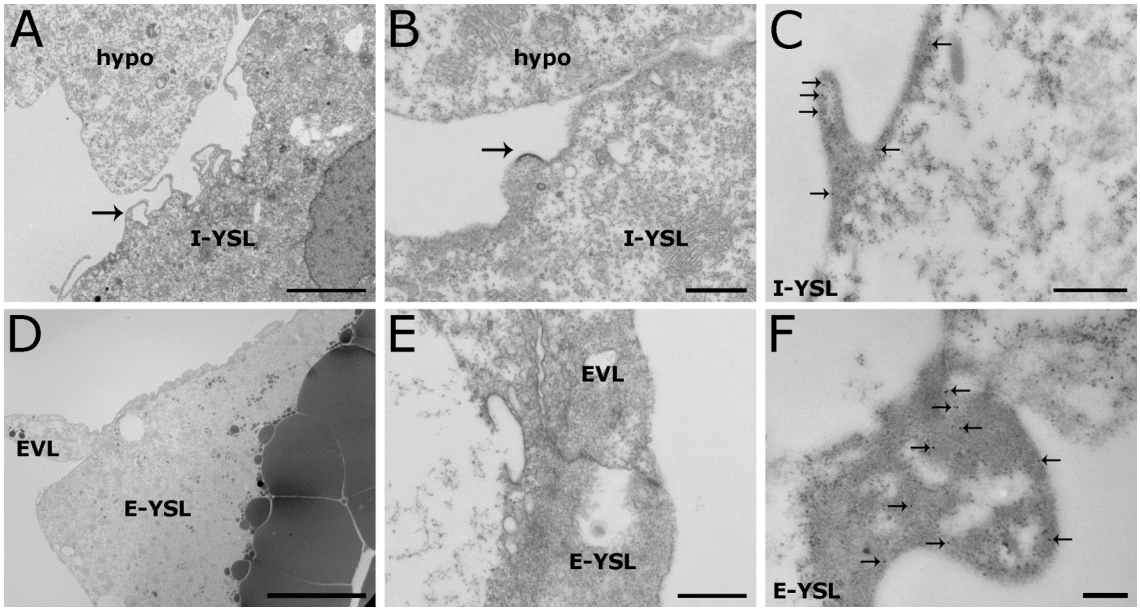

Figure 3.5 – Membrane specializations in the YSL of shield stage embryos visualized by TEM. Longitudinal sections of shield stage wild-type embryos were taken. Animal pole is on top in (A-C,E,F) and on the left in (D). (A) Microvilli-like membrane protrusions in the I-YSL, in a region of close contact with a hypoblast cell (hypo). (B) Electron-dense structure in the membrane of the I-YSL (arrow). Note that the apposing membrane of a hypoblast cell does not show a similar structure. (C) Antibody staining for actin, detected by 12nm-gold particles (arrows), in a microvilli-like protrusion of the I-YSL (D) Membrane folds in the E-YSL membrane. (E) Tight junction connecting an EVL cell to the E-YSL. (F) Antibody staining for actin, detected by 12nm-gold particles (arrows), in a membrane fold of the E-YSL. Abbreviations: EVL, enveloping layer cell; E-YSL, external yolk syncytial layer; hypo, hypoblast cell; I-YSL, internal yolk syncytial layer; n, nucleus; YG, yolk granule. Scale bars: (A) 5 µm; (B,C,E) 500 nm; (D) 10 µm; (F) 200 nm.

In the E-YSL, membrane ruffles were associated with the leading edge of the epibolizing E-YSL (Fig. 3.5D). Similar structures were also detected in the leading EVL cells. Tight junctions were present at the linkage between EVL cells and the E-YSL, already before the beginning of gastrulation and persisted throughout the process (Figs. 3.5E,3.6B). Consistent with this, it has been shown that the same region is positively immunolabeled for known components of vertebrate tight junctions, ZO-1 and Claudin-1 (Köppen et al, 2006). Besides the protrusions and folds present in the YSL membrane, we verified that the cortical actin belt occupying the entire surface of the YSL membrane (I- and E-YSL) was thicker than in embryonic cells (data not shown).

In *Fundulus* it has been shown that the length of I-YSL protrusions and the number of E-YSL membrane folds decrease during epiboly, an event that was proposed to contribute to the expansion of the YSL membrane in detriment of YCL membrane (Betchaku and Trinkaus, 1978). We observed the same tendency in our zebrafish samples (Figs. 3.6A,B). Additionally, at late epiboly stages (80% epiboly), we detected a second region of membrane folding at the contact site between the epibolizing DEL and E-YSL, which has not been described in *Fundulus* (Figs. 3.6C,D). The contact between I-YSL membrane and hypoblast cells was more extensive at 80% epiboly than at earlier stages, and was marked by structures resembling adherens junctions (Figs. 3.6E,F).

In conclusion, the YSL membrane is highly rich in protrusions and folds, which, as suggested for *Fundulus* (Betchaku and Trinkaus, 1978), could constitute a reserve of plasma membrane necessary for YSL epiboly movements. The large membrane folds observed in the E-YSL probably correspond to the actin positive accumulations seen before by light microscopy, proposed to be important for YSL contractility at its leading edge and functioning as the driving force for epiboly (Cheng et al., 2004; Köppen et al., 2006; Zalik et al., 1999). The second region of membrane folding observed at the leading edge of the DEL at mid-gastrulation stages (also detected by light microscopy; Cheng et al., 2004; Köppen et al., 2006) could provide an additional force necessary for vegetal migration. The whole cortex of the YSL is actin rich, indicating that the entire tissue has the potential to be contractile. The presence of numerous microvilli and junctions at the contact between I-YSL and hypoblast cells suggests that these two layers might interact during gastrulation movements.

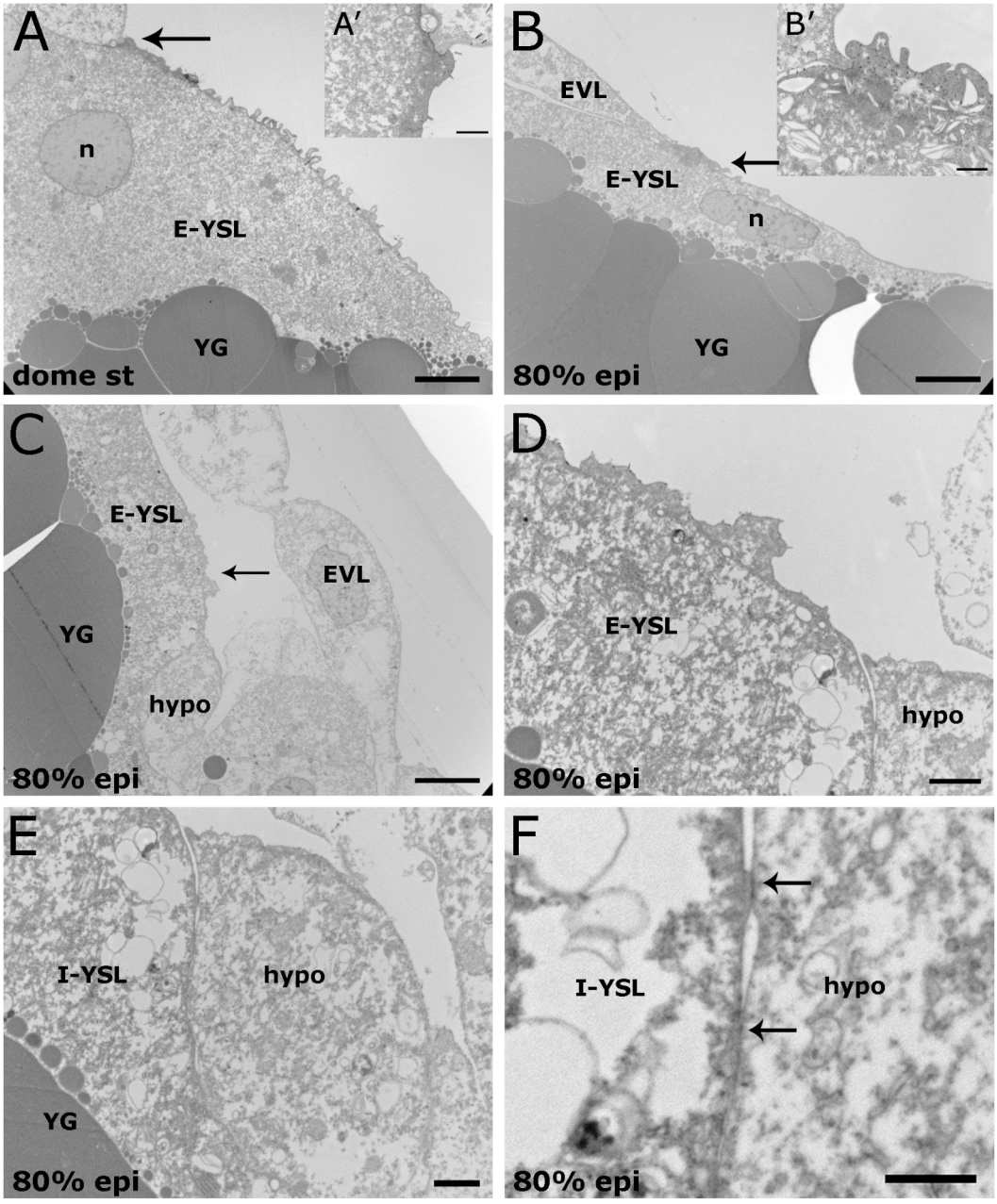

Figure 3.6 – Membrane specializations in the YSL at blastula and mid-gastrula stages visualized by TEM. Longitudinal sections of dome (A,A') and 80% epiboly (B-F) stage wild-type embryos were taken. Animal pole is on top in (A,C), on the left in (B,B'), and on the right in (D-F). (A) E-YSL of a dome stage embryo with many highly electron-dense membrane folds. Arrow indicates region magnified in (A'). (A') Tight junctions are already established between EVL and E-YSL at this early stage. (B) 80% epiboly embryo showing smaller membrane folds than in (A) in the E-YSL. Arrow indicates region magnified in (B'). (B') Tight junctions between EVL and E-YSL persist throughout gastrulation. (C) Embryo at 80% epiboly showing second zone of membrane folds (likely rich in actin) in the E-YSL at the contact site with the blastoderm (arrow). (D) Magnified region of image depicted in (C) showing highly electron-dense membrane folds in the E-YSL at the contact site with the blastoderm. (E) Same embryo as in (C,D), showing hypoblast cell in close contact with the I-YSL. (F) Magnified region of image depicted in (E), showing structures that resemble adherens junctions (arrows) between a hypoblast cell and the I-YSL membrane. Abbreviations: epi, epiboly; dome st, dome stage; EVL, enveloping layer cell; E-YSL, external yolk syncytial layer; hypo, hypoblast cell; I-YSL, internal yolk syncytial layer; n, nucleus; YG, yolk granule. Scale bars: (A-C) 10 µm; (D-F) 2 µm.

3.3 Organization of the microtubule cytoskeleton in the YSL

3.3.1 Analysis of microtubule cytoskeleton localization

Another component of the YSL that we focused on was the microtubule cytoskeleton, since it is likely to be of great importance for YSL movement (Solnica-Krezel and Driever, 1994; Strähle and Jesuthasan, 1993). For that, we performed tubulin immunostainings in whole embryos at different developmental stages and analyzed them by confocal microscopy. Additionally, we used a live microtubule-marker, Tau-GFP, and analyzed its dynamic distribution during gastrulation by two-photon confocal microscopy.

Our α-tubulin antibody stainings showed that the YSL is composed of an extremely dynamic and dense network of microtubules. During the first stages of YSL development (between high and sphere stage, 3.3-4 hpf), the nuclei underwent mitosis and not many interphase-like microtubules were visible (Fig. 3.7A). Only between dome and 30% epiboly stage, about 30 minutes later, divisions had stopped and interphase-like microtubules were visible originating from all nuclei toward the vegetal pole (Fig. 3.7B). These microtubules likely originate from two or more microtubule organizing centers (MTOCs) associated with each nucleus, as suggested by anti-γ-tubulin staining (Fig. 3.7B'). During gastrulation stages, a more extensive mesh of microtubule filaments became apparent within the I-YSL (Figs. 3.7C,D). In the E-YSL, microtubules were arranged in a more parallel way relative to the axis of the embryo.

Next, we analyzed the organization of YSL microtubules in the live embryo. For that, we used of a GFP-tagged microtubule binding protein – Tau – used previously to label microtubules in the live zebrafish embryo and *Drosophila*, without causing any secondary effects for development (Geldmacher-Voss et al., 2003; Kaltschmidt et al., 2000). Tau is a microtubule-associated protein (MAP), belonging to the MAP2/tau family, and mainly found in neurons (reviewed by Dehmelt and Halpain, 2005). We injected Tau-GFP-encoding mRNA into the YSL of wild-type embryos and examined them at different gastrulation stages via two-photon confocal time-lapse microscopy. Consistent with our tubulin antibody stainings, we observed that the YSL contains a dense microtubule network. The distribution of microtubules varied within the YSL. In the I-YSL, microtubule filaments were not arranged with a clear orientation and were

observed in all angles (Figs. 3.8A-F). In dorsal and paraxial regions of the I-YSL, the microtubule network was very dense and single microtubule filaments were hardly distinguishable (Figs. 3.8A-C; Movie 3). In ventral regions, less microtubules were apparent (Figs. 3.8D-F; Movie 4). In more vegetal regions, namely in the E-YSL and YCL, microtubules were organized in a more parallel way relative to the animal-vegetal axis of the embryo (Figs. 3.9A,B; Movie 5). Interestingly, the E-YSL nuclei seemed to move along these parallel arrays of microtubules.

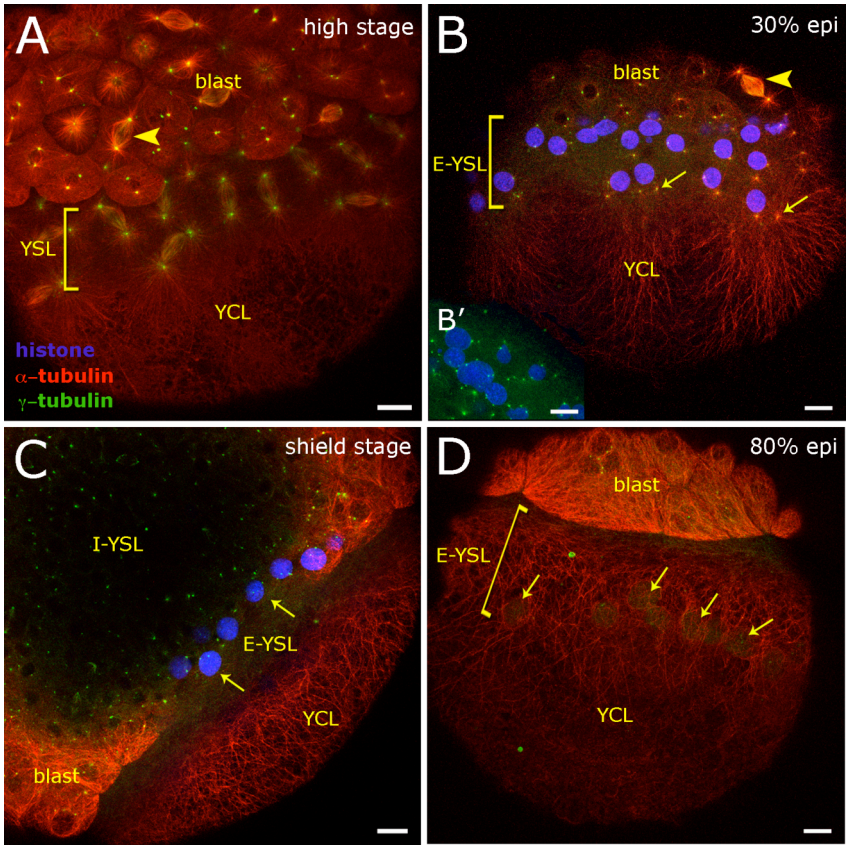

Figure 3.7 – Organization of YSL microtubules during blastula and gastrula stages by single-photon confocal microscopy performed in fixed embryos. Images are projections of 15-50 Z-slices. (A-D) α-tubulin antibody labels the microtubules (red); γ-tubulin antibody stains microtubule-organizing centers (MTOCs; green). (B-C) Histone protein localizes only to nuclei in the YSL (since it has been previously injected into the YSL; blue). (A) Embryo at high stage. YSL nuclei are dividing synchronously at this stage, as evidenced by metaphasic spindle microtubules. Some of the blastodermal cells are also dividing (arrowhead), although not synchronously. YCL has no detectable microtubules. (B) Embryo at 30% epiboly. YSL nuclei stopped dividing, in contrast to blastoderm cells (arrowhead). Microtubules irradiate from MTOCs associated with E-YSL nuclei (arrows) and reach the YCL. (B') Inset of (B) showing E-YSL nuclei associated with multiple MTOCs. (C) Shield stage embryo. YCL contains a more complex network of microtubules. Microtubules in I-YSL and E-YSL are not visible in this image since the thickness of the tissue does not allow efficient penetration of the antibody and accessibility by single confocal imaging. Some MTOCs are visible in the I-YSL and E-YSL and a few E-YSL nuclei are also visible (arrows). The blastoderm is out of focus in the centre of the image. (D) Embryo at 80% epiboly. YCL and E-YSL microtubules are visible. I-YSL is not accessible. MTOCs are not visible in the YSL at this stage. Faint staining shows E-YSL nuclei in between microtubule filaments (arrows). Abbreviations: blast, blastoderm; YCL, yolk cytoplasmic layer; E-YSL, external yolk syncytial layer; I-YSL, internal yolk syncytial layer; epi, epiboly. Scale bars, 10 µm.

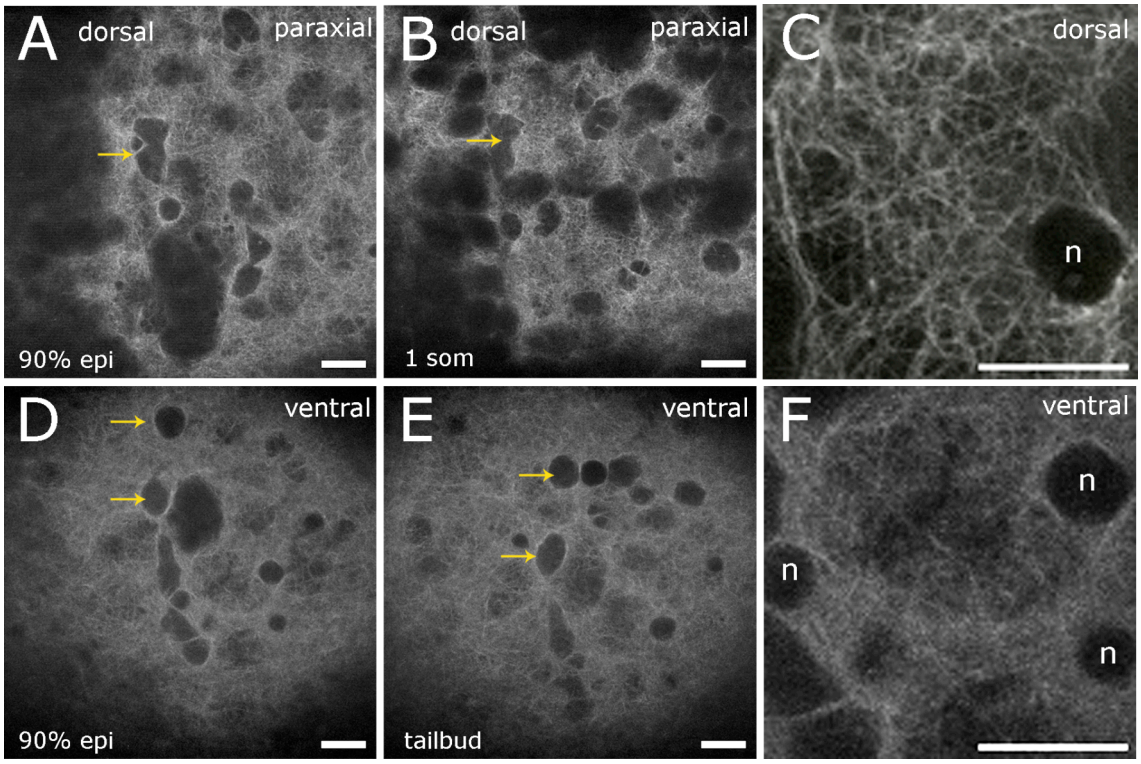

Figure 3.8 – Organization of I-YSL microtubules during gastrulation in the live embryo. Embryos were injected with Tau-GFP mRNA in the YSL and imaged by two-photon confocal microscopy. Animal pole is always on top. All images represent single Z-slices. (A-C) I-YSL microtubules in dorsal and paraxial regions. The same YSL nucleus is indicated by the arrow in both images. (A) Embryo at 90% epiboly (B) Embryo at 1 somite stage. (C) Magnified image of the I-YSL dorsal region showing detail of microtubule filaments around an I-YSL nucleus (n). (D-F) I-YSL microtubules in ventral region. The same 2 I-YSL nuclei are indicated by the arrows in both images. (D) Embryo at 90% epiboly. (E) Embryo at tailbud stage. (F) Magnified image of the I-YSL ventral region showing detail of microtubule filaments surrounding I-YSL nuclei(n). Note the difference in intensity of staining and density of filaments between (C) and (F). Abbreviations: epi, epiboly; n, YSL nucleus; som, somite. Scale bars, 10 µm.

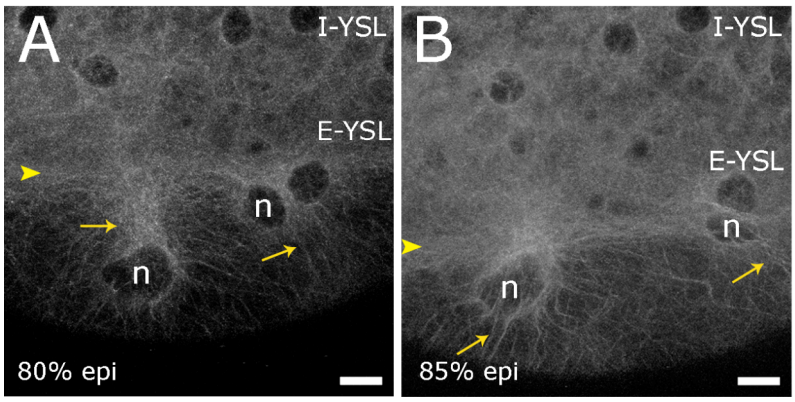

Figure 3.9 – Organization of E-YSL microtubules during gastrulation in the live embryo. Embryos were injected with Tau-GFP mRNA in the YSL and imaged by two-photon confocal microscopy. Animal pole is on top. Images are projections of 20 Z-slices. (A) Embryo at 80% epiboly. (B) Embryo at 85% epiboly. At the leading edge of epiboly (arrowhead) microtubules are arranged perpendicularly to the animal-vegetal axis of the embryo. In more vegetal regions of the E-YSL (arrows), microtubules are arranged parallel to the axis. Abbreviations: I-YSL, internal yolk syncytial layer; E-YSL, external yolk syncytial layer; epi, epiboly; n, YSL nucleus. Scale bars, 10 µm.

3.3.2 Orientation of microtubule growth and its relation to convergence movement

In order to better understand the dynamics of the microtubules in the YSL, we assayed for the direction and rate of growth of microtubule filaments in different regions of the gastrulating embryo. For this, we injected a GFP-tagged version of EB3 (End-binding protein 3), a plus end-tracking protein (+TIP; Nakagawa et al., 2000), in the YSL. +TIPs specifically associate with distal ends of microtubules and regulate microtubule dynamics and intracellular transport on microtubules (for a review see Schuyler and Pellman, 2001). EB3-GFP and other GFP-tagged +TIPs have been used in earlier studies to analyze microtubule polymerization dynamics in different cell types, since the dynamic behavior of microtubules is not altered significantly by low expression levels of these proteins (Stepanova et al., 2003).

In cultured cells, EB3-GFP fluorescent dots typically move as "comet-like dashes" toward the cell cortex (Stepanova et al., 2003). We observed a similar pattern in our zebrafish blastodermal cells (Fig. 3.10A; Movie 6). In contrast, in the YSL the distribution of EB3-GFP dots appeared more dispersed and was not restricted to a specific region of the cell (Figs. 3.10A-C; Movies 6-8). The movement of EB3 dots showed no clear bias to one direction, as described for other types of cells, including zebrafish blastoderm cells. Our preliminary observations indicate that E-YSL microtubule plus-ends grew preferentially to the vegetal pole, while in the I-YSL no directionality was detected (data not shown), but a quantitative analysis is necessary to confirm this.

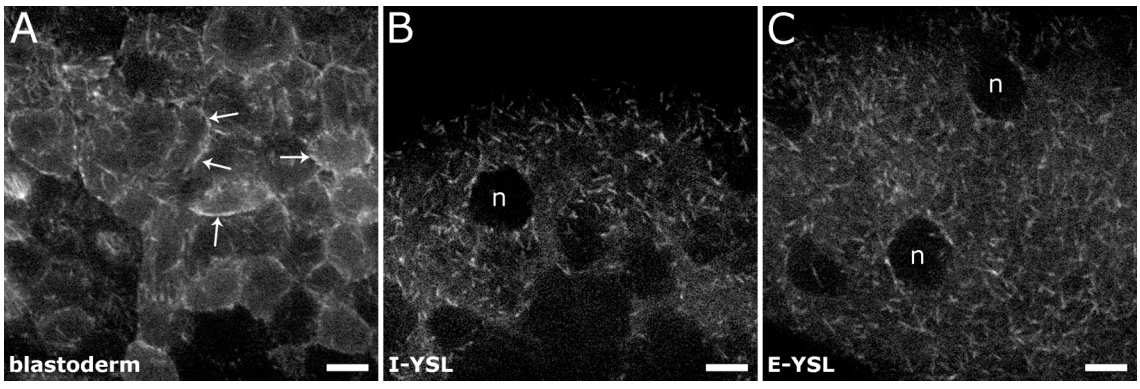

Figure 3.10 – Dynamics of microtubule plus-ends in the blastoderm and YSL during gastrulation. Embryos were injected with EB3-GFP mRNA in the YSL and imaged by two-photon confocal microscopy. Animal pole is on top. All images represent single Z-slices. (A) Blastodermal cells. Most of the EB3-GFP positive dots are concentrated at cortical region of the cell (arrows). (B-C) In the I-YSL (B) and E-YSL (C) EB3-GFP positive dots are dispersed through the whole cytoplasm. n, YSL nucleus. Scale bars, 20 µm.

In summary, the YSL microtubule network is remarkably dynamic and elaborate, suggesting that microtubules could be involved in the movement of YSL nuclei during gastrulation.

3.4 Evidence of cytoplasmic streaming within the I-YSL

During our analysis of YSL nuclei movement, we detected that not only the nuclei, but also the cytoplasm seemed to undergo a global convergence and extension movement. Cytoplasmic streaming has been implicated as one of the mechanisms regulating the movement of particles, including nuclei and vesicles, in a variety of biological systems such as plants, *Drosophila* and *Caenorhabditis elegans* (Foe and Alberts, 1983; Shimmen and Yokota, 2004; Theurkauf, 1994; Wolke et al., 2007). To clarify whether the same process occurs in the YSL, we investigated the movement of polystyrene beads inserted into the YSL of gastrulating embryos. This type of beads has been widely used to study the dynamics of cytoplasmic and fluid flow in *C. elegans* and zebrafish embryos, as well as in mammalian blood flow studies, since they do not bind unspecifically to molecules or organelles in the cell (Essner et al., 2005; Fukada et al., 1989; Khoobehi et al., 1997; Lynn and Ahmed, 2006; Wolke et al., 2007).

Beads of different diameters were placed in the YSL at sphere stage, when YSL nuclei movement starts. Two-photon confocal time-lapse imaging revealed that beads converged to the dorsal side and moved to animal pole, similar to the I-YSL nuclei (Figs. 3.11A-D; Movies 9,10). However, we failed to detect beads undergoing epiboly movements within the E-YSL as observed for E-YSL nuclei.

These findings strongly indicate that there is a flow of cytoplasm within the I-YSL during gastrulation, which is mainly directed dorsal side of the embryo. It is thus possible that the convergence movement performed by the I-YSL nuclei is a result of this cytoplasmic streaming, and that the transport/movement of other particles within the cytoplasm may occur via the same mechanism.

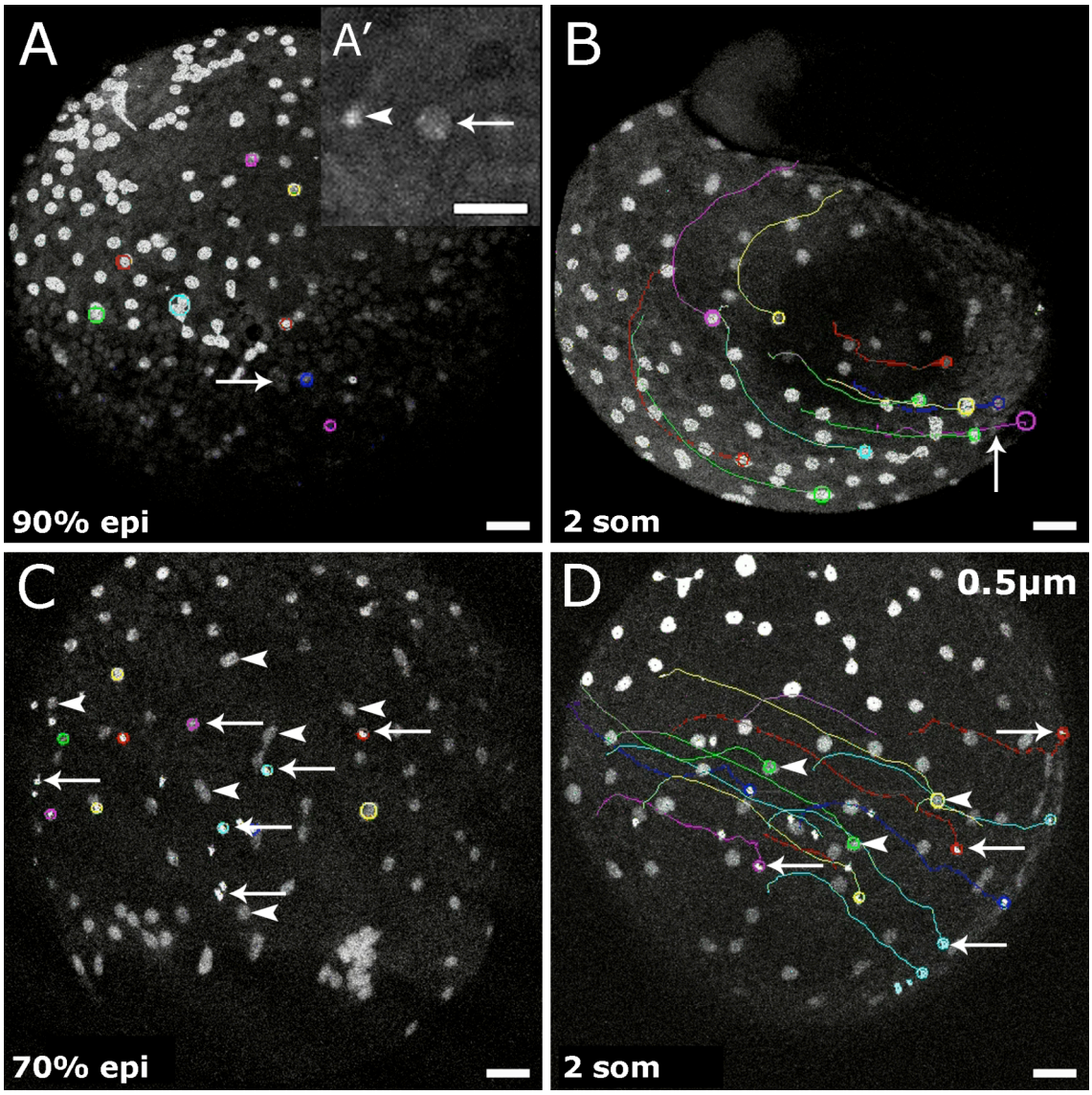

Figure 3.11 – Movement of beads in the YSL during gastrulation. Embryos were imaged by two-photon confocal microscopy during gastrulation. Images in (A-D) are projections of 35 Z-slices, image (A') is a projection of 7 Z-slices. Some of the trajectories of nuclei and beads obtained with the Motion Tracking Software are shown. The circles indicate the end-point of each track. Animal pole is on top; dorsal is on the right. (A-B) Embryo injected with histone in the YSL and subsequently implanted with a single 20-µm diameter polystyrene bead in the YSL at sphere stage (n=3). (A) Embryo at 90% epiboly. The bead (arrow) is on the lateral-ventral side of the I-YSL. (A') High magnification of the bead (arrow) shown in (A) close to a YSL nucleus (arrowhead). (B) Embryo at 2-somite stage. The same bead (arrow) is now closer to the dorsal side of the embryo similar to the I-YSL nuclei in the same region. (C-D) Embryo injected with a mixture of histone and 0.5 µm-diameter fluorescent beads in the YSL at sphere stage (n=3). The beads appear larger than 0.5 µm because they are overexposed. Some of the beads and nuclei are indicated by arrows and arrowheads respectively. (C) Embryo at 70% epiboly. The beads (arrows) are on the lateral side of the embryo. (D) Embryo at 2-somite stage. The beads (arrows) have moved to more paraxial/dorsal regions of the embryo similar to I-YSL nuclei (arrowheads). Abbreviations: epi, epiboly; som, somite. Scale bars: (A-D), 50 µm; (A'), 40 µm.

3.5 Regulation of blastodermal cell movement by YSL nuclei movement

One of the main goals of this thesis was to understand how YSL nuclei convergence and extension movement is related to hypoblast movement. Do both tissues interact to achieve these highly coordinated movements? If so, does the YSL regulate hypoblast movement or is it the hypoblast that is necessary for the movement of YSL nuclei? An alternative hypothesis is conceivable: YSL and hypoblast movements can be completely independent of each other and controlled by a common, unknown mechanism. In order to answer these questions, we first decided to investigate how hypoblast movement is affected when we interfere with YSL nuclei movement, and second, how YSL nuclei behave in the absence of a proper hypoblast cell layer.

In order to understand whether YSL nuclei are necessary for hypoblast movement, we decided to interfere with YSL nuclei movement. As discussed in the introduction, it has been proposed that microtubules serve an important role in YSL movement (Solnica-Krezel and Driever, 1994; Strähle and Jesuthasan, 1993). Still, it remained unclear from these studies how precisely E-YSL nuclei movement is affected and whether I-YSL nuclei movement is impaired at all, when the microtubule cytoskeleton is disrupted. Furthermore, these studies involved experimental approaches that interfered with the microtubules of the whole embryo and not specifically the YSL, and from blastula stages onwards.

Therefore, we initially tested several methods to specifically interfere with the YSL microtubules without directly affecting the blastoderm. We injected different microtubule-destabilizing or stabilizing drugs (e.g. colchicine, paclitaxel) or proteins (e.g. Katanin, XKCM1) into the YSL. Unfortunately, these approaches failed to interfere with the YSL cytoskeleton (data not shown). We assume that, as drugs are very small molecules, they diffuse through the whole embryo and yolk and thus become too diluted to exert visible effects. In the case of protein/mRNA over-expression, it is conceivable that the YSL has mechanisms that compensate for their deleterious activity. For these reasons, we decided to incubate embryos in different microtubule-interfering drugs. Nocodazole and colchicine are microtubule-depolymerizing drugs used extensively in cell culture and in vitro studies to disrupt the microtubule cytoskeleton (Downing, 2000; Jordan and Wilson, 1998; Luduena and Roach, 1991). When we tried

to incubate zebrafish embryos in medium containing these drugs, we observed effects on the YSL as well as on blastodermal cells, as accessed by tubulin antibody staining (data not shown). Therefore, we discarded these results as too unspecific. More promising effects resulted from the drug paclitaxel (also known as taxol). This molecule, originally isolated from the yew tree, belongs to the Taxane family and serves as a useful anti-cancer drug. Taxanes bind microtubules with very high affinity, leading to an increase in microtubule polymerization and stability (Jordan and Wilson, 2004; Schiff et al., 1979). When we incubated gastrulating embryos in paclitaxel, they displayed striking abnormalities in YSL microtubule organization (Figs. 3.12A,B). In particular, microtubules of the E-YSL and YCL were dramatically affected: we detected bundle-like accumulations of microtubules at the leading edge of the epibolizing E-YSL and a strong decrease in tubulin staining in the YCL. To our surprise, blastodermal microtubules were largely normal (Figs. 3.12A',B'), suggesting that this treatment primarily affects the E-YSL and YCL. Microtubules in the I-YSL could not be directly analyzed due to the thickness of the tissue. When we analyzed the actin cytoskeleton, no effects of paclitaxel treatment were detected on the E-YSL/EVL actin ring (Figs. 3.12C,D).

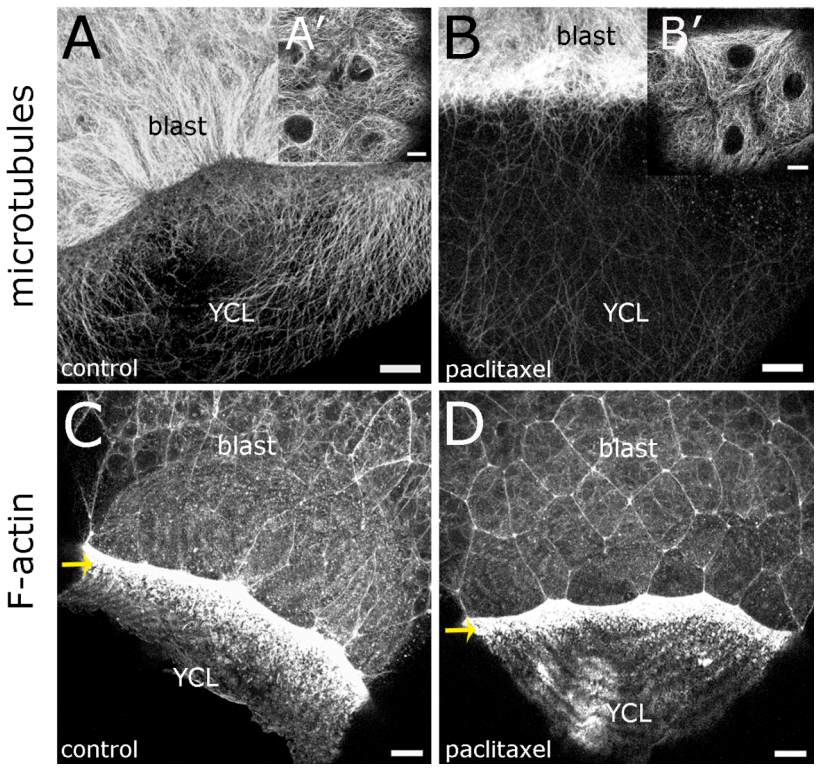

Figure 3.12 – Treatment of gastrulating embryos with paclitaxel interferes with E-YSL and YCL microtubules but not with actin. Images are projections of 25-55 Z-slices. Animal pole is on top. (A,C) Control embryos were incubated in medium containing DMSO at 60% epiboly and fixed at 85% epiboly. (B,D) Embryos were incubated in medium containing paclitaxel at 60% epiboly and fixed when control embryos were at 85% epiboly. (A-B) Embryos stained with α-tubulin antibody. (A) Control embryo with microtubules in the E-YSL and YCL regions. (A') Detail from blastoderm of embryo in

(A) showing normal microtubule network in blastodermal cells. (B) Paclitaxel-treated embryo showing reduced microtubule network in the YCL and accumulation of microtubules in E-YSL. (B') Detail from blastoderm of embryo in (B) showing normal microtubule network in blastodermal cells. (C-D) Embryos stained for F-actin. (C) Control embryo showing strong actin ring in the E-YSL at the contact sire with EVL (arrow). (D) Paclitaxel-treated embryo showing similar actin ring in the E-YSL (arrow) as in control embryo. EVL cells are less elongated than in controls due to delayed epiboly. Abbreviations: blast, blastoderm; epi, epiboly; E-YSL, external yolk syncytial layer; YCL, yolk cytoplasmic layer. Scale bars, 10 μm.

We then decided to evaluate how interfering with the E-YSL and YCL microtubules influences YSL nuclei movement. For that, we imaged histone-labeled YSL nuclei by two-photon confocal time-lapse microscopy, and observed that their movement was severely reduced in paclitaxel-treated embryos (Figs. 3.13A,B,D,E,G,H; Movies 11-13). The nuclei did not move to the vegetal pole of the embryo, where the microtubules seemed to be mostly affected, resulting in an accumulation of nuclei in the animal pole of the embryo. Some of these YSL nuclei still converged to the dorsal side and moved further animally but in a more random way. Notably, the E-YSL cytoplasm of paclitaxel-treated embryos was advancing further vegetally than the nuclei (arrow in Fig. 3.13G, and Movie 13), while in the controls, several E-YSL nuclei moved ahead of the bulk of E-YSL cytoplasm (Movie 11).

In addition, paclitaxel treatment affected DEL and EVL epiboly. Mild phenotypes were observed when incubating the embryos from 75% epiboly until tailbud stage, with epiboly of E-YSL, EVL and DEL slowing down but reaching completion (Fig. 3.13F). On the other hand, when incubating the embryos from the onset of gastrulation, epiboly was severely impaired and typically halted after covering about 80% of the yolk, for all three layers (Figs. 3.13I). The distance between the leading edge of the epibolizing E-YSL/EVL and the leading edge of the DEL was shorter than in control embryos (data not shown). Interestingly, convergence and extension movement of the DEL was only mildly affected by this treatment (Figs. 3.13C,F,I; data not shown), indicating that proper YSL nuclei movement is not essential for these movements to occur. Embryos that did complete epiboly continued developing normally for the next days, while embryos that failed to complete epiboly showed tail and yolk extension defects (data not shown).

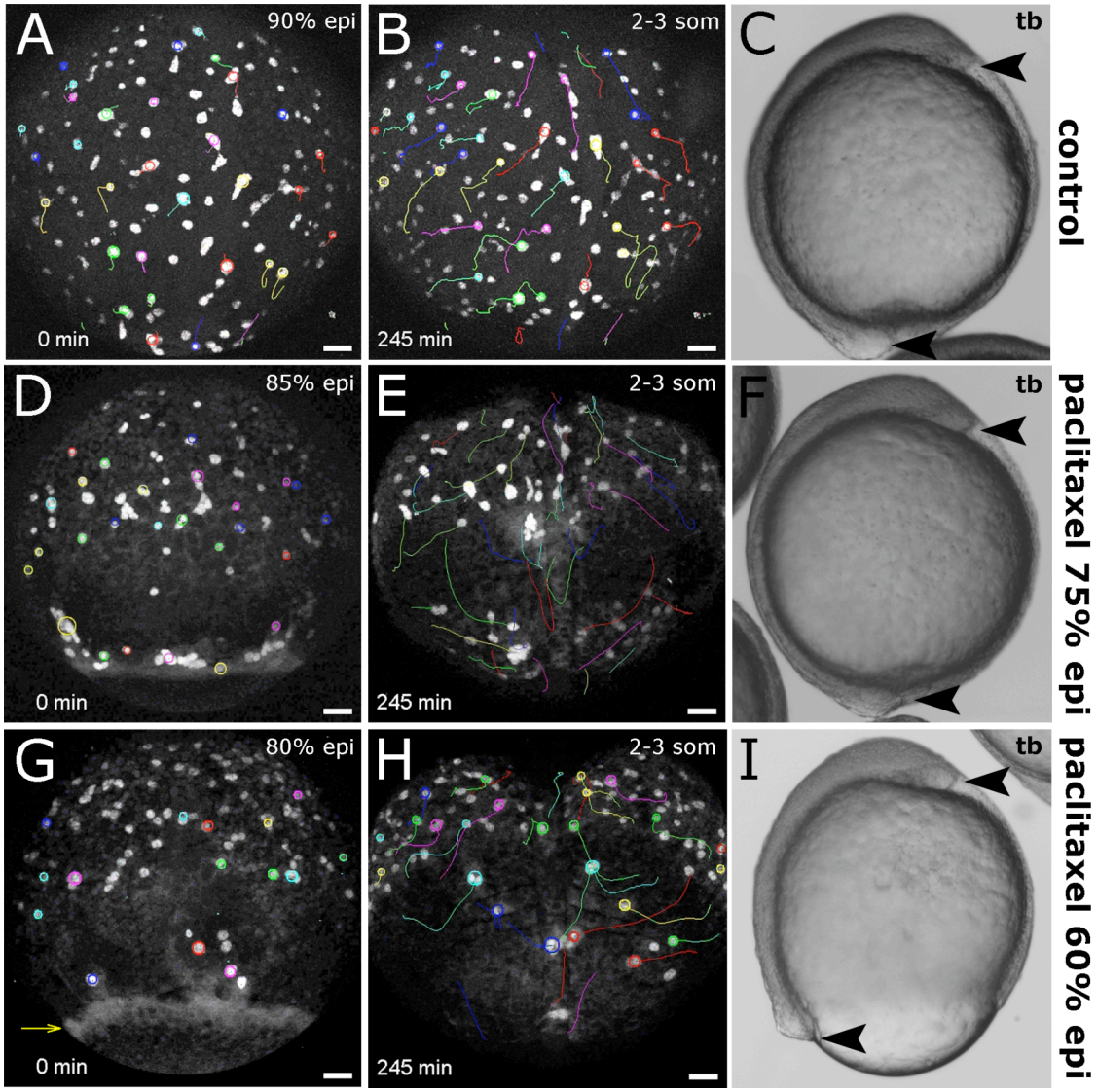

Figure 3.13 – Treatment of gastrulating embryos with paclitaxel interferes with YSL nuclei movement. (A,B,D,E,G,H) Still images of histone-injected embryos taken from two-photon confocal time-lapses. Images are projections of 35 Z-slices. Dorsal views are shown; animal pole is on top. Some of the nuclear trajectories obtained with the Motion Tracking Software are shown. The circles indicate the end-point of each track. (A) Control embryo at 90% epiboly. (B) Same embryo as in (A) at 2-3 somite stage. (D) 75%-epiboly-paclitaxel-treated embryo at 85% epiboly. A delay in epiboly is already visible (arrow), and the distribution of YSL nuclei is abnormal. (E) Same embryo as in (D) at 2-3 somite stage. Epiboly is completed, but YSL nuclei show impaired movement trajectories and irregular distribution, although they partially converge and extend. (G) 60%-epiboly-paclitaxel-treated embryo at 80% epiboly. A delay in epiboly is visible (arrow), and YSL nuclei shown an irregular distribution. E-YSL nuclei are behind the leading edge of E-YSL/EVL epiboly (arrow). (H) Same embryo as in (G) at 2-3 somite stage. E-YSL nuclei do not undergo epiboly, and most of the I-YSL nuclei are restricted to the animal-most region of the embryo. Some YSL nuclei still converge to the dorsal side although not as efficiently as in control embryos. (C,F,I) Bright-field images from embryos at tailbud stage. Dorsal is on the left; animal pole in on top. (C) Control embryos show complete epiboly and normal developed axis (delimited by arrowheads). (F) 75%-epiboly-paclitaxel-treated embryo showing complete epiboly at tailbud stage, and a normally extended axis (arrowheads). (I) 60%-epiboly-paclitaxel-treated embryo showing blockage of epiboly and shorter body axis (arrowheads). epi, epiboly; som, somite; tb, tailbud. Scale bars, 50 µm.

Together these data suggest that E-YSL and YCL microtubules are necessary for the epibolic movement of E-YSL nuclei, similar to what has been proposed before (Solnica-Krezel and Driever, 1994; Strähle and Jesuthasan, 1993). The vegetal progression of the YSL itself appears to be less dependent on the microtubules than the movement of the YSL nuclei. Besides epiboly, other gastrulation movements seem to be partly independent of YSL microtubules and YSL nuclei movement, although this can be due to a remaining fraction of functional microtubules in the I-YSL after drug treatment.

3.6 Regulation of YSL nuclei movement by the overlying hypoblast

Our experiments so far lead us to postulate that proper I-YSL nuclei convergence and extension movement is not crucial for the movement of the overlying hypoblast. Hence, we next tested whether, conversely, hypoblast morphogenesis is necessary for I-YSL nuclei movement. For that, we assessed how I-YSL nuclei behave in loss-of-function conditions affecting different aspects of hypoblast formation and migration. First, we looked at mutant embryos that do not form a hypoblast layer; and second, we looked at mutants where cell movements are impaired but patterning occurs normally.

3.6.1 I-YSL nuclei convergence movement is reduced in the absence of hypoblast cells in maternal zygotic *oep* mutant embryos

To analyze the movement of YSL nuclei in the absence of hypoblast cells, we used embryos that lack both maternal and zygotic activity of One-eyed pinhead protein (MZ*oep* mutants) and do not form a hypoblast cell layer (Gritsman et al., 1999). Oep is a conserved transmembrane EGF-CFC protein that functions as an extracellular co-factor for Nodal/TGFβ signaling and is essential during zebrafish gastrulation (Gritsman et al., 1999; Zhang et al., 1998). It has been shown that MZ*oep* mutants have severe defects in germ layer formation, anterior-posterior axis positioning and organizer development (Gritsman et al., 1999). Involution of hypoblast cells at the germ ring margin does not occur, and therefore no mesendoderm-derived tissues form. The epiblast cell layer undergoes normal epiboly and convergence movement, but the anterior-posterior axis is not well established and remains short.

In order to analyze I-YSL nuclei movement in MZ*oep* mutant embryos, we again performed Nomarski time-lapse imaging during gastrulation (Fig. 3.14A; Movie 14). Tracking of the I-YSL nuclei in these movies revealed abnormal convergence movement. I-YSL nuclei underwent largely normal extension movements towards the animal pole, but strikingly they frequently moved to lateral/ventral positions, rather than converging to the dorsal side (Fig. 3.14B; Movie 14). As expected, no involution occurred to generate a hypoblast layer, while epiblast cells underwent epiboly and convergence movements (data not shown).

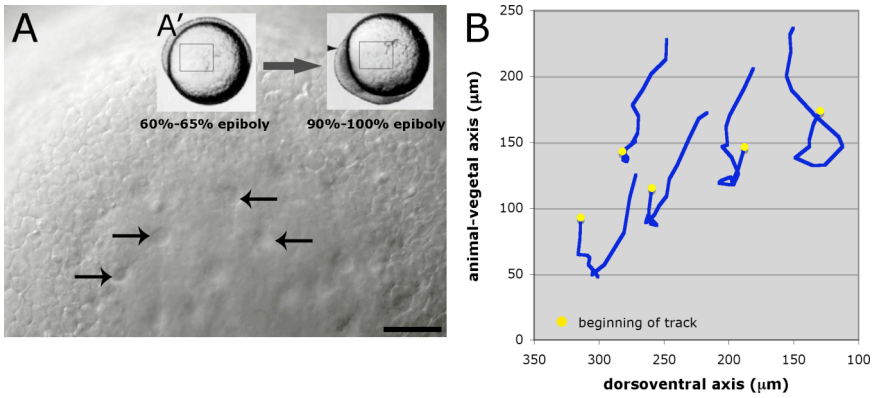

Figure 3.14 – I-YSL nuclei movement during gastrulation in MZ*oep* embryos imaged by Nomarski optics. Dorsal side is on the left; animal pole is on top. (A) Nomarski image of the paraxial region of an MZ*oep* embryo as indicated in square box in (A'). (A') Representation of the region and time period imaged during the time-lapse. MZ*oep* embryos were imaged from 60%-65% until 90% epiboly. MZ*oep* embryos do not form a dorsal embryonic shield but the dorsal side is still slightly thickened when compared to the rest of the margin. The arrowhead indicates the position of the future head. (B) Graphical representation of typical examples of the trajectories of I-YSL nuclei. I-YSL nuclei move toward the animal pole but do not converge to the dorsal side. Approximately ten tracks from each embryo (n=6) were obtained manually by recording their coordinates at every 10 minutes/5 frames. Yellow circles represent beginning of each track. Scale bar, 50 µm.

To more precisely investigate these phenotypes, we performed two-photon confocal time-lapse microscopy of histone-labeled YSL nuclei in MZ*oep* embryos. We observed that, similar to wild-type embryos, E-YSL nuclei underwent epiboly. In contrast, I-YSL nuclei located in dorsal and lateral regions had the tendency to move away from the dorsal side and towards the lateral side of the embryo, even though they were able to move in direction to the animal pole (Figs. 3.15A,B; Movie 15).

To quantify the tracks obtained, we used the Motion Tracking software (see methods). To focus on convergence movements, we only analyzed tracks of nuclei initially located in the animal half of the embryo (I-YSL), excluding the nuclei initially located in the dorsal side of the embryo, given that they only display extension movements. When calculating the total speed of the selected I-YSL nuclei, we received

similar values for both wild type and MZ*oep* (Fig. 3.16). This suggests that the overall speed of the nuclei is not dramatically influenced by hypoblast cells. We then calculated the net speed of the nuclei separately for the *x* and *y* axes ("net dorsal speed" and "net animal-vegetal speed" respectively; see methods for details). This provides a more accurate way to distinguish the dorsalward movement and the degree of animal-vegetal extension. As expected, we observed that in MZ*oep* embryos, I-YSL nuclei showed a significantly lower net dorsal speed when compared to wild type (Fig. 3.16). The negative sign of the MZ*oep* values reflects the net movement of the I-YSL nuclei away from the dorsal side. On the other hand, the net animal-vegetal speed was higher in MZ*oep* than in wild-type (Fig. 3.16).

Altogether, these results strongly suggest that blastodermal cells influence I-YSL nuclei convergence movement.

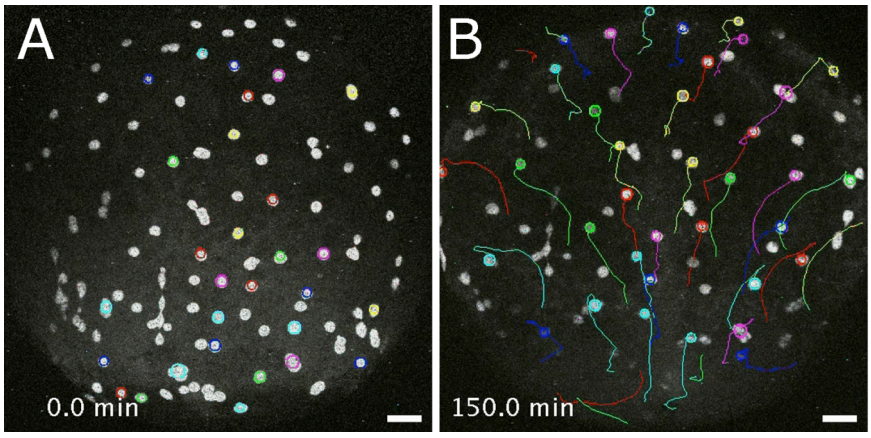

Figure 3.15 – Two-photon confocal time-lapse imaging of YSL nuclei during gastrulation in MZ*oep* embryos. Still images of a histone-injected embryo from 70% epiboly until 2-somite stage. All images are projections of 35 Z-slices. Some of the nuclear trajectories obtained with the Motion Tracking Software are shown. The circles indicate the end-point of each track. Embryos are shown on a dorsal view; animal pole is on top. (A) Embryo at 75% epiboly. (B) Embryo at 2-somite stage. I-YSL nuclei move to the animal pole but do not converge to the dorsal side. E-YSL nuclei move to the vegetal pole. n=5. Scale bars, 50 µm.

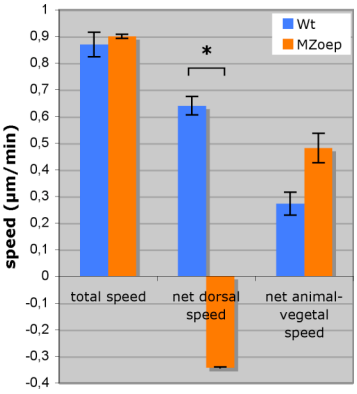

Figure 3.16 – Comparison of the speed of I-YSL nuclei movements between wild-type and MZ*oep* embryos during gastrulation. The total speed of I-YSL nuclei is similar wild-type and MZ*oep* embryos (p=0.6588). Net dorsal speed and net animal-vegetal speed were calculated by dividing the net displacement in the *x* or *y* axis, respectively, by the total time. The net dorsal speed of I-YSL nuclei is significantly lower in MZ*oep* embryos compared to wild-type (p=0.0031). The negative sign of the MZ*oep* value indicates that the net movement of the nuclei is away from dorsal in contrast to wild-type. Net animal-vegetal speed of I-YSL nuclei is not significantly higher in MZ*oep* compared to wild-type (p=0.0792). The trajectories of 30 to 47 paraxial and lateral I-YSL nuclei from each embryo (wild-type, n=4; MZ*oep*, n=2) were considered for quantification. All the trajectories considered were 150 minutes long (75% epiboly to 1 somite stage). Unpaired Student's *t* tests were performed to test the differences between the mean values of wild-type *versus* MZ*oep*. Error bars represent the standard error of the mean.

3.6.2 Oep expression within the YSL is not sufficient for YSL nuclei movement in MZ*oep* mutant embryos

Our observations indicate that the convergence movement of I-YSL nuclei could be dependent on the blastoderm. Alternatively, it is possible that the observed defect in I-YSL nuclei movement results from the absence of Oep protein in the YSL of MZ*oep* mutants. To distinguish between these two possibilities, we checked whether *oep* is expressed in the YSL of wild-type embryos during gastrulation. We performed in situ hybridizations for *oep* mRNA in shield stage wild-type embryos, and then sectioned them to better visualize the YSL. No (or very weak) expression was detected in the YSL, but was only found in the blastoderm (Figs. 3.17A-C), consistent to what has been observed in previous studies (Zhang et al., 1998).

To discard the possibility that weak Oep expression has a function in the YSL, we ectopically expressed Oep in the YSL of MZ*oep* embryos. We did this by injecting full-length *oep* mRNA into the YSL, which has been described as a functional mRNA (Gritsman et al., 1999; Zhang et al., 1998). When we analyzed the movements of the I-YSL nuclei in the injected embryos by Nomarski imaging, we verified that they were identical to MZ*oep* embryos, showing no convergence movements to the dorsal side, but still migrating toward the animal pole (Fig. 3.18; Movie 15).

These observations provide evidence that the function of Oep protein in the YSL is not sufficient for the convergence movement of I-YSL nuclei in MZ*oep* mutants, thus strengthening our hypothesis that convergence of I-YSL nuclei is dependent on the blastoderm.

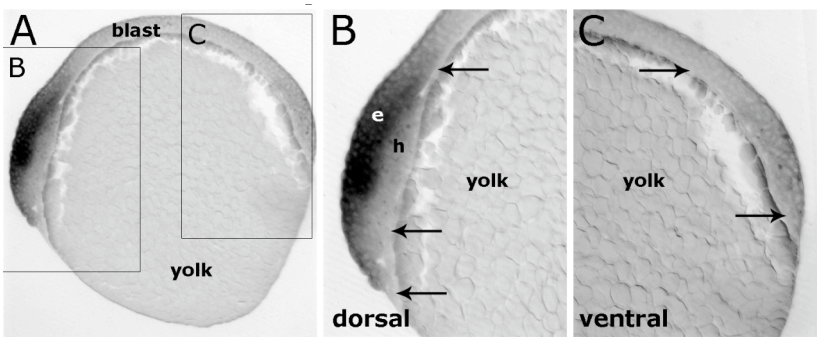

Figure 3.17 – Expression of *oep* mRNA in shield stage wild-type embryos. (A) In situ hybridizations were performed on whole-mount shield stage embryos, which where then sectioned in longitudinal orientation. (B,C) Magnified dorsal (B) and ventral (C) regions of embryo shown in (A). (B) *oep* is expressed in the blastoderm but not in the dorsal YSL. (C) *oep* is not expressed in the ventral YSL.

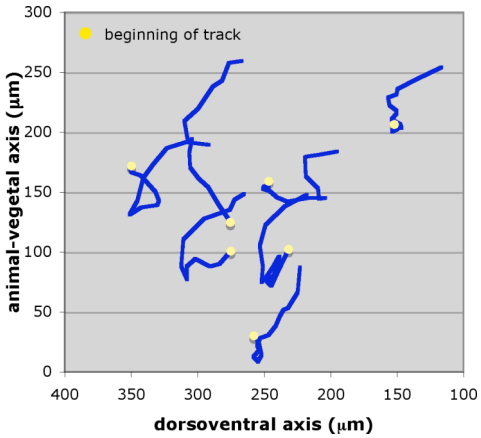

Figure 3.18 – I-YSL nuclei movement in MZ*oep* mutant embryos ectopically expressing *oep* in the YSL. I-YSL nuclei move toward the animal pole but do not converge to the dorsal side similar to what is observed in uninjected MZ*oep* embryos (compare with Fig. 3.14B). 100 pg of *oep* mRNA were injected in the YSL at sphere stage and embryos imaged using Nomarski optics from 60%-65% until 90% epiboly. Dorsal side is on the left; animal pole is on top. Paraxial region was imaged as shown in Fig. 3.13A. Typical examples of the trajectories of I-YSL nuclei are shown. Approximately ten tracks from each embryo (n=3) were obtained manually by recording their coordinates at every 10 minutes/5 frames. Yellow circles represent beginning of each track.

3.6.3 Transplanted hypoblast-like cells partially rescue the convergence of I-YSL nuclei in MZ*oep* embryos

To investigate whether absence of the hypoblast cell layer is the cause of the nuclear movement defect observed in the I-YSL of MZ*oep* embryos, we addressed whether hypoblast cells can regulate I-YSL nuclei movement. We developed an assay whereby we transplanted "hypoblast-like" cells into the margin of MZ*oep* embryos (Fig. 3.19A) and examined if they induced I-YSL nuclei to move to the dorsal side as in a wild-type embryo. To obtain hypoblast-like cells for transplantation, we over-expressed *cyclops/nodal-related2* (*cyc/ndr2*) mRNA in wild-type donor embryos, a Nodal/TGFβ signal responsible for mesendoderm induction (Feldman et al., 1998; Rebagliati et al., 1998). Cyc/Ndr2 over-expression confers mesendodermal identity to the majority of the cells of the embryo, as confirmed by expression of several mesendodermal markers (Alexander and Stainier, 1999; Chen and Schier, 2001; Erter et al., 1998; Montero et al., 2003; Y. Arboled, pers. com.; see also Appendix). To analyze I-YSL nuclei movement in MZ*oep* embryos transplanted with hypoblast-like cells, we performed two-photon confocal time-lapse microscopy. We observed that at the side of the embryo where the transplanted cells were located, I-YSL nuclei tended to move to the dorsal side, in contrast to the nuclei on the opposite side of the embryo, which lacked hypoblast cells (Figs. 3.19B-G; Movie 17). To analyze this in more detail, we labeled the transplanted cells with a membrane-targeted form of GFP (GAP43-GFP) and performed high magnification time-lapse. In most of these movies, we observed that from mid-gastrulation stages (about 80% epiboly) onwards, transplanted cells behaved like typical

hypoblast cells: they actively migrated to the dorsal side of the embryo, in close contact with the yolk cell (Figs. 3.19I-L; Movie 18). The I-YSL nuclei underlying these cells also moved to the dorsal side of the embryo, seemingly "following" the transplanted cells, in contrast to what happens in non-transplanted M*Zoep* embryos (Figs. 3.19I-L; Movie 18). This effect seemed to be local, as I-YSL nuclei located at a distance from the transplanted cells did not move to the dorsal side. Taken together, these results strongly suggest that convergence of I-YSL nuclei is directed by the overlying hypoblast cells.

Cyc/Ndr2 is a secreted Nodal/TGFβ signaling molecule that has been shown to have short-range effects during mesendodermal patterning (Chen and Schier, 2001). In order to clarify whether the influence of hypoblast cells on I-YSL nuclei movement results from putative Cyc/Ndr2 over-expression, we performed two additional experiments: first, we transplanted cells obtained from purely wild-type embryos into M*Zoep* embryos; and second, we transplanted cells taken from embryos over-expressing a constitutively active form of Taram-A (Tar*), the putative receptor for Nodal signaling, which confers mesendodermal identity to the cells as Cyc/Ndr2 over-expression (Aoki et al., 2002; Renucci et al., 1996; data not shown). In both these situations, transplanted cells behaved similarly to Cyc/Ndr2 over-expressing cells, and I-YSL nuclei seemed to follow them to the dorsal side of the embryo (Movies 19,20). Therefore, we conclude that the movement of I-YSL nuclei is influenced by the transplanted hypoblast-like cells and not by an independent effect of Cyc/Ndr2 over-expression.

Based on these data, we propose that the convergence movement of hypoblast cells toward the dorsal side causes the I-YSL nuclei to move in the same direction.

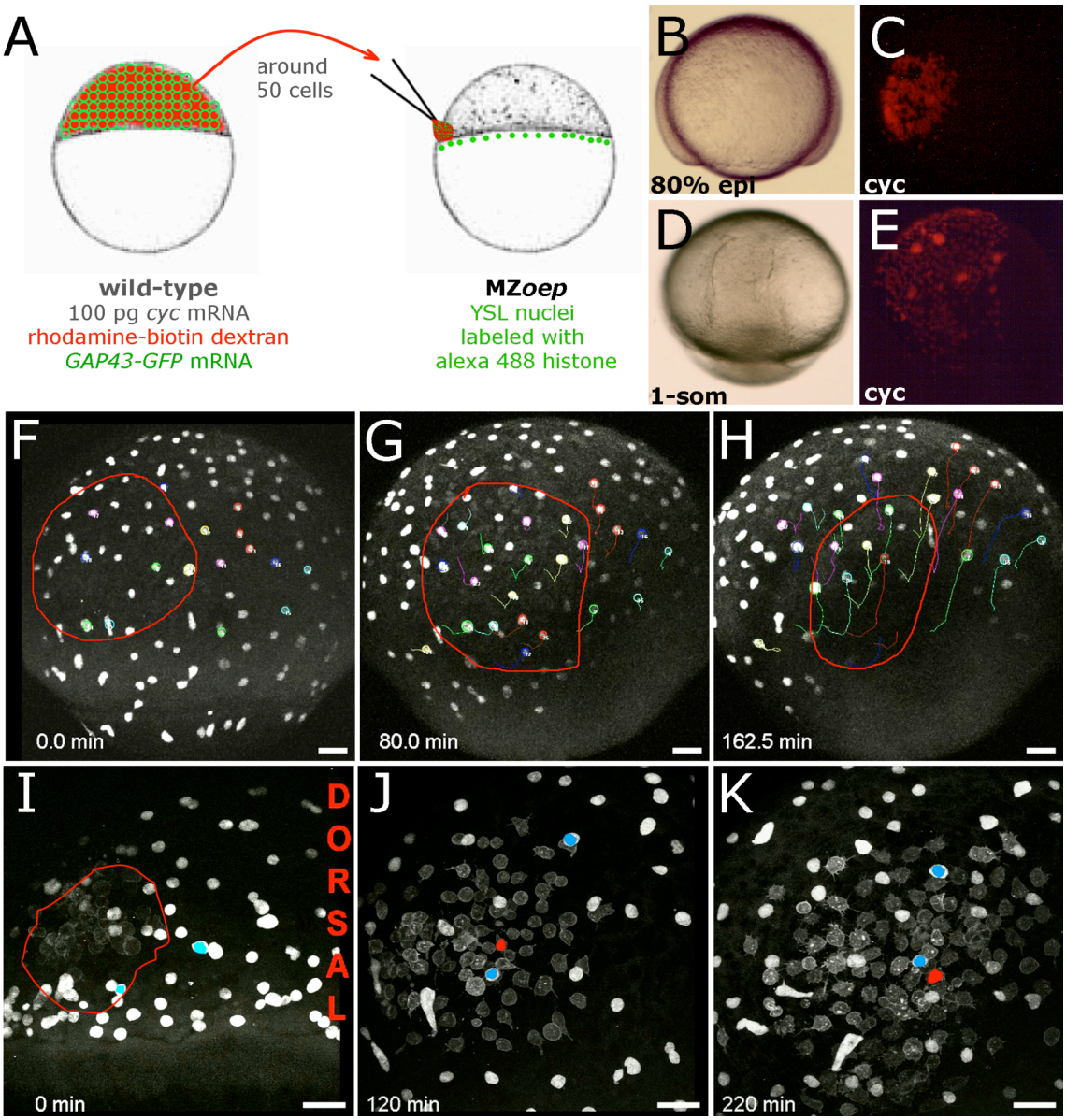

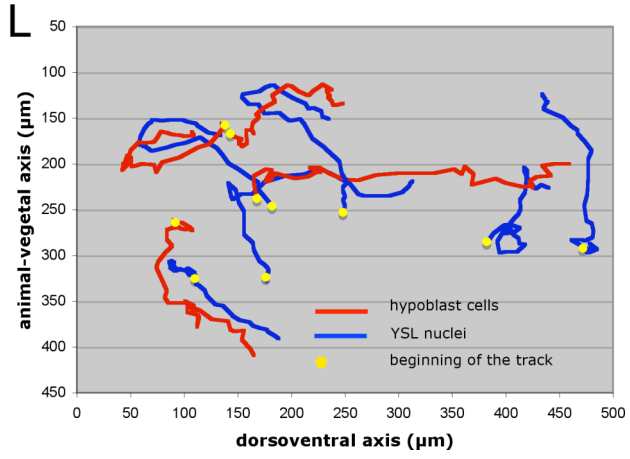

Figure 3.19 – Transplantion of hypoblast-like cells into MZ*oep* mutant embryos induces convergence movement of I-YSL nuclei. (A) Schematic view of the transplantation procedure. Wild-type donor embryos are injected at one-cell stage with *cyc* mRNA to induce mesendodermal cell fates in the whole embryo; *GAP43-GFP* mRNA to label cell membranes (I-K); and rhodamine-biotin dextran to allow the detection of donor cells in host embryos. Host MZ*oep* embryos are injected in the YSL with histone to label YSL nuclei. When donor and host embryos are at sphere stage, ca. 50 cells are transplanted from the animal pole of a donor to the blastoderm margin of an MZ*oep* embryo. (B-E) Images of MZ*oep* transplanted embryos before (B,C) and after (D,E) imaging by two-photon confocal microscopy. Dorsal views are shown; animal pole is on top. Brightfield (B,D) and fluorescence (C,E) images are shown. The

transplanted cells labeled with rhodamine dextran move from the lateral region (C) to the dorsal side of the embryo (E). (F-H) Still images of histone-labeled YSL nuclei obtained by two-photon confocal microscopy. Images are projections of 35 slices. Dorsal views are shown; animal pole is on top. Some of the nuclear trajectories obtained with the Motion Tracking Software are shown. The circles indicate the end-point of each track. (F) Embryo at 80% epiboly. Transplanted cells (delimited by red circle) are located in paraxial regions of the embryo. (G) Embryo at 95% epiboly. Transplanted cells moved toward the dorsal side of the embryo. I-YSL nuclei directly underneath the transplanted cells move also to the dorsal side, while I-YSL nuclei on the right side of the embryo do not. (H) Embryo at 2-somite stage. Transplanted cells are on the dorsal side. I-YSL nuclei directly underneath them displayed a net displacement toward dorsal, while I-YSL nuclei in similar regions on the other side of the embryo not containing transplanted cells show no directed movement towards dorsal. Similar observations were obtained from 3 embryos. (I-K) Still images of histone-labeled YSL nuclei and GAP43-GFP-labeled transplanted cells obtained by two-photon confocal microscopy. Images are projections of 35 slices. A transplanted cell (red) and two I-YSL nuclei (blue) are artificially labeled. Dorsal side is on the right; animal pole is on top. (I) Embryo at 65% epiboly. Transplanted cells are clustered together in the lateral side of the embryo (J) Embryo at 75% epiboly. Cells start to become more motile and spread. (K) Embryo at 90% epiboly. Cells and I-YSL nuclei move toward the dorsal side. (L) Graphical representation of the tracks manually obtained from the time-lapse in (I-K). Cell tracks are in red; I-YSL nuclei tracks are in blue; yellow circles represent the beginning of each track. Transplanted cells move to the dorsal side and I-YSL nuclei directly underneath them move in a similar way. I-YSL nuclei far from the cells only move to the animal pole. Similar observations were obtained in 5 embryos. Scale bars, 50 μm.

3.6.4 Convergence of I-YSL nuclei is reduced in Slb/Ppt loss-of-function

Our results suggest that convergence of I-YSL nuclei is dependent on hypoblast cell movement. It is possible that I-YSL nuclei movement is not dependent on a patterning signal, but rather on a mechanical influence of hypoblast migration. To clarify this, we investigated I-YSL nuclei movement in embryos showing impaired hypoblast movement but normal patterning. Non-canonical Wnt signaling is crucial for regulating convergence and extension movements during zebrafish gastrulation, but to be dispensable for early germ layer patterning (reviewed in Myers et al., 2002b; Tada et al., 2002; see also introduction). The genes *silberblick(slb)/wnt11* and *pipetail(ppt)/wnt5* have been identified as the two main ligands from this pathway involved in gastrulation movements (Heisenberg et al., 2000; Kilian et al., 2003; Rauch et al., 1997). Therefore, we examined the movement of the I-YSL nuclei in embryos deficient for both genes (Figs. 3.20A,B; Movie 21). For this, we used *slb/wnt11* mutants that were injected with a morpholino oligonucleotide against *ppt/wnt5* (which we call here *slb/ppt*). We found that in these embryos, the total speed of I-YSL nuclei was only slightly reduced, while the net dorsal speed was dramatically decreased compared to wild type (Fig. 3.20C). On the other hand, the net animal-vegetal speed was approximately the same in *slb/ppt* and wild-type embryos (Fig. 3.20C). These results indicate that the convergence of I-YSL nuclei is partially impaired in *slb/ppt* loss-of function.

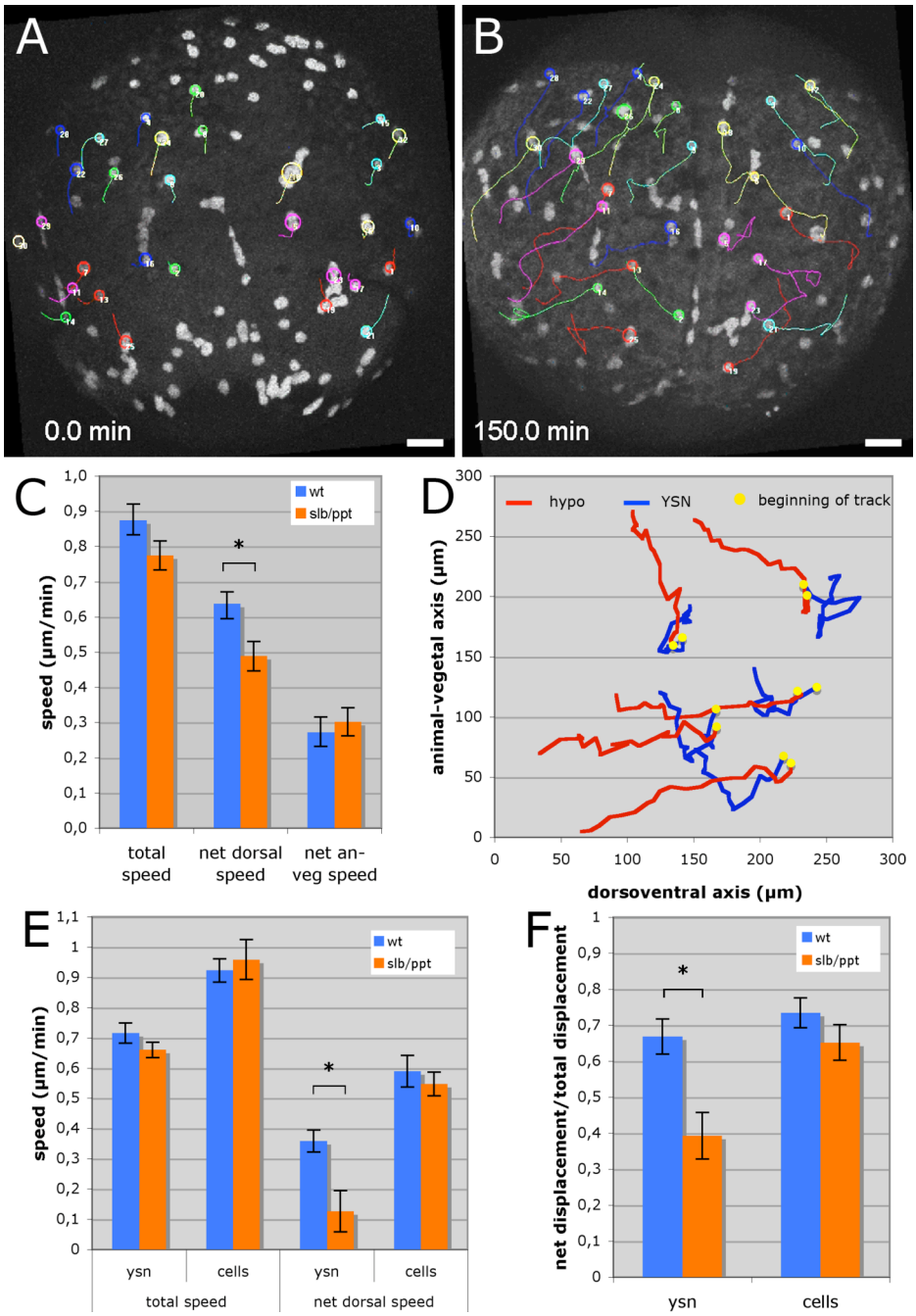

Figure 3.20 – Analysis of I-YSL nuclei and hypoblast cell movements during gastrulation in *slb/ppt* mutant embryos. (A-B) Still images of a histone-injected embryo from 70% epiboly until 1-somite stage obtained by two-photon confocal microscopy. All images are projections of 35 Z-slices. Some of the nuclear trajectories obtained with the Motion Tracking Software are shown. The circles indicate the end-point of each track. Embryos are shown on a dorsal view; animal pole is on top. (A) Embryo at 70% epiboly. (B) Embryo at 1-somite stage. I-YSL nuclei move to the animal pole and converge to the dorsal side. (C) Comparison of the speed of I-YSL nuclei movements between wild-type and *slb/ppt* embryos. The total speed and net animal-vegetal speed of I-YSL nuclei are similar in wild-type and *slb/ppt* embryos ($p>0.05$). The net dorsal speed is significantly lower in *slb/ppt* compared to wild-type ($p=0.0290$). Trajectories of 30 to 42 paraxial and lateral I-YSL nuclei from each embryo (wild-type, n=4; *slb/ppt*, n=4) were considered. All the trajectories were 150 minutes long (75% epiboly to 1 somite stage). (D) Typical trajectories of hypoblast cells and I-YSL nuclei obtained from Nomarski DIC time-lapses of paraxial regions of *slb/ppt* embryos from 65% until 90% epiboly (n=4). Dorsal is on the left, animal pole

in on top. Hypoblast cells (red) and I-YSL nuclei (blue) undergo similar convergence and extension movements. Yellow circles represent the beginning of each track. (E-F) Comparison of I-YSL nuclei and hypoblast cell speed and directionality in wild-type and *slb/ppt*. Trajectories of cells and nuclei from different embryos were quantified. (E) Total and net dorsal speed are similar between wild-type (n=14) and *slb/ppt* (n=13) hypoblast cells ($p>0.05$); *slb/ppt* I-YSL nuclei (n=7) show lower net dorsal speed than wild-type (n=9; $p=0.0228$) but similar total speed ($p=0.2144$). (F) The directionality of *slb/ppt* I-YSL nuclei is significantly lower than wild-type I-YSL nuclei ($p=0.0023$). For all quantifications (C,E,F) unpaired Student's *t* tests were performed to test the differences between the mean values of wild-type *versus slb/ppt*. Error bars represent the standard error of the mean. Abbreviations: hypo, hypoblast cells; ysn, yolk syncytial nuclei. Scale bars, 50 µm.

As explained above, mutants in components of non-canonical Wnt signaling display defective convergence and extension movements of hypoblast cells. To directly compare hypoblast and I-YSL nuclei movements, we performed Nomarski DIC time-lapses of paraxial regions in early gastrulating *slb/ppt* embryos. As expected, hypoblast cells moved in a less directed fashion compared to the wild type (Figs. 3.20D,F; Movie 23). Interestingly, *slb/ppt* I-YSL nuclei showed a much lower directionality rate when compared to wild type I-YSL nuclei (Fig.3.20F). Concerning the total speed, no difference between *slb/ppt* and wild type I-YSL nuclei and hypoblast cells was detected (Fig. 3.20E). As observed before by two-photon microscopy, the net dorsal speed of I-YSL nuclei was reduced in *slb/ppt* embryos compared to the wild-type. In contrast, hypoblast cells showed similar values in wild type and mutant cases (Fig. 3.20F), consistent with previous observations indicating that *slb* mutant cells display low net animal-vegetal speed but normal net dorsal speed (Heisenberg et al., 2000).

Together these observations again support our hypothesis that convergence of I-YSL nuclei depend on a mechanical influence coming from hypoblast cell movement and not on a patterning event.

3.7 E-cadherin links hypoblast movement to I-YSL nuclei movement

Our results have shown that I-YSL nuclei movement is influenced by the movement of the overlying hypoblast. However, the cellular mechanism that mediates this tissue interaction remains unclear. There are several hypotheses that could explain our observations. Based on our results, we can largely exclude the involvement of a patterning molecule in this process. Still, it is possible that a chemoattractant molecule is secreted by the hypoblast, or that non-canonical Wnt signaling autonomously or non-

autonomously regulates convergence of I-YSL nuclei. Alternatively, this interaction might have a more mechanical basis. The adhesion properties of the hypoblast cells, which migrate in very close contact to the I-YSL membrane, might induce a local change on the I-YSL cytoskeleton, leading to the observed nuclear movement.

3.7.1 E-cadherin is necessary for proper I-YSL nuclei movement

A strong candidate for mediating YSL/hypoblast interaction is the adhesion molecule E-cadherin (called Cadherin1 in zebrafish). E-cadherin is a transmembrane protein, and its extracellular domain forms Ca^{2+}-dependent homophilic trans-dimers that provide a specific interaction between adjacent cells. The cytoplasmic domain of cadherins is connected to the actin cytoskeleton via anchor proteins called catenins (reviewed by Adams and Nelson, 1998; Gumbiner, 2005). It was known from previous work that E-cadherin is strongly expressed on the surface of the YSL and hypoblast cells, and more weakly on epiblast cells (Montero et al., 2005, Ulrich et al., 2005). We confirmed this by performing antibody stainings for E-cadherin on sections of wild-type gastrulating embryos (Figs. 3.21A,B). Furthermore, in our transplantation assay (see Section 3.6.3), we observed that transplanted hypoblast-like cells showed increased levels of cadherins when compared to MZ*oep* host cells (Figs. 3.21C-E).

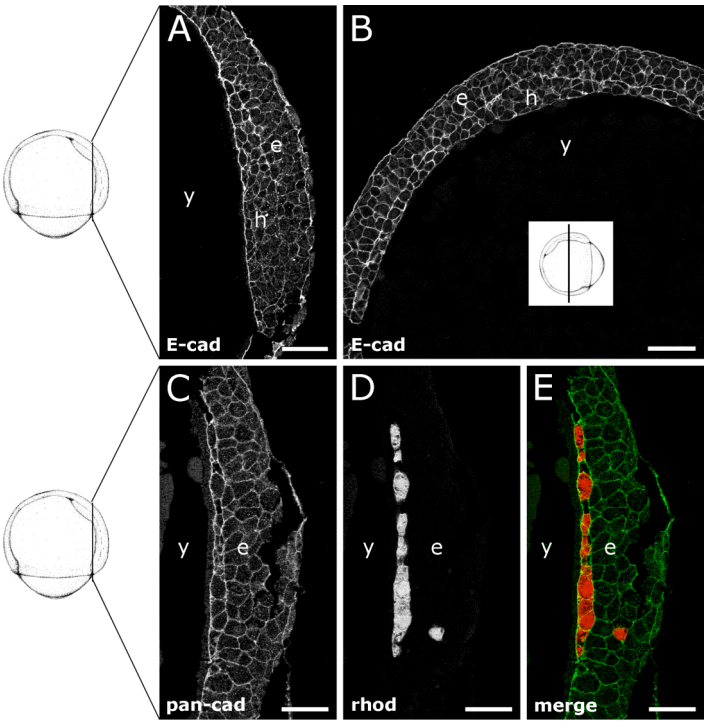

Figure 3.21 – Cadherin localization during gastrulation. Mid-gastrula stage embryos were sectioned and stained for E-cadherin or pan-cadherin. Images represent single Z-slices. (A,B) E-cadherin antibody staining on wild-type embryos. (A) Longitudinal section at the axial level as shown in scheme on the left. Animal pole is on top. (B) Transversal section at the level indicated in the scheme. Dorsal is on top. E-cadherin is strongly expressed in the membrane of hypoblast cells (h) and yolk (y), and more weakly in epiblast cells (e). (C-E) Pan-cadherin antibody staining in MZ*oep* embryos transplanted with hypoblast-like cells. Longitudinal section at the axial level as shown in the scheme. Animal pole is on top. (C) Pan-cadherin staining. (D) Transplanted cells marked with rhodamine-dextran. (E) Merged image of (C,D). Transplanted cells (red)

show higher expression of cadherins (green) than MZ*oep* host cells. Abbreviations: e, epiblast; e-cad, e-cadherin; h, hypoblast; pan-cad, pan-cadherin; rhod, rhodamine-dextran; y, yolk. Scale bars: (A,B) 50 µm; (C-E) 30 µm.

Therefore, we interfered with E-cadherin function specifically in the YSL and determined the effects on I-YSL nuclei movement. For that, we injected a morpholino against the start codon of the zebrafish *cadherin1* (*chd1*) gene into the YSL and performed two-photon confocal time-lapse imaging. We observed a striking effect: I-YSL nuclei moved more randomly and rapidly compared to wild type, while E-YSL nuclei underwent normal epiboly (Figs. 3.22A,B; Movie 23). Specifically, we found that I-YSL nuclei in *cdh1* morphants have a higher total speed than control embryos, while net dorsal speed and net animal-vegetal speed are normal (Fig. 3.23A). It is important to note that the observed effect was transient, since the movement of the nuclei seemed to recover after 90% epiboly and resemble wild type movements. Preliminary observations indicate that injection of a morpholino targeting the UTR region of *cdh1* into the YSL also affects YSL nuclei movement (data not shown).

The effect of *cdh1* morpholinos on the YSL is likely specific because when the same morpholinos are injected in one-cell stage embryos, the observed phenotype is identical to the phenotype of *cdh1* mutants (Babb and Mars, 2004; Kane et al., 2005; Montero et al, 2005; Shimizu et al., 2005). We could not perform a "rescue experiment" by co-injecting *cdh1* mRNA, since to date neither we nor other labs could obtain the zebrafish *cdh1* cDNA necessary to synthesize full-length mRNA for injection (Kane et al., 2005; Shimizu et al., 2005).

As an additional approach to study E-cadherin function, we analyzed the (zygotic) *cdh1* mutant allele hab^{tx230} (previously known as weg^{tx230}), which produces a truncated form of E-cadherin protein and is likely a functional null (Kane et al., 2005). *cdh1*/*hab* mutants display several defects in gastrulation movements without major patterning defects. Most severely affected is the epiboly movement of the deep cells, which arrests at about the 80% epiboly stage (Kane et al., 1996). In addition, both hypoblast and epiblast cells show defects in radial intercalation, and hypoblast cells do not undergo proper anterior migration (Kane et al., 2005; Montero et al., 2005). On the other hand, both EVL and E-YSL undergo normal epiboly (Kane et al., 1996). Thus we decided to analyze the movement of I-YSL nuclei in these mutants and to compare them to hypoblast cell movements. Using two-photon confocal time-lapse microscopy, we

observed that E-YSL nuclei underwent epiboly, as described before. Surprisingly, I-YSL nuclei seemed to converge normally to the dorsal side, contrary to the random movement observed in *chd1* YSL-morphants (Figs. 3.22C,D; Movie 24). Quantification showed that, in the mutant, total speed, net dorsal speed and net animal-vegetal extension speed were only slightly affected when compared to wild type (Fig. 3.23B).

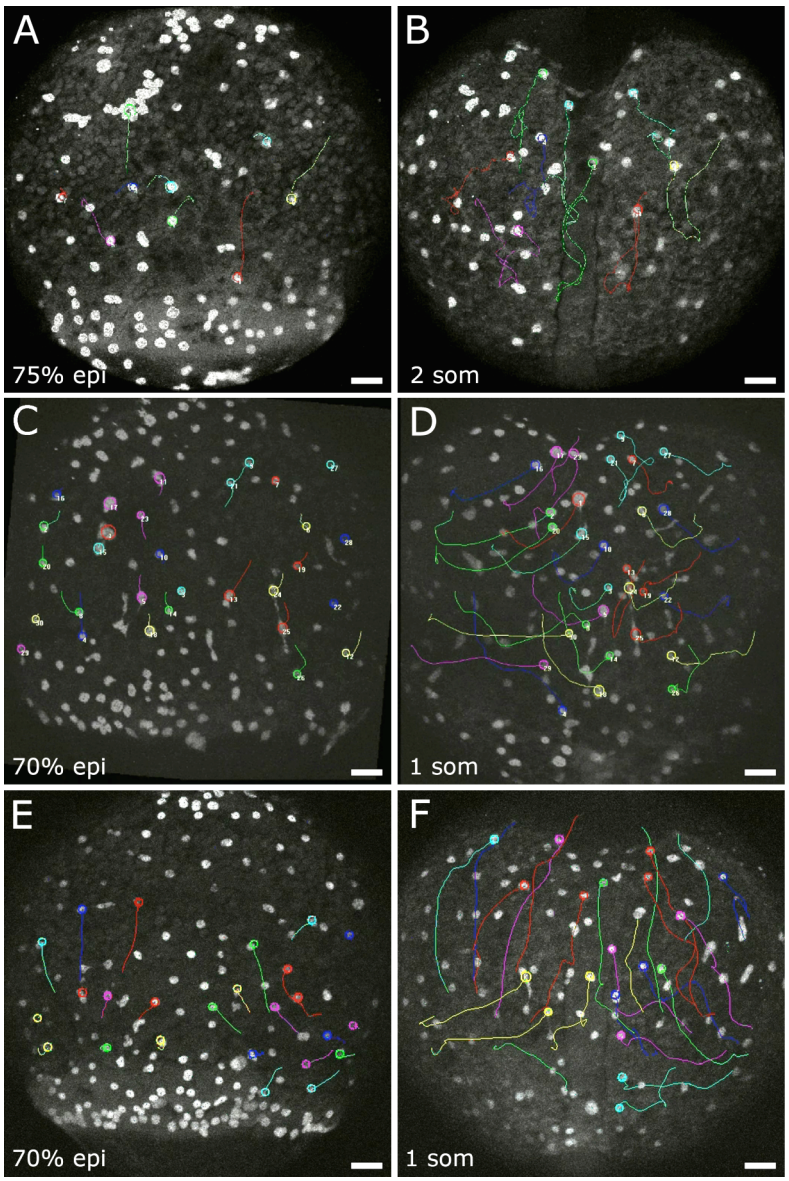

Figure 3.22 – Two-photon confocal time-lapse imaging of YSL nuclei movement during gastrulation in *cdh1* YSL-morphant and *cdh1/hab* mutant embryos. Still images of histone-labeled embryos from 65%-75% epiboly until 1-somite stage. All images are projections of 35 Z-slices. Some of the nuclear trajectories obtained with the Motion Tracking Software are shown. The circles indicate the end-point of each track. Embryos are shown on a dorsal view; animal pole is on top. (A,B) Embryo injected with 16 ng of *cdh1* ATG morpholino in the YSL. (A) Embryo at 65% epiboly. (B) Embryo at 2-somite stage. I-YSL nuclei still undergo convergence and extension movements, but display higher displacements and move more randomly than in wild-type. (C-D) *chd1/hab* mutant embryo. (C) Embryo at 75% epiboly. (D) Embryo at 1-somite stage. I-YSL nuclei converge to the dorsal side of the embryo. (E-F) *chd1/hab* embryo with a mild phenotype ("hab-mild"). (E) Embryo at 70% epiboly. (F) Embryo at 2-somite stage. I-YSL nuclei undergo convergence and extension movements, but display impaired movements similar to that observed in (B). In (A,B) time-lapses were performed at room temperature (22-24ºC); in (C-F) time-lapses were performed at 29ºC; respective wild-type controls were performed under identical conditions. Scale bars, 50 µm.

Our analyses of *cdh1*/*hab* mutant embryos yielded several other interesting observations. We found that a considerable number of embryos of a *cdh1*/*hab* clutch, although not showing the typical defective epiboly phenotype, displayed partially impaired I-YSL nuclei movement resembling the phenotype seen in *chd1* YSL-morphant embryos (Figs. 3.23E,F; Movie 25). We then compared the average speed and directionality between four groups of embryos: *a) cdh1*/*hab* embryos with the described epiboly phenotype ("hab"); *b) cdh1*/*hab* embryos with a mild phenotype during gastrulation and I-YSL nuclei movement ("hab-mild"); *c) cdh1*/*hab* embryos without a visible phenotype ("hab-wt"); and finally *d)* wild-type embryos. Again, total speed was similar for all conditions (Fig. 3.23B). In contrast, "hab-mild" embryos showed a significantly lower net dorsal speed compared to all other classes of embryos. These results indicate that I-YSL nuclei in "hab-mild" embryos have a similar phenotype as *cdh1* YSL-morphants, suggesting they might be heterozygous mutants for *cdh1*.

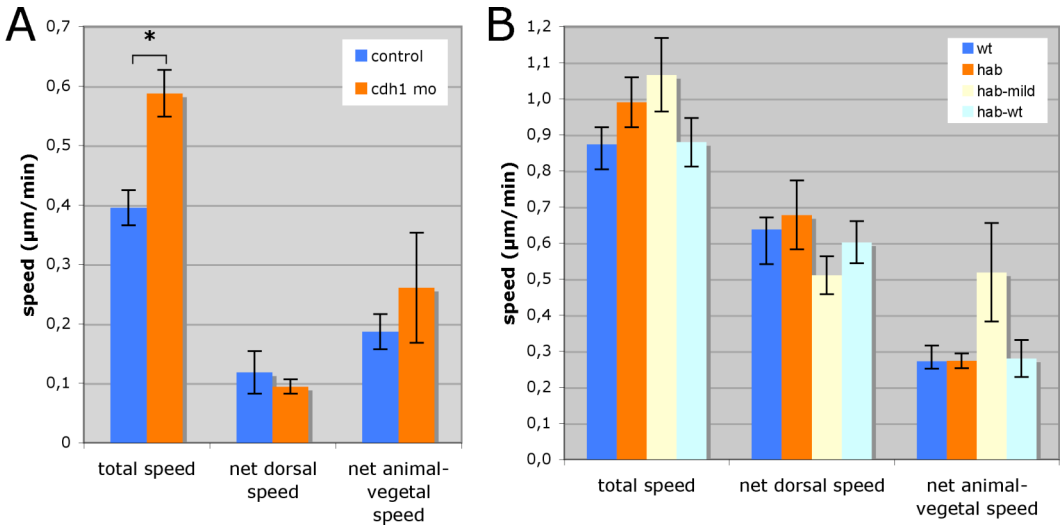

Figure 3.23 - Comparison of the speed of I-YSL nuclei movement between wild-type and *chd1* YSL-morphant (A) and *cdh/hab* mutant embryos (B). (A) The total speed of I-YSL nuclei in *chd1* morphant embryos (n=3) is significantly higher than in control embryos (n=3; p=0.0199). The net dorsal speed and net animal-vegetal speed are similar in control and morphant embryos (p>0.05). (B) Total, net dorsal, and net animal-vegetal speeds are similar in all classes of embryos (wild-type, n=4; hab, n=3; hab-mild, n=4; hab-wt, n=3; p>0.05). Trajectories of 30 to 50 paraxial and lateral I-YSL nuclei from each embryo were considered. In (A) trajectories of both wild-type and *cdh1* YSL-morphants were 300 minutes long (65% epiboly to 2-somite stage; room temperature). In (B) trajectories were 150 minutes long (70%-75% epiboly to 1-somite stage; 29ºC). Unpaired Student's *t* tests were performed to test the differences between the mean values of wild-type and morphant/mutant embryos.

3.7.2 E-cadherin is necessary for the coordination between I-YSL nuclei and hypoblast cell movements

We have shown that I-YSL nuclei move very similarly to hypoblast cells and that convergence of I-YSL nuclei is dependent on the movement of the hypoblast. Furthermore, reducing E-cadherin function caused defective I-YSL nuclei movement. E-cadherin-mediated adhesion may therefore be necessary for the coordination between I-YSL and hypoblast during convergence movements. In order to address this, we performed Nomarski time-lapse imaging of paraxial tissue of *cdh1/hab* mutants, including the ones with a mild phenotype ("hab-mild"). We found that the movements of I-YSL nuclei and hypoblast cells were similar in this mutant (Figs. 3.24A,B; Movies 26,27). However, we detected that I-YSL nuclei moved faster, whereas hypoblast cells moved slower than in the wild-type (Fig. 3.24C). Therefore, contrary to wild type, *cdh1*/*hab* mutant hypoblast cells tended to move slower than the underlying I-YSL nuclei, indicating that there might be a defect in the coordination between these two layers. In addition, we found that in the mutant, both I-YSL nuclei and hypoblast mutant cells displayed a lower net dorsal speed, contrary to what we obtained from the analysis of two-photon time-lapse movies (Fig. 3.24C). This discrepancy might be due to the fact that two-photon time-lapses were performed in slightly different conditions than those used in DIC movies (e.g. temperature, orientation of the embryo), thus it will be necessary to re-analyze this in more detail. In what respects the directionality of movement, we observed that mutant cells and I-YSL nuclei meandered more when compared to wild type (Fig. 3.24D).

These results led us to investigate how hypoblast cells move when E-cadherin function is impaired specifically in the YSL. We found that in *cdh1* YSL-morphants, I-YSL nuclei displayed erratic and rapid movements, as observed by two-photon confocal microscopy (Figs. 3.25A-C; Movie 28). Preliminary quantifications indicate that in the morphant, hypoblast cells also show defects in their movement: total and net dorsal speed, as well as directionality, were reduced (Figs. 3.25A-C). Despite this, we observed that *cdh1* YSL-morphant embryos undergo normal involution, convergence and extension, and epiboly movements, continuing to normally develop during the following days (see Appendix). This indicates that proper convergence of I-YSL nuclei might not be crucial for blastoderm gastrulation. However, the phenotype observed on

I-YSL nuclei movement is not very severe, considering that they eventually converge to the dorsal side. So far, we were not able to strongly interfere with the movement of I-YSL nuclei without simultaneously affecting E-YSL nuclei, and consequently blastoderm epiboly, but such experiments will be necessary to clarify this issue.

In summary, we have shown that E-cadherin function is necessary, not only within the YSL but also in the blastoderm, to coordinate convergence of I-YSL nuclei with hypoblast cell movement.

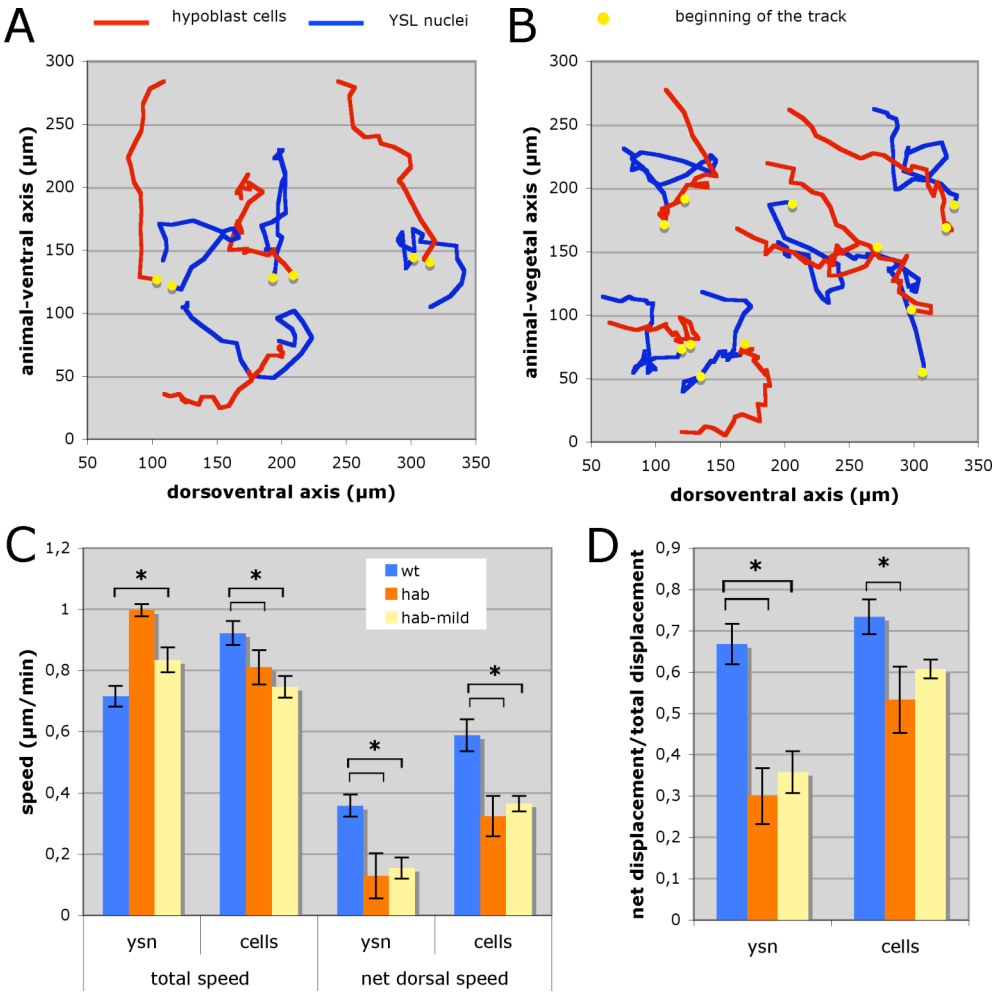

Figure 3.24 - Comparison of hypoblast cell and I-YSL nuclei movements between wild-type and *cdh1/hab* mutants during gastrulation. (A-B) Typical trajectories of hypoblast cells and I-YSL nuclei obtained from Nomarski DIC time-lapses of paraxial regions of *chd1/hab* embryos from 65% until 90% epiboly (n=8). Dorsal is on the left, animal pole in on top. (A) *cdh1/hab* mutant embryo. Hypoblast cells (red) and I-YSL nuclei (blue) partially converge and extend but their movements appear more random and uncoordinated with each other in comparison to wild-type. (B) *cdh1/hab* mutant embryo with a mild phenotype (hab-mild). Hypoblast and I-YSL nuclei movements are similar to that observed in (A). (C,D) Comparison of I-YSL nuclei and hypoblast cell speed and directionality in wild-type and *cdh1/hab* mutants. (C) Total speed of I-YSL nuclei is higher in *cdh1/hab* mutants (n=4) than in wild-type (n=9; p=0.0131), while the total speed of hypoblast cells is lower in *cdh1/hab* (n=7) than wild-type (n=12; p=0.0265); I-YSL nuclei in "hab-mild" embryos (n=10) move with similar speed as in wild-type (n=9;

p>0.05), while hypoblast cells move slower in the mutants (n=21; p=0.0007). The net dorsal speed of I-YSL nuclei and hypoblast cells is significantly lower in the two classes of mutants in comparison to wild-type (p<0.05). (D) The directionality of *cdh1/hab* I-YSL nuclei and hypoblast cells is significantly lower compared to wild-type (p<0.05), except in the case of "hab" hypoblast cells. Unpaired Student's *t* tests were performed to test the differences between the mean values of wild-type *versus* *chd1* mutants/morphants. Trajectories of cells and nuclei from different embryos from each class were quantified. Error bars represent the standard error of the mean. Red tracks represent hypoblast cell trajectories; blue tracks represent I-YSL nuclei trajectories; yellow circles represent the beginning of each track.

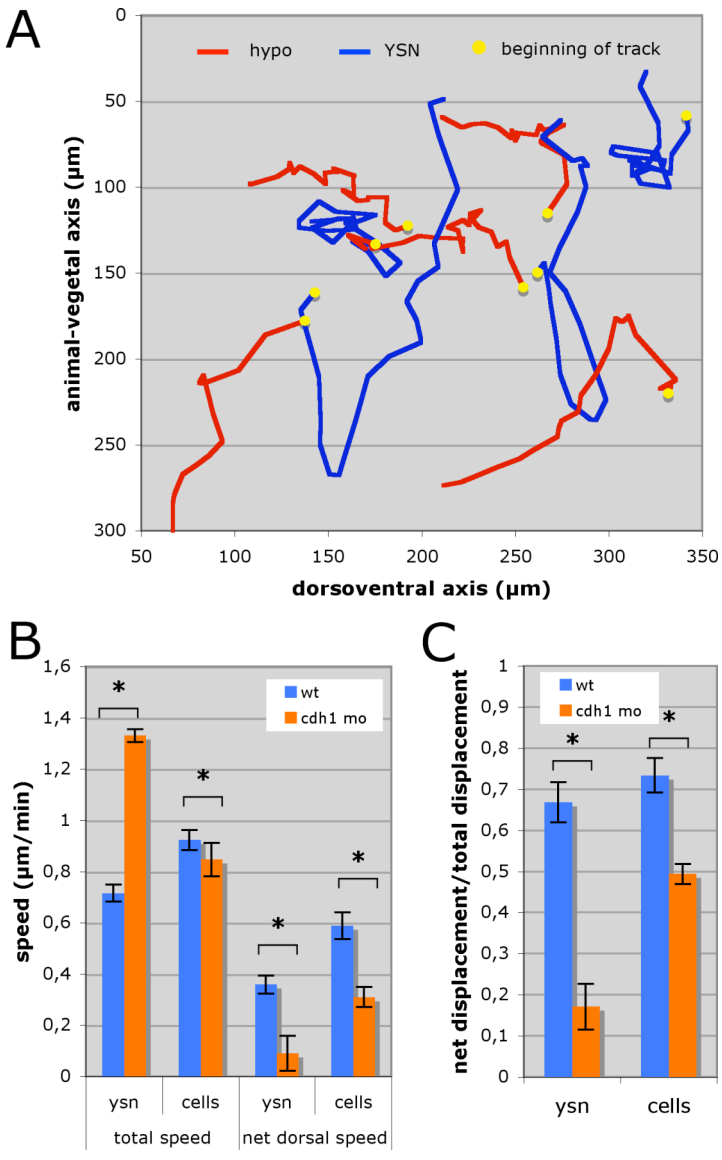

Figure 3.25 - Comparison of hypoblast cell and I-YSL nuclei movements between wild-type and *cdh1* YSL-morphants during gastrulation. (A) Typical trajectories of hypoblast cells and I-YSL nuclei obtained from Nomarski DIC time-lapses of paraxial regions of *chd1* YSL-morphant embryos from 65% until 90% epiboly (n=3). Dorsal is on the left, animal pole in on top. (B) The total speed of I-YSL nuclei *cdh1* YSL-morphant embryos (n=3) is higher whereas that of hypoblast cells is lower (n=11) than in wild-type (p<0.05). Net dorsal speed of I-YSL nuclei and hypoblast cells is lower in the morphants than in wild-type (p<0.05). (C) The directionality of I-YSL nuclei and hypoblast cells in the morphants is lower than in wild-type (p<0.05). Unpaired Student's *t* tests were performed to test the differences between the mean values of wild-type *versus* *chd1* mutants/morphants. Error bars represent the standard error of the mean. Trajectories of cells and nuclei from different embryos were quantified. Red tracks represent hypoblast cell trajectories; blue tracks represent I-YSL nuclei trajectories; yellow circles represent the beginning of each track. Abbreviations: hypo, hypoblast cells; ysn, yolk syncytial nuclei.

4. Discussion

The main goal of this thesis was to understand the relationship between I-YSL nuclei and hypoblast movements. Our major finding was that I-YSL nuclei convergence movement is influenced by the movement of the overlying hypoblast cells. We propose that the interaction between I-YSL and hypoblast is regulated by E-cadherin-mediated adhesion.

4.1 Relevance of studying YSL nuclei movement for understanding nuclear migration in other systems

Much of what we know about the mechanisms of nuclear migration comes from studies of fungi and invertebrate model systems (Morris, 2003). Correct movement and positioning of nuclei in cells and syncytia are required in a variety of biological contexts, and in a wide range of organisms, including vertebrates. Recently, it has been proposed that neuronal migration in the human brain is mediated by a similar mechanism to that responsible for long-range nuclear migration in filamentous fungi (Morris et al., 1998). Dosage insufficiency of LIS1, the human homologue of a nuclear migration protein in the filamentous fungi *Aspergillus nidulans*, NUDF (Xiang et al., 1995), causes a disease known as lissencephaly. This deficiency is characterized by a failure of neurons to migrate from the paraventricular replicative zone to the cerebral cortex, causing the cortex to be underpopulated with neurons (Dobyns and Truwit, 1995). Striking similarities between the *A. nidulans* NUDF and the mammalian LIS1 led to the idea that neuronal migration and nuclear migration are related (Morris et al., 1998). These authors have proposed that migration of cortical neurons involves a process called nucleokinesis (Klominek et al., 1991). Cells migrate by extending a long process followed by translocation of the nucleus to the anterior limit of the process. The residual trailing process retracts, followed by reiteration of the same sequence of steps. Based on analysis of LIS1 knockout mice, Morris and colleagues have suggested that translocation of the nucleus during nucleokinesis involves dynein, dynactin and microtubules, similar to nuclear migration in filamentous fungi (Morris et al., 1998).

Another example of nuclear movement and positioning in vertebrates is the

neuromuscular junction (NMJ). Vertebrate skeletal muscle fibers contain hundreds of nuclei, of which three to six are functionally specialized and stably anchored beneath the postsynaptic membrane at the NMJ (Sanes and Lichtman, 2001). Studies have suggested that these nuclei migrate through the cytoplasm of the newly formed myotube (Englander and Rubin, 1987), but the mechanisms and the roles they play in neuromuscular development are still poorly understood. The only insight comes from a study showing that colchicine treatment of muscle cells in culture impairs the migration of these nuclei, indicating that microtubules are involved in this process. In contrast, disrupting the actin cytoskeleton has no effect (Englander and Rubin, 1987).

In the zebrafish embryo, highly coordinated nuclear movements occur within the large yolk cell, and probably constitute a tightly regulated process involving the YSL cytoskeleton and interaction with overlying blastoderm. Therefore, the zebrafish YSL might constitute a good model system to study nuclear migration in vertebrates.

4.2 Internal YSL nuclei undergo convergence and extension similar to the overlying hypoblast cells

The previous study by D'Amico and Cooper (2001) has shown that I-YSL nuclei movement is analogous to the convergence and extension movement of the overlying blastoderm. In the first part of this thesis, we analyzed this in more detail, by taking a more quantitative approach. We established a high-resolution method to visualize YSL nuclei movement by two-photon confocal time-lapse microscopy and further quantification of the movement using a 2D tracking software (the latter in collaboration with Prof. Yannis Kalaidzidis, MPI-CBG Dresden). Our observations were similar to the obtained by the previous study: I-YSL nuclei undergo long-range convergence and extension movement that resemble the movement of the overlying hypoblast cells. I-YSL nuclei initially move toward the animal pole, starting to converge only at midgastrulation stages; the speed and direction of movement of I-YSL nuclei also varies according to their animal-vegetal and dorsoventral position. A similar dynamics has been described for hypoblast cells (Myers et al., 2002a; Sepich et al., 2000; Sepich et al., 2005), indicating that these two layers might interact during gastrulation movements, or at least be regulated by the same mechanism.

However, after quantitatively analyzing these movements, we found that hypoblast and I-YSL nuclei movements also differ in several aspects. Lateral hypoblast cells move significantly faster and in a more dorsal-directed way than the underlying I-YSL nuclei. While lateral hypoblast cells have been described to increase their speed as they approach the dorsal side, this feature has not been observed for the I-YSL nuclei (our unpublished observations from tracking in 3D). Beside this, lateral hypoblast cells start their convergence movement slightly earlier than I-YSL nuclei, suggesting that convergence of I-YSL nuclei might be initiated as a consequence of hypoblast movement. This is in contrast to what happens in the E-YSL, where the nuclei always move ahead of the blastoderm margin toward the vegetal pole (Kimmel et al., 1995; Trinkaus, 1993; this study). Finally, we did not observe a one-to-one relationship between the trajectory of I-YSL nuclei and immediately overlying hypoblast cells.

Together, these data show that I-YSL movement is similar, but not identical, to the convergence and extension movement of overlying hypoblast cells. A possible explanation for the observed difference is that nuclear movement relies on molecular mechanisms different from cell migration. Alternatively, I-YSL nuclei and hypoblast cell movements might be regulated by distinct signaling pathways.

4.3 YSL nuclei movement *versus* YSL movement

In our study, we were interested in studying nuclear movement within the YSL assuming it provides a reasonable read-out for the movement of the whole YSL. Implanted beads into the YSL move identically to I-YSL nuclei in their long-range convergence and extension movement. On the other hand, when we interfere with nuclear movement either by disrupting the microtubule network or by targeting E-cadherin translation in the YSL, we observe some degree of uncoupling of nuclear and cytoplasmic movements in I-YSL and E-YSL. Therefore, in this discussion we will consider YSL nuclei and YSL movements as separate aspects of yolk syncytial movement.

4.4 How do nuclei move within the YSL?

One of the aims of this thesis was to study how the YSL nuclei move within the YSL. What are the cellular mechanisms that generate such a coordinated movement of a

syncytium? Our results indicate that the microtubule cytoskeleton has an essential role for E-YSL nuclei epiboly movement and is at least partially required for I-YSL nuclei convergence and extension. Besides this, cytoplasmic streaming might also be an important component of the convergence and extension movement in the I-YSL.

4.4.1 The role of microtubules for YSL nuclei movement

Parallel arrays of microtubules oriented in the animal-vegetal axis of the embryo seem to originate in the E-YSL and continue to grow in the YCL toward the vegetal pole, while the I-YSL contains a dense network of microtubules without a clear polarity. Furthermore, interfering with the microtubule network through of microtubule-stabilizing or -destabilizing drugs, cold treatment, or UV irradiation results in the impairment of epiboly movement (Solnica-Krezel and Driever, 1994; Strähle and Jesuthasan, 1993; this study). Most of these treatments clearly affect epiboly of the E-YSL, EVL and DEL, but also have dramatic effects on the overall development of the embryo, leading to lethality before the end of gastrulation (Solnica-Krezel and Driever, 1994; our unpublished observations). Therefore, we decided that they are inadequate to specifically address the role of microtubules on YSL nuclei movement. In contrast, the microtubule-stabilizing drug paclitaxel seems to have a more specific effect on epiboly (Solnica-Krezel and Driver, 1994; this study). Paclitaxel stabilizes and promotes polymerization of microtubule filaments (Nogales, 2001), and when we treated embryos with this drug, we observed a strong enrichment of microtubules in the E-YSL, while the YCL showed a dramatic loss of parallel arrays of microtubules. While the exact mechanism is still unclear, several studies have described that treatment of cells with paclitaxel can lead to microtubule bundling (e.g. Green and Goldman, 1983; Tokunaka et al., 1983; Wehland et al., 1983), which is consistent with the observed effects on the zebrafish E-YSL. Importantly, this effect is restricted to the E-YSL and YCL, whereas microtubules in embryonic cells remain intact (Solnica-Krezel and Driever, 1994; this study). This might be due to the fact that paclitaxel is very water-insoluble and has a low transmembrane permeability (Jia et al., 2003; Swindell and Krauss, 1991), preventing it from diffusing across the rather impermeable EVL (Finn, 2007; Keller and Trinkaus, 1987). Therefore, paclitaxel is a very useful reagent for studying microtubule requirement within the YSL. In the previous study, effects of this drug on epiboly of the

three layers (E-YSL, EVL, DEL) were roughly analyzed, but it remained unclear to what extent YSL nuclear movement was affected, in particular in the I-YSL (Solnica-Krezel and Driever, 1994). For this reason, we recapitulated these experiments and analyzed YSL nuclear movement in more detail, by taking advantage of high-resolution two-photon confocal time-lapse microscopy. Our time-lapse analysis of paclitaxel-treated embryos revealed strongly impaired movement of YSL nuclei, in particular during epiboly. Most of the E-YSL and I-YSL nuclei concentrate in the animal pole of the embryo and show partially randomized movement. Interestingly, some degree of convergence and extension is still detected in these nuclei, but this is likely due to the fact that more animal regions of the I-YSL were not so severely affected by the treatment. Therefore, more specific tools to interfere with the whole YSL microtubule network, such as knocking-down proteins that regulate microtubule polymerization endogenously, are needed for future studies of the YSL cytoskeleton.

Microtubules are involved in nuclear migration in many different systems (Morris, 2003). In both fungi and animal cells, microtubules, the motor protein dynein, dynactin, and other microtubule plus-end binding proteins appear to interact with proteins at the cell cortex to generate forces acting on the nuclear microtubule organizing center (MTOC). Striking examples of long-range nuclear movement within a syncytium, resembling the case of the teleost YSL, occur in the hyphae of filamentous fungi. In this system, nuclei have to move over very long distances, as some fungal colonies have a diameter of several miles (Smith et al., 1992). As the fungal colony grows, the nuclei first move apart as a result of mitosis, then move towards the hyphal tip, resulting in a relatively even distribution along the mycelium (Suelmann et al., 1997). This process highly resembles the morphogenesis of the YSL in zebrafish, where nuclei first divide and spread evenly within the YSL cytoplasm during blastula stages and then start moving in a specific direction (dorso-animally or vegetally) during gastrulation. In fungi, it is thought that the separation of the daughter nuclei during mitosis may partly contribute to the even spacing of nuclei along the hyphae (Aist, 2002; Inoue et al., 1998). This might also constitute a mechanism regulating the distribution of nuclei in the zebrafish YSL.

Dynein-dependent interactions between microtubules and the cell cortex are involved in the movement of interphase nuclei along the hyphae (Osmani et al., 1990;

Xiang et al., 1994). Furthermore, studies in fungi as well as in *Drosophila* and *C. elegans* embryos provide strong evidence that dynein and microtubule-dependent forces exerted on the centrosome are responsible for nuclear migration (Gönczy et al., 1999; Freeman et al., 1986; Malone et al., 1999; Raff and Glover, 1989; Veith et al., 2005). Therefore, it would be of great interest to investigate the role of dynein and other microtubule motors for the movements of YSL nuclei.

Plus-end microtubule dynamics have also been proposed as a mechanism of nuclear migration in several eukaryotic cells (Reinsch and Gönczy, 1998; Xiang and Fischer, 2004). In the zebrafish I-YSL, it is unlikely that the same process plays a major role in nuclear movement, since microtubule plus-end protein EB3 does not seem to move in the same direction as the nuclei. The situation might be different in the E-YSL, where EB3 dynamics appear to follow the vegetalward movement of the nuclei, indicating that plus-end microtubule dynamics might be involved.

4.4.2 Cytoplasmic streaming and I-YSL nuclei movement

Another important finding of this work is that the cytoplasm of the I-YSL flows in the same direction and speed as the I-YSL nuclei toward dorsal regions of the embryo. We have shown that beads implanted or injected in the YSL undergo convergence movement, similar to the I-YSL nuclei moving in their vicinity. This event does not seem to be dependent on the size of the bead, suggesting that passive flow can account for the movement of both smaller (e.g. vesicles) and larger organelles (e.g. nuclei). Convergence of YSL cytoplasm has also been observed in the gastrulae of another teleost species, the white-sucker *Catostomus commersoni*, evidenced by the movement of chalk particles implanted at the margin of the YSL (Long, 1980). Together, we propose that substantial cytoplasmic streaming within the I-YSL contributes to the displacement of molecules, nuclei and other organelles within the cytoplasm. Interestingly, we never observed movement of beads toward the vegetal pole, suggesting that movement and transport of particles in this region could be regulated by a different mechanism. Alternatively, the position of bead injection or implantation may bias for movement to more animal regions. Indeed, Long (1980) has observed that the direction of chalk particle movement varied according to the stage when they were implanted at the YSL margin. Implantation before or during early epiboly stages

resulted in movement within the animal two thirds of the YSL, while implantation during mid-epiboly stages caused particles to move toward the vegetal pole. In both cases, particles consistently converged to the dorsal side. Technical limitations have so far prevented us from performing similar experiments to ultimately prove whether cytoplasmic flow also occurs in the zebrafish E-YSL.

Cytoplasmic streaming occurs in several organisms and biological processes. In the syncytial *Drosophila* embryo, this phenomenon is important for axial nuclear migration (von Dassow and Schubiger, 1994). Furthermore, there is a steady flow of cytoplasm from the nurse cells into the enlarging oocyte through cytoplasmic bridges (Mahajan-Miklos and Cooley, 1994). More recently, it has been shown that in *C. elegans* there is a bulk streaming of cytoplasmic materials from the core of the gonad into the enlarging oocytes (Wolke et al., 2007). In all of these systems, actin/myosin contraction is the main regulator of cytoplasmic streaming, although microtubules are also present and usually align in the direction of streaming (Bohrmann and Biber, 1994; Theurkauf et al., 1992; von Dassow and Schubiger, 1994; Wheatley et al., 1995; Wolke et al., 2007). In plants and algae, cytoplasmic streaming has been a major subject of study (for a review see Shimen, 2007). Here, myosins mediate the movement of organelles along oriented actin cables. Our electron microscopy analysis has revealed that the whole I-YSL contains a thick belt of cortical actin, but the potential role of actin and myosin in mediating streaming within the I-YSL remains to be directly addressed. It would also be interesting to investigate whether organelles, such the Golgi apparatus and the ER, also move within the I-YSL as a result of cytoplasmic streaming, as observed in plants and algae.

Altogether these results lead us to propose that in the I-YSL, cytoplasmic streaming and nuclear movement display the same movement direction. It is tempting to speculate that while actin regulates cytoplasmic streaming, microtubules direct the nuclei to go along with this flow. It is still unclear whether microtubules are also subject of cytoplasmic streaming and passively drag attached nuclei with them, or whether they provide a more static framework along which nuclei move via motor proteins. Investigating the presence and function of specific microtubule motors and centrosomes in the YSL will hopefully clarify this issue.

4.5 Importance of YSL nuclei movement during gastrulation

Our data suggest that E-YSL nuclei movement is important for epiboly of the E-YSL, EVL and DEL, while I-YSL nuclei movement is not essential for blastoderm convergence and extension. In this section we will discuss this in more detail.

4.5.1 Role of nuclear movement for YSL and blastoderm epiboly

We observed that E-YSL/EVL and deep cell epiboly is only partially delayed when E-YSL nuclei movement is impaired by paclitaxel treatment. In these embryos, the leading edge of the E-YSL/EVL can advance further than E-YSL nuclei, whereas it always trails behind the nuclei in untreated embryos. These observations implicate other factors besides microtubule dynamics and E-YSL nuclear movement in mediating epiboly. A good candidate is the actin/myosin ring present at the leading edge of the E-YSL/EVL, whose structure is not affected in paclitaxel-treated embryos. Actin/myosin-mediated contraction at this position likely causes a shortening of the margin and further progression toward the vegetal pole (Cheng et al., 2004; Köppen et al., 2006; Trinkaus, 1984). A similar "purse string-like" mechanism has been described during the closure of epithelial edges in other systems, such as dorsal closure in the *Drosophila* embryo (Martin and Wood, 2002), ventral closure in the hypodermis of *C. elegans* (Williams-Masson et al., 1997), and wound healing of embryonic skin and *Xenopus* oocytes (Bement et al., 1999; Kiehart, 1999; Nodder and Martin, 1997).

Another mechanism that has been proposed to be part of the motor that drives YSL epiboly in another teleost fish, *Fundulus*, is localized endocytosis occurring at the leading edge of the E-YSL (Betchaku and Trinkaus, 1978; Betchaku and Trinkaus, 1986; Trinkaus, 1984). Endocytosis of YCL plasma membrane occurs specifically at the E-YSL/YCL interface during epiboly stages (Betchaku and Trinkaus, 1986; Solnica-Krezel and Driever, 1994), and it has been postulated that this leads to the disappearance of the YCL and enables the YSL to expand vegetally. The large amount of membrane necessary for expansion of the YSL is in turn provided by numerous and long microvilli present in the I-YSL, which shorten during epiboly (Betchaku and Trinkaus, 1978), a feature that we also observed in our TEM analysis of zebrafish embryos. However, functional investigations of YCL endocytosis and I-YSL microvilli have not been performed in *Fundulus* or zebrafish embryos. Future studies should test

whether endocytosis and microvilli shortening still occur in paclitaxel-treated embryos. In addition, interfering with endocytosis and microvilli formation/stability will clarify the importance of these factors for YSL epiboly.

In summary, we propose that E-YSL nuclei movement is dependent on microtubules and is necessary for E-YSL/EVL and DEL epiboly but that other factors such as actin/myosin contraction and endocytosis must also be essential.

4.5.2 Role of the YSL for blastoderm epiboly

In paclitaxel-treated embryos, we observed a decrease of the distance between the leading edges of E-YSL/EVL and DEL in comparison to controls. This indicates that epiboly is more strongly affected in the E-YSL/EVL than in the DEL. Therefore, it is possible that E-YSL/EVL epiboly is necessary for DEL epiboly in a permissive way rather than as a major driving force. In this context, the E-YSL/EVL would function more as a substrate that deep cells use to epibolize. Three additional independent findings support this model. First, experiments in the *Fundulus* embryo have revealed that when the connection between EVL and E-YSL is physically disrupted, the E-YSL undergoes epiboly at a normal rate, while the blastoderm retracts. After some time, the blastoderm reattaches to the I-YSL surface and slowly recovers epiboly movements (Trinkaus, 1951). It is however not clear whether this reattachment is only mediated by the EVL or also by the deep cells. Second, *cdh1/hab* mutants show an arrest in DEL epiboly, whereas E-YSL/EVL movement is not affected; moreover, the epiblast layer has a cell-autonomous defect in cell intercalation, which might be the cause for its impaired movement (Kane et al., 1996; Kane et al., 2005; Shimizu et al., 2005). Third, *spg/pou5f1* mutants show a blockage of DEL but not EVL and E-YSL epiboly by a yet unknown mechanism (Reim and Brand, 2006). Together, our and previous observations strongly suggest that DEL epiboly is at least partially autonomous; additional studies are required to clarify the contributions of the E-YSL and EVL. For example, it would be useful to know what happens to DEL epiboly when E-YSL/EVL tight junctions are specifically impaired or when the EVL is not present at all. Furthermore, E-YSL epiboly is a completely autonomous process.

At the interface between the DEL leading edge and YSL, actin accumulations and membrane folds are present (Cheng et al., 2004; this study). Our TEM observations

show that these structures are very similar to the ones observed at the EVL/E-YSL interface. We propose that this additional actin ring might also be involved in epiboly of the deep cells, possibly independently of EVL epiboly.

4.5.3 Is the movement of I-YSL nuclei important for blastoderm convergence and extension movement?

We have shown that interfering with the movement of YSL nuclei does not significantly affect other gastrulation movements besides epiboly, namely involution, and convergence and extension. This is a somewhat surprising observation, in light of previous studies (D'Amico and Cooper, 2001; Keller et al., 2003; Long, 1984). The striking similarity between the convergence and extension movement of I-YSL nuclei and blastodermal cells led to three hypotheses: first, the I-YSL might influence the direction of hypoblast cell movement; second, hypoblast cell movement might direct I-YSL nuclei movement; and finally, the movement of I-YSL nuclei and hypoblast cells could be completely autonomous events (D'Amico and Cooper, 2001). Until now, the first and third hypotheses were considered to be the most likely, based on the following arguments: *a)* hypoblast cells, presumably endodermal progenitors, use the I-YSL membrane as a substrate for migration (Trinkaus and Erickson, 1983; Warga and Nüsslein-Volhard, 1999); *b)* blastoderm epiboly is at least partially dependent on E-YSL epiboly (Solnica-Krezel and Driever, 1994; Strähle and Jesuthasan, 1993; Trinkaus, 1951; this study); *c)* E-YSL nuclei movement is completely independent of the overlying blastoderm (Trinkaus, 1951), suggesting the same may apply for the I-YSL; *d)* the YSL has a common evolutionarily origin to the endodermal layer (Agassiz and Whitman, 1884; Bolker, 1994; Collazo et al., 1994), and it has been suggested that the presence of an "endodermal" YSL could be a consequence of the highly derived mode of gastrulation of teleost fishes, caused by a transition in the cleavage pattern from holoblastic to meroblastic (Cooper and Virta, 2007); and finally, *e)* the extension movement of the I-YSL nuclei seem to be homologous to the autonomous movement of vegetal endoderm in *Xenopus* (Cooper and Virta, 2007; D'Amico and Cooper, 2001; Keller et al., 2003).

We have shown that in embryos where YSL microtubules are impaired from the onset of gastrulation, both E-YSL and I-YSL nuclei movements are affected. The most

animally located I-YSL nuclei partially converge and extend, but in the most severe cases almost no nuclei are observed in the three vegetal quarters of the YSL, and still the blastoderm is able to converge and extend. In addition, knocking down E-cadherin function in the YSL leads to a specific effect on I-YSL nuclei movement, without a detectable effect on blastoderm convergence and extension. Therefore, it is reasonable to suggest that proper I-YSL nuclei movement is not essential for convergence and extension movement of the blastoderm. Still, several aspects have to be considered. The effect of E-cadherin knockdown on I-YSL nuclei movement is only transient and in the end of gastrulation the nuclei start to converge to the dorsal side and extend along the antero-posterior axis similar to normal embryos. These defects may be too mild to cause any visible effects on the blastoderm. In addition, our preliminary observations indicate that, in these morphants, flow of cytoplasm still occurs towards the dorsal side. Although this has to be analyzed more carefully, it is tempting to suggest that this cytoplasmic streaming might be an important factor in the transport and asymmetric localization of specific proteins, RNAs or other molecules necessary for guiding hypoblast cell movement; in this scenario, nuclear movement could result from bulk streaming of cytoplasm and might be dispensable for hypoblast movement.

Another hypothesis, which does not exclude the previous, is that the convergence and extension movement of hypoblast cells is guided by the I-YSL plasma membrane (Trinkaus and Erickson, 1983; Warga and Nüsslein-Volhard, 1999). It is well established that during gastrulation of other vertebrate embryos, the interaction between migrating mesodermal cells and its substrate – the extracellular matrix (ECM) – is absolutely crucial (Brown and Sanders, 1991; George et al., 1993; Klinowska et al., 1994; Winklbauer et al., 1996). In the *Xenopus* embryo, where this process has been most studied, mesodermal cells use the blastocoel roof as substrate; this tissue is covered with an extensive network of fibronectin fibrils that are essential for cell migration, lamellipodia extension and for determining the direction of cell movement (reviewed in Winklbauer et al., 1996). In the zebrafish, fibronectin has so far not been directly implicated in gastrulation. Although mRNA for the *fibronectin1* (*fn1*) gene is expressed in mesendodermal progenitors during gastrulation (Trinh and Stainier, 2004), a clear fibronectin matrix has to not been detected at the interface between hypoblast and I-YSL (Montero et al., 2005). On the other hand, preliminary analysis of *fn1/natter*

maternal and zygotic mutants seems to indicate that maternal Fn1 is necessary during gastrulation stages (Trinh and Stainier, 2004), and the function of a second fibronectin gene (*fn1b*) remains to be investigated (Jülich et al., 2005; Sun et al., 2005). Furthermore, the YSL is necessary to induce *fn1* expression in the embryo and consequently myocardial migration during somitogenesis stages (Sakaguchi et al., 2006). Besides fibronectin, other ECM molecules such as laminin could be involved in zebrafish gastrulation. Zebrafish mutants for *laminin γ1* (*lamc1*) and *laminin β1* (*lamb1*) chains, the first of which is expressed in the YSL (Thisse et al., 2004), show defects in notochord differentiation and have a shortened body axis, consistent with a defect during gastrulation of the chordamesoderm (Parsons et al., 2002). Interestingly, knocking down the function of the galactosyltransferase β4GalT1 impairs convergence and extension and notochord formation, possibly due to reduced galactosylation of laminin (Machingo et al., 2006).

4.6 Influence of the blastoderm on I-YSL nuclei movement

4.6.1 Hypoblast movement is necessary for I-YSL nuclei convergence movement

In our study, we have discovered that blastoderm movement influences the movement of the underlying I-YSL nuclei. We have observed that, in MZ*oep* mutants that lack mesendodermal progenitor cells (Gristman et al., 1999), I-YSL nuclei do not converge to the dorsal side as in wild-type embryos. This does not result from a defect in the intrinsic ability of the nuclei to move, since I-YSL nuclei still move animally and E-YSL nuclei move vegetally, with total speeds similar to the wild type case. Furthermore, we can partially rescue this phenotype by transplanting mesendodermal cells from a wild-type embryo into the MZ*oep* mutant. These results strongly suggest that convergence of I-YSL nuclei requires the presence of a proper hypoblast cell layer.

In *slb/ppt* embryos, which show impaired blastoderm convergence and extension but normal patterning (Heisenberg et al., 2000; Kilian et al., 2003; Rauch et al., 1997), I-YSL nuclei convergence movement is also reduced. This strongly suggests that the hypoblast influences the I-YSL independently of early embryonic patterning.

Several hypotheses can be proposed based on these observations. First, we can imagine that the hypoblast secretes a chemoattractant-like molecule that is necessary to

guide I-YSL nuclei movement. This would be consistent with our observation that transplanted hypoblast-like cells can locally influence I-YSL nuclei movement in MZ*oep* embryos. Alternatively, both hypoblast and I-YSL nuclei might move in response to a gradient of guidance cues that leads them to the dorsal side and animal pole. Such a gradient has been previously invoked to explain the movement of hypoblast cells (Miyagi et al., 2004; Sepich et al., 2005; Yamashita et al., 2002), which resembles the directed migration of chemotaxing cells (Dormann and Weijer, 2006). While the identity and the source of such an attractant molecule remain elusive, it has been shown that Stat3 activation is required for anterior and dorsalward migration of hypoblast cells (Yamashita et al., 2002). Stat3 belongs to the family of "signal transducers and activators of transcription" that act in response to cytokines (Darnell Jr, 1997; Hirano et al., 2000). Although the requirement of Stat3 for I-YSL nuclei movement has not been addressed, its phosphorylation occurs in dorsal YSL nuclei as well as in dorsal hypoblast cells during gastrulation (Yamashita et al., 2002). In addition, Stat3 likely induces activation of non-canonical Wnt/PCP signaling in lateral hypoblast cells (Miyagi et al., 2004), the major regulator of convergence and extension movements during gastrulation (Myers et al., 2002b; Tada et al., 2002). The Wnt/PCP ligands, Slb/Wnt11 and Ppt/Wnt5, regulate hypoblast movement in a cell non-autonomous way. Our analysis of I-YSL nuclei movement in *slb/ppt* embryos suggests that the same mechanism might regulate convergence and extension of I-YSL nuclei, as proposed by Cooper and Virta (2007).

A third and more likely possibility is that the influence of the hypoblast on the I-YSL is a result of mechanical effects induced by the collective movement of cells. It is an important but underappreciated fact that gastrulation is a biomechanical process (Keller et al., 2003); the embryonic form results from patterned forces generated by cells and tissues, and according to their mechanical properties. Therefore, we can imagine that the movement of I-YSL nuclei (and possibly also cytoplasm) is a consequence of the shape changes of the overlying blastoderm as a whole. It is possible that the migration of hypoblast cells on the I-YSL membrane causes a local deformation that leads to cytoskeletal changes and consequently movement of nuclei within the I-YSL. This view is consistent with most of our observations. First, the movement of I-YSL nuclei usually reflects the movement of the overlying blastoderm; the converse is

not true, as evidenced in E-cadherin YSL-morphants and paclitaxel-treated embryos. A second argument comes from our transplantation experiments. Hypoblast cells transplanted into MZ*oep* embryos move in a directed fashion toward the dorsal side after mid-gastrulation stages, and only the I-YSL nuclei located immediately underneath these cells are affected. This experiment shows that hypoblast cells can respond to signals supposedly coming from the dorsal side of embryo, independently of Nodal signaling, and probably depending on the activity of the Wnt/PCP pathway. Furthermore, it argues against the previously stated Stat3-Wnt/PCP hypothesis to explain I-YSL nuclei movement, which would predict I-YSL nuclei convergence in the absence of hypoblast cells in MZ*oep* mutants. Although it is still possible that something else besides lack of hypoblast cells prevents I-YSL nuclei convergence in MZ*oep* mutants, our results strongly suggest that this movement depends on an interaction between I-YSL and hypoblast cells.

4.6.2 E-cadherin as a link between hypoblast and I-YSL

The interaction between hypoblast and I-YSL might be mediated by E-cadherin (see proposed model in Fig. 4.1). We have shown that in E-cadherin mutants the movement of hypoblast cells and I-YSL nuclei to the dorsal side occurs in a more random, uncoupled fashion. I-YSL nuclei move faster than in wild type, whereas mutant hypoblast cells are slower. Therefore, in the E-cadherin mutant, I-YSL nuclei move faster than hypoblast cells, while the opposite occurs in wild type. This shows that in this mutant, the movement of I-YSL nuclei is partly uncoupled from the overlying hypoblast and strongly suggests that E-cadherin is necessary for maintaining the mechanical link between hypoblast and I-YSL. How then does E-cadherin-mediated adhesion specifically affect I-YSL nuclei movement? E-cadherin is known to mediate stable cell interactions, as part of epithelial adherens junctions and desmosomes, but it also mediates dynamic cell rearrangements and cell migration (reviewed by Adams and Nelson, 1998; Gumbiner, 2005). Adhesion through classical cadherins requires homotypic binding of the extracellular domain of cadherins on adjacent cells and the attachment of the intracellular domain to the actin cytoskeleton. Classical cadherins interact with actin through different complexes composed of cytosolic proteins, namely α-catenin, β-catenin, plakoglobin, and p120. Catenins are not only important to regulate

the direct physical linkage of cadherin to actin, but they also control the state of the adhesive bond on the outside of the cell and indirectly regulate the state of the cytoskeleton through the activation of signaling pathways. An interesting study has shown that mechanical coupling between cultured fibroblast cells, mediated by cadherins, β-catenin and actin, can lead to cytoplasmic deformation and flow of vesicles and particles along the axis of a specific type of cell protrusion (Ragsdale et al., 1997). Therefore, it is possible that E-cadherin adhesion sites between hypoblast cells and the I-YSL membrane link to the I-YSL actin cytoskeleton, triggering nuclear and/or cytoplasmic rearrangements within the I-YSL and causing the nuclei to move in the same direction as the overlying hypoblast cells.

An alternative is that the microtubule cytoskeleton is involved in mediating the membrane-nucleus interaction. A recent study has demonstrated that cadherin-based cell-cell contacts regulate non-centrosomal microtubule dynamics by stabilizing the microtubule minus end through an unknown signaling pathway (Chausovsky et al., 2000). Although we have not so far detected defects in microtubule organization in E-cadherin mutants (our unpublished observations), it is possible that E-cadherin affects I-YSL nuclei movement by controlling microtubule dynamics in the YSL.

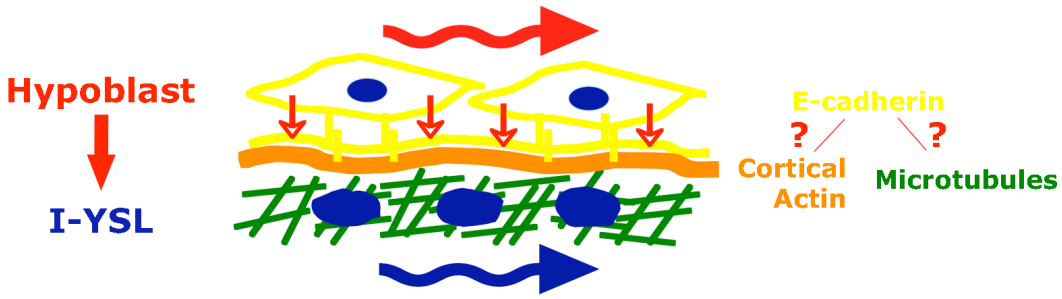

Figure 4.1 – Model of how E-cadherin-mediated adhesion might regulate I-YSL nuclei movement. E-cadherin protein, which is strongly expressed in the membrane of hypoblast cells and I-YSL (yellow), provides a link between hypoblast cells and I-YSL. It is yet unclear whether this molecule acts on I-YSL nuclei movement through microtubules (green) and/or actin cytoskeleton (orange).

To understand how E-cadherin-mediated adhesion is established between hypoblast and I-YSL and how it coordinates their convergence and extension movements, it will be necessary to investigate whether components of the cadherin/catenin complex interact with cytoskeletal components at the interface between these tissues.

4.7 Significance of I-YSL nuclei movement for embryonic development

Taking into account that the YSL is involved in inducing the dorsal Spemann-Mangold organizer as well as mesendodermal cell fates (Chen and Kimelman, 2000; Mizuno et al., 1996; Mizuno et al., 1999; Ober and Sculte-Merker, 1999; Rodaway et al., 1999), it was reasonable to expect that proper I-YSL nuclei convergence and extension movement is necessary for these processes. Our results do not seem to support such a hypothesis, as embryos where YSL nuclei movement was impaired apparently did not have major patterning defects. Moreover, many genes are exclusively expressed in the whole YSL or in specific regions of the YSL during blastula and gastrula stages (Sakaguchi et al., 2002), indicating that nuclear movement could be important for maintaining asymmetric gene expression. While the function of most of these genes has not been fully characterized, some of them have been shown to have an important role during early stages of zebrafish embryogenesis. Many of these include genes coding for enzymes involved in early metabolism and nutrition-related functions, essential before the major organs are formed at later stages. Some examples are enzymes involved in steroidogenesis (Hsu et al., 2002), iron transport (Donovan et al., 2000), lipid metabolism (Marza et al., 2005; Mudumana et al., 2004), and creatine metabolism (Wang et al., 2007).

A different class of genes expressed in the YSL during gastrulation is composed of homeobox transcription factors. For example, *mtx1* and *mtx2* are important for morphogenetic movements, respectively, myocardial migration and epiboly (Bruce et al., 2005; Hirato et al., 2000; Sakaguchi et al., 2006). In contrast, the conserved endodermal gene *hhex* seems to serve patterning roles, and was shown to function as a transcriptional repressor of ventralizing and posteriorizing molecules in the overlying blastoderm (Ho et al., 1999). Furthermore, specific knock-down of early *hhex* expression in the YSL leads to later defects in digestive organ chirality, suggesting that the YSL has a role in establishing left-right asymmetry of endodermal organs (Wallace et al., 2001). *hhex* is inititally expressed in the dorsal marginal YSL at sphere stage of development, similar to other dorsal organizer genes, such as *dharma* (Fekany et al., 1999; Koos and Ho, 1999; Shimizu et al., 2000; Yamanaka et al., 1998) and *squint* (Feldman et al., 1998). During the late blastula period and until the end of gastrulation, *hhex* is expressed in the YSL along the dorsal axis and extends to the presumptive head

region at the animal pole (Bischof and Driever, 2004; Ho et al., 1999). This change in expression domain is correlated with the morphological redistribution of dorsal I-YSL nuclei as they translocate toward the animal pole region (D'Amico and Cooper, 2001; this study). However, we observed that the expression pattern of *hhex* was not affected in our E-cadherin YSL-morphants (see Appendix), which show defective movement of dorsal I-YSL nuclei, indicating that proper I-YSL nuclei movement is not essential for maintaining restricted *hhex* expression in the YSL. Again, it remains possible that the degree of impairment of I-YSL nuclei movement in the morphants is too weak or too transient to cause a detectable change of gene expression; alternatively, cytoplasmic streaming and/or cytoskeletal motors might be able to maintain restricted expression of this gene within the dorsal YSL, independently of I-YSL nuclei movement. It would be interesting to examine the expression of other YSL specific genes in these morphants, or in embryos where microtubules and I-YSL convergence and extension movement are more severely impaired.

In conclusion, I-YSL and E-YSL are critical tissues for early development of the zebrafish embryo, including germ layer patterning and early metabolism and nutrition. These functions are probably related to the highly derived mode of gastrulation characteristic of teleost fishes, which evolved as result of changes in yolk structure and early cleavage patterns (Cooper and Virta, 2007). To fully understand whether I-YSL convergence and extension plays a role in the distribution of molecules important for these functions, as well as in blastoderm gastrulation movements, it will be necessary to find ways to interfere more specifically and efficiently with the movement occurring in this compartment. This will surely constitute the major challenge to future studies.

References

Adams, C. L. and Nelson, W. J. (1998). Cytomechanics of cadherin-mediated cell-cell adhesion. *Curr Opin Cell Biol* **10**, 572-7.

Adler, P. N. and Lee, H. (2001). Frizzled signaling and cell-cell interactions in planar polarity. *Curr Opin Cell Biol* **13**, 635-40.

Agassiz, A. and Whitman, C. O. (1884). On the development of some pelagic fish eggs. Preliminary Notice. *Proc Natl Acad Sci U S A* **20**, 23-75.

Aist, J. R. (2002). Mitosis and motor proteins in the filamentous ascomycete, Nectria haematococca, and some related fungi. *Int Rev Cytol* **212**, 239-63.

Akimenko, M. A., Ekker, M., Wegner, J., Lin, W. and Westerfield, M. (1994). Combinatorial expression of three zebrafish genes related to distal-less: part of a homeobox gene code for the head. *J Neurosci* **14**, 3475-86.

Alexander, J., Rothenberg, M., Henry, G. L. and Stainier, D. Y. (1999). casanova plays an early and essential role in endoderm formation in zebrafish. *Dev Biol* **215**, 343-57.

Alexander, J. and Stainier, D. Y. (1999). A molecular pathway leading to endoderm formation in zebrafish. *Curr Biol* **9**, 1147-57.

Amsterdam, A., Lin, S. and Hopkins, N. (1995). The Aequorea victoria green fluorescent protein can be used as a reporter in live zebrafish embryos. *Dev Biol* **171**, 123-9.

Aoki, T. O., Mathieu, J., Saint-Etienne, L., Rebagliati, M. R., Peyrieras, N. and Rosa, F. M. (2002). Regulation of nodal signalling and mesendoderm formation by TARAM-A, a TGFbeta-related type I receptor. *Dev Biol* **241**, 273-88.

Babb, S. G. and Marrs, J. A. (2004). E-cadherin regulates cell movements and tissue formation in early zebrafish embryos. *Dev Dyn* **230**, 263-77.

Barth, K. A. and Wilson, S. W. (1995). Expression of zebrafish nk2.2 is influenced by sonic hedgehog/vertebrate hedgehog-1 and demarcates a zone of neuronal differentiation in the embryonic forebrain. *Development* **121**, 1755-68.

Beddington, R. S. and Robertson, E. J. (1998). Anterior patterning in mouse. *Trends Genet* **14**, 277-84.

Bement, W. M., Mandato, C. A. and Kirsch, M. N. (1999). Wound-induced assembly and closure of an actomyosin purse string in Xenopus oocytes. *Curr Biol* **9**, 579-87.

Betchaku, T. and Trinkaus, J. P. (1978). Contact relations, surface activity, and cortical microfilaments of marginal cells of the enveloping layer and of the yolk syncytial and yolk cytoplasmic layers of fundulus before and during epiboly. *J Exp Zool* **206**, 381-426.

Betschaku, T. and Trinkaus, J. P. (1986). Programmed endocytosis during epiboly of *Fundulus heteroclitus*. *American Zoologist* **26**, 193-199.

Bischof, J. and Driever, W. (2004). Regulation of hhex expression in the yolk syncytial layer, the potential Nieuwkoop center homolog in zebrafish. *Dev Biol* **276**, 552-62.

Bohrmann, J. and Biber, K. (1994). Cytoskeleton-dependent transport of cytoplasmic particles in previtellogenic to mid-vitellogenic ovarian follicles of Drosophila: time-lapse analysis using video-enhanced contrast microscopy. *J Cell Sci* **107 (Pt 4)**, 849-58.

Bolker, J. A. (1994). Comparison of gastrulation in frogs and fish. *American Zoologist* **34**, 313-22.

Bouwmeester, T. and Leyns, L. (1997). Vertebrate head induction by anterior primitive endoderm. *Bioessays* **19**, 855-63.

Brown, A. J. and Sanders, E. J. (1991). Interactions between mesoderm cells and the extracellular matrix following gastrulation in the chick embryo. *J Cell Sci* **99 (Pt 2)**, 431-41.

Bruce, A. E., Howley, C., Dixon Fox, M. and Ho, R. K. (2005). T-box gene eomesodermin and the homeobox-containing Mix/Bix gene mtx2 regulate epiboly movements in the zebrafish. *Dev Dyn* **233**, 105-14.

Burnside, M. B. and Jacobson, A. G. (1968). Analysis of morphogenetic movements in the neural plate of the newt Taricha torosa. *Dev Biol* **18**, 537-52.

Carmany-Rampey, A. and Schier, A. F. (2001). Single-cell internalization during zebrafish gastrulation. *Curr Biol* **11**, 1261-5.

Chausovsky, A., Bershadsky, A. D. and Borisy, G. G. (2000). Cadherin-mediated regulation of microtubule dynamics. *Nat Cell Biol* **2**, 797-804.

Chen, J. N., Haffter, P., Odenthal, J., Vogelsang, E., Brand, M., van Eeden, F. J., Furutani-Seiki, M., Granato, M., Hammerschmidt, M., Heisenberg, C. P. et al. (1996). Mutations affecting the cardiovascular system and other internal organs in zebrafish. *Development* **123**, 293-302.

Chen, J. N., van Eeden, F. J., Warren, K. S., Chin, A., Nusslein-Volhard, C., Haffter, P. and Fishman, M. C. (1997). Left-right pattern of cardiac BMP4 may drive asymmetry of the heart in zebrafish. *Development* **124**, 4373-82.

Chen, S. and Kimelman, D. (2000). The role of the yolk syncytial layer in germ layer patterning in zebrafish. *Development* **127**, 4681-9.

Chen, Y. and Schier, A. F. (2001). The zebrafish Nodal signal Squint functions as a morphogen. *Nature* **411**, 607-10.

Cheng, J. C., Miller, A. L. and Webb, S. E. (2004). Organization and function of microfilaments during late epiboly in zebrafish embryos. *Dev Dyn* **231**, 313-23.

Cole, L., Davies, D., Hyde, G. J. and Ashford, A. E. (2000). ER-Tracker dye and BODIPY-brefeldin A differentiate the endoplasmic reticulum and golgi bodies from the tubular-vacuole system in living hyphae of Pisolithus tinctorius. *J Microsc* **197**, 239-49.

Collazo, A., Bolker, J. A. and Keller, R. (1994). A phylogenetic perspective on teleost gastrulation. *American Naturalist* **144**, 133-52.

Concha, M. L. and Adams, R. J. (1998). Oriented cell divisions and cellular morphogenesis in the zebrafish gastrula and neurula: a time-lapse analysis. *Development* **125**, 983-94.

Cooper, M. S., D'Amico, L. A. and Henry, C. A. (1999). Confocal microscopic analysis of morphogenetic movements. *Methods Cell Biol* **59**, 179-204.

Cooper, M. S. and Virta, V. C. (2007). Evolution of gastrulation in the ray-finned (actinopterygian) fishes. *J Exp Zoolog B Mol Dev Evol*. **308B**.

D'Amico, L. A. and Cooper, M. S. (2001). Morphogenetic domains in the yolk syncytial layer of axiating zebrafish embryos. *Dev Dyn* **222**, 611-24.

Darnell, J. E., Jr. (1997). STATs and gene regulation. *Science* **277**, 1630-5.

Dehmelt, L. and Halpain, S. (2005). The MAP2/Tau family of microtubule-associated proteins. *Genome Biol* **6**, 204.

Dickmeis, T., Mourrain, P., Saint-Etienne, L., Fischer, N., Aanstad, P., Clark, M., Strahle, U. and Rosa, F. (2001). A crucial component of the endoderm formation pathway, CASANOVA, is encoded by a novel sox-related gene. *Genes Dev* **15**, 1487-92.

Dobyns, W. B. and Truwit, C. L. (1995). Lissencephaly and other malformations of cortical development: 1995 update. *Neuropediatrics* **26**, 132-47.

Donovan, A., Brownlie, A., Zhou, Y., Shepard, J., Pratt, S. J., Moynihan, J., Paw, B. H., Drejer, A., Barut, B., Zapata, A. et al. (2000). Positional cloning of zebrafish ferroportin1 identifies a conserved vertebrate iron exporter. *Nature* **403**, 776-81.

Dormann, D. and Weijer, C. J. (2006). Chemotactic cell movement during Dictyostelium development and gastrulation. *Curr Opin Genet Dev* **16**, 367-73.

Downing, K. H. (2000). Structural basis for the interaction of tubulin with proteins and drugs that affect microtubule dynamics. *Annu Rev Cell Dev Biol* **16**, 89-111.

Driever, W., Solnica-Krezel, L., Schier, A. F., Neuhauss, S. C., Malicki, J., Stemple, D. L., Stainier, D. Y., Zwartkruis, F., Abdelilah, S., Rangini, Z. et al. (1996). A genetic screen for mutations affecting embryogenesis in zebrafish. *Development* **123**, 37-46.

Edgar, B. A., Kiehle, C. P. and Schubiger, G. (1986). Cell cycle control by the nucleo-cytoplasmic ratio in early Drosophila development. *Cell* **44**, 365-72.

Englander, L. L. and Rubin, L. L. (1987). Acetylcholine receptor clustering and nuclear movement in muscle fibers in culture. *J Cell Biol* **104**, 87-95.

Erter, C. E., Solnica-Krezel, L. and Wright, C. V. (1998). Zebrafish nodal-related 2 encodes an early mesendodermal inducer signaling from the extraembryonic yolk syncytial layer. *Dev Biol* **204**, 361-72.

Essner, J. J., Amack, J. D., Nyholm, M. K., Harris, E. B. and Yost, H. J. (2005). Kupffer's vesicle is a ciliated organ of asymmetry in the zebrafish embryo that initiates left-right development of the brain, heart and gut. *Development* **132**, 1247-60.

Ettensohn, C. A. (1985). Gastrulation in the sea urchin embryo is accompanied by the rearrangement of invaginating epithelial cells. *Dev Biol* **112**, 383-90.

Fekany, K., Yamanaka, Y., Leung, T., Sirotkin, H. I., Topczewski, J., Gates, M. A., Hibi, M., Renucci, A., Stemple, D., Radbill, A. et al. (1999). The zebrafish bozozok locus encodes Dharma, a homeodomain protein essential for induction of gastrula organizer and dorsoanterior embryonic structures. *Development* **126**, 1427-38.

Feldman, B., Gates, M. A., Egan, E. S., Dougan, S. T., Rennebeck, G., Sirotkin, H. I., Schier, A. F. and Talbot, W. S. (1998). Zebrafish organizer development and germ-layer formation require nodal-related signals. *Nature* **395**, 181-5.

Fink, R. D. and Trinkaus, J. P. (1988). Fundulus deep cells: directional migration in response to epithelial wounding. *Dev Biol* **129**, 179-90.

Finn, R. N. (2007). The physiology and toxicology of salmonid eggs and larvae in relation to water quality criteria. *Aquat Toxicol* **81**, 337-54.

Foe, V. E. and Alberts, B. M. (1983). Studies of nuclear and cytoplasmic behaviour during the five mitotic cycles that precede gastrulation in Drosophila embryogenesis. *J Cell Sci* **61**, 31-70.

Freeman, M., Nusslein-Volhard, C. and Glover, D. M. (1986). The dissociation of nuclear and centrosomal division in gnu, a mutation causing giant nuclei in Drosophila. *Cell* **46**, 457-68.

Fukada, E., Seaman, G. V., Liepsch, D., Lee, M. and Friis-Baastad, L. (1989). Blood modeling using polystyrene microspheres. *Biorheology* **26**, 401-13.

Gard, D. L. (1993). Confocal immunofluorescence microscopy of microtubules in amphibian oocytes and eggs. *Methods Cell Biol* **38**, 241-64.

Geldmacher-Voss, B., Reugels, A. M., Pauls, S. and Campos-Ortega, J. A. (2003). A 90-degree rotation of the mitotic spindle changes the orientation of mitoses of zebrafish neuroepithelial cells. *Development* **130**, 3767-80.

George, E. L., Georges-Labouesse, E. N., Patel-King, R. S., Rayburn, H. and Hynes, R. O. (1993). Defects in mesoderm, neural tube and vascular development in mouse embryos lacking fibronectin. *Development* **119**, 1079-91.

Giraldez, A. J., Cinalli, R. M., Glasner, M. E., Enright, A. J., Thomson, J. M., Baskerville, S., Hammond, S. M., Bartel, D. P. and Schier, A. F. (2005). MicroRNAs regulate brain morphogenesis in zebrafish. *Science* **308**, 833-8.

Glickman, N. S., Kimmel, C. B., Jones, M. A. and Adams, R. J. (2003). Shaping the zebrafish notochord. *Development* **130**, 873-87.

Gonczy, P., Pichler, S., Kirkham, M. and Hyman, A. A. (1999). Cytoplasmic dynein is required for distinct aspects of MTOC positioning, including centrosome separation, in the one cell stage Caenorhabditis elegans embryo. *J Cell Biol* **147**, 135-50.

Green, K. J. and Goldman, R. D. (1983). The effects of taxol on cytoskeletal components in cultured fibroblasts and epithelial cells. *Cell Motil* **3**, 283-305.

Gritsman, K., Zhang, J., Cheng, S., Heckscher, E., Talbot, W. S. and Schier, A. F. (1999). The EGF-CFC protein one-eyed pinhead is essential for nodal signaling. *Cell* **97**, 121-32.

Gumbiner, B. M. (2005). Regulation of cadherin-mediated adhesion in morphogenesis. *Nat Rev Mol Cell Biol* **6**, 622-34.

Haffter, P., Granato, M., Brand, M., Mullins, M. C., Hammerschmidt, M., Kane, D. A., Odenthal, J., van Eeden, F. J., Jiang, Y. J., Heisenberg, C. P. et al. (1996). The identification of genes with unique and essential functions in the development of the zebrafish, Danio rerio. *Development* **123**, 1-36.

Hammerschmidt, M., Pelegri, F., Mullins, M. C., Kane, D. A., Brand, M., van Eeden, F. J., Furutani-Seiki, M., Granato, M., Haffter, P., Heisenberg, C. P. et al. (1996). Mutations affecting morphogenesis during gastrulation and tail formation in the zebrafish, Danio rerio. *Development* **123**, 143-51.

Heisenberg, C. P., Brand, M., Jiang, Y. J., Warga, R. M., Beuchle, D., van Eeden, F. J., Furutani-Seiki, M., Granato, M., Haffter, P., Hammerschmidt, M. et al. (1996). Genes involved in forebrain development in the zebrafish, Danio rerio. *Development* **123**, 191-203.

Heisenberg, C. P., Tada, M., Rauch, G. J., Saude, L., Concha, M. L., Geisler, R., Stemple, D. L., Smith, J. C. and Wilson, S. W. (2000). Silberblick/Wnt11 mediates convergent extension movements during zebrafish gastrulation. *Nature* **405**, 76-81.

Helenius, J., Brouhard, G., Kalaidzidis, Y., Diez, S. and Howard, J. (2006). The depolymerizing kinesin MCAK uses lattice diffusion to rapidly target microtubule ends. *Nature* **441**, 115-9.

Helmchen, F. and Denk, W. (2005). Deep tissue two-photon microscopy. *Nat Methods* **2**, 932-40.

Hirano, T., Ishihara, K. and Hibi, M. (2000). Roles of STAT3 in mediating the cell growth, differentiation and survival signals relayed through the IL-6 family of cytokine receptors. *Oncogene* **19**, 2548-56.

Hirata, T., Yamanaka, Y., Ryu, S. L., Shimizu, T., Yabe, T., Hibi, M. and Hirano, T. (2000). Novel mix-family homeobox genes in zebrafish and their differential regulation. *Biochem Biophys Res Commun* **271**, 603-9.

Ho, C. Y., Houart, C., Wilson, S. W. and Stainier, D. Y. (1999). A role for the extraembryonic yolk syncytial layer in patterning the zebrafish embryo suggested by properties of the hex gene. *Curr Biol* **9**, 1131-4.

Ho, R. K. (1992). Cell movements and cell fate during zebrafish gastrulation. *Dev Suppl*, 65-73.

Hsu, H. J., Liang, M. R., Chen, C. T. and Chung, B. C. (2006). Pregnenolone stabilizes microtubules and promotes zebrafish embryonic cell movement. *Nature* **439**, 480-3.

Inoue, S., Yoder, O. C., Turgeon, B. G. and Aist, J. R. (1998). A cytoplasmic dynein required for mitotic aster formation in vivo. *J Cell Sci* **111 (Pt 17)**, 2607-14.

Irvine, K. D. and Wieschaus, E. (1994). Cell intercalation during Drosophila germband extension and its regulation by pair-rule segmentation genes. *Development* **120**, 827-41.

Jessen, J. R., Topczewski, J., Bingham, S., Sepich, D. S., Marlow, F., Chandrasekhar, A. and Solnica-Krezel, L. (2002). Zebrafish trilobite identifies new roles for Strabismus in gastrulation and neuronal movements. *Nat Cell Biol* **4**, 610-5.

Jia, L., Schweizer, J., Wang, Y., Cerna, C., Wong, H. and Revilla, M. (2003). Effect of nitric oxide on cytotoxicity of Taxol: enhanced Taxol transcellular permeability. *Biochem Pharmacol* **66**, 2193-9.

Jones, C. M., Broadbent, J., Thomas, P. Q., Smith, J. C. and Beddington, R. S. (1999). An anterior signalling centre in Xenopus revealed by the homeobox gene XHex. *Curr Biol* **9**, 946-54.

Jordan, M. A. and Wilson, L. (1998). Use of drugs to study role of microtubule assembly dynamics in living cells. *Methods Enzymol* **298**, 252-76.

Jordan, M. A. and Wilson, L. (2004). Microtubules as a target for anticancer drugs. *Nat Rev Cancer* **4**, 253-65.

Julich, D., Geisler, R. and Holley, S. A. (2005). Integrinalpha5 and delta/notch signaling have complementary spatiotemporal requirements during zebrafish somitogenesis. *Dev Cell* **8**, 575-86.

Kaltschmidt, J. A., Davidson, C. M., Brown, N. H. and Brand, A. H. (2000). Rotation and asymmetry of the mitotic spindle direct asymmetric cell division in the developing central nervous system. *Nat Cell Biol* **2**, 7-12.

Kane, D. and Adams, R. (2002). Life at the edge: epiboly and involution in the zebrafish. *Results Probl Cell Differ* **40**, 117-35.

Kane, D. A., Hammerschmidt, M., Mullins, M. C., Maischein, H. M., Brand, M., van Eeden, F. J., Furutani-Seiki, M., Granato, M., Haffter, P., Heisenberg, C. P. et al. (1996). The zebrafish epiboly mutants. *Development* **123**, 47-55.

Kane, D. A. and Kimmel, C. B. (1993). The zebrafish midblastula transition. *Development* **119**, 447-56.

Kane, D. A., McFarland, K. N. and Warga, R. M. (2005). Mutations in half baked/E-cadherin block cell behaviors that are necessary for teleost epiboly. *Development* **132**, 1105-16.

Kane, D. A., Warga, R. M. and Kimmel, C. B. (1992). Mitotic domains in the early embryo of the zebrafish. *Nature* **360**, 735-7.

Keller, R., Davidson, L., Edlund, A., Elul, T., Ezin, M., Shook, D. and Skoglund, P. (2000). Mechanisms of convergence and extension by cell intercalation. *Philos Trans R Soc Lond B Biol Sci* **355**, 897-922.

Keller, R., Davidson, L. A. and Shook, D. R. (2003). How we are shaped: the biomechanics of gastrulation. *Differentiation* **71**, 171-205.

Keller, R. E. and Spieth, J. (1984). Neural crest cell behavior in white and dark larvae of Ambystoma mexicanum: time-lapse cinemicrographic analysis of pigment cell movement in vivo and in culture. *J Exp Zool* **229**, 109-26.

Keller, R. E. and Trinkaus, J. P. (1987). Rearrangement of enveloping layer cells without disruption of the epithelial permeability barrier as a factor in Fundulus epiboly. *Dev Biol* **120**, 12-24.

Khoobehi, B., Shoelson, B., Zhang, Y. Z. and Peyman, G. A. (1997). Fluorescent microsphere imaging: a particle-tracking approach to the hemodynamic assessment of the retina and choroid. *Ophthalmic Surg Lasers* **28**, 937-47.

Kiehart, D. P. (1999). Wound healing: The power of the purse string. *Curr Biol* **9**, R602-5.

Kikuchi, Y., Agathon, A., Alexander, J., Thisse, C., Waldron, S., Yelon, D., Thisse, B. and Stainier, D. Y. (2001). casanova encodes a novel Sox-related protein necessary and sufficient for early endoderm formation in zebrafish. *Genes Dev* **15**, 1493-505.

Kilian, B., Mansukoski, H., Barbosa, F. C., Ulrich, F., Tada, M. and Heisenberg, C. P. (2003). The role of Ppt/Wnt5 in regulating cell shape and movement during zebrafish gastrulation. *Mech Dev* **120**, 467-76.

Kimmel, C. B., Ballard, W. W., Kimmel, S. R., Ullmann, B. and Schilling, T. F. (1995). Stages of embryonic development of the zebrafish. *Dev Dyn* **203**, 253-310.

Kimmel, C. B. and Law, R. D. (1985a). Cell lineage of zebrafish blastomeres. I. Cleavage pattern and cytoplasmic bridges between cells. *Dev Biol* **108**, 78-85.

Kimmel, C. B. and Law, R. D. (1985b). Cell lineage of zebrafish blastomeres. II. Formation of the yolk syncytial layer. *Dev Biol* **108**, 86-93.

Kimmel, C. B. and Warga, R. M. (1987). Indeterminate cell lineage of the zebrafish embryo. *Dev Biol* **124**, 269-80.

Kimmel, C. B., Warga, R. M. and Kane, D. A. (1994). Cell cycles and clonal strings during formation of the zebrafish central nervous system. *Development* **120**, 265-76.

Kisseleva, T., Bhattacharya, S., Braunstein, J. and Schindler, C. W. (2002). Signaling through the JAK/STAT pathway, recent advances and future challenges. *Gene* **285**, 1-24.

Klinowska, T. C., Ireland, G. W. and Kimber, S. J. (1994). A new in vitro model of murine mesoderm migration: the role of fibronectin and laminin. *Differentiation* **57**, 7-19.

Klominek, J., Sundqvist, K. G. and Robert, K. H. (1991). Nucleokinesis: distinct pattern of cell translocation in response to an autocrine motility factor-like substance or fibronectin. *Proc Natl Acad Sci U S A* **88**, 3902-6.

Koos, D. S. and Ho, R. K. (1998). The nieuwkoid gene characterizes and mediates a Nieuwkoop-center-like activity in the zebrafish. *Curr Biol* **8**, 1199-206.

Koppen, M., Fernandez, B. G., Carvalho, L., Jacinto, A. and Heisenberg, C. P. (2006). Coordinated cell-shape changes control epithelial movement in zebrafish and Drosophila. *Development* **133**, 2671-81.

Kuhl, M. (2002). Non-canonical Wnt signaling in Xenopus: regulation of axis formation and gastrulation. *Semin Cell Dev Biol* **13**, 243-9.

Lele, Z., Bakkers, J. and Hammerschmidt, M. (2001). Morpholino phenocopies of the swirl, snailhouse, somitabun, minifin, silberblick, and pipetail mutations. *Genesis* **30**, 190-4.

Lentz, T. L. and Trinkaus, J. P. (1967). A fine structural study of cytodifferentiation during cleavage, blastula, and gastrula stages of Fundulus heteroclitus. *J Cell Biol* **32**, 121-38.

Leptin, M. (2005). Gastrulation movements: the logic and the nuts and bolts. *Dev Cell* **8**, 305-20.

Liao, W., Ho, C. Y., Yan, Y. L., Postlethwait, J. and Stainier, D. Y. (2000). Hhex and scl function in parallel to regulate early endothelial and blood differentiation in zebrafish. *Development* **127**, 4303-13.

Lipsky, N. G. and Pagano, R. E. (1985). A vital stain for the Golgi apparatus. *Science* **228**, 745-7.

Long, W. L. (1980). Analysis of yolk syncytium behavior in *Salmo and Catostomus*. *The Journal of Experimental Zoology* **214**, 323-31.

Long, W. L. (1984). Cell movements in teleost fish development. *Bioscience* **34**, 84-88.

Luduena, R. F. and Roach, M. C. (1991). Tubulin sulfhydryl groups as probes and targets for antimitotic and antimicrotubule agents. *Pharmacol Ther* **49**, 133-52.

Lynn, C. N. and Ahmed, J. (2006). A technique for tracking intravascular fluorescent microspheres for the determination of arteriolar blood flow in rats. *Biomed Sci Instrum* **42**, 90-5.

Machingo, Q. J., Fritz, A. and Shur, B. D. (2006). A beta1,4-galactosyltransferase is required for convergent extension movements in zebrafish. *Dev Biol* **297**, 471-82.

Mahajan-Miklos, S. and Cooley, L. (1994). Intercellular cytoplasm transport during Drosophila oogenesis. *Dev Biol* **165**, 336-51.

Makita, R., Mizuno, T., Koshida, S., Kuroiwa, A. and Takeda, H. (1998). Zebrafish wnt11: pattern and regulation of the expression by the yolk cell and No tail activity. *Mech Dev* **71**, 165-76.

Malone, C. J., Fixsen, W. D., Horvitz, H. R. and Han, M. (1999). UNC-84 localizes to the nuclear envelope and is required for nuclear migration and anchoring during C. elegans development. *Development* **126**, 3171-81.

Mani-Ponset, L., Guyot, E., Diaz, J. P. and Connes, R. (1996). Utilization of yolk reserves during post-embryonic development in three teleostean species: the seam bream *Sparus aurata*, the sea bass *Dicentrarchus labrax*, and the pike-perch *Stizostedion lucioperca*. *Mar. Biol.* **126**, 539-47.

Martin, P. and Wood, W. (2002). Epithelial fusions in the embryo. *Curr Opin Cell Biol* **14**, 569-74.

Martinez-Barbera, J. P., Rodriguez, T. A. and Beddington, R. S. (2000). The homeobox gene Hesx1

is required in the anterior neural ectoderm for normal forebrain formation. *Dev Biol* **223**, 422-30.

Marza, E., Barthe, C., Andre, M., Villeneuve, L., Helou, C. and Babin, P. J. (2005). Developmental expression and nutritional regulation of a zebrafish gene homologous to mammalian microsomal triglyceride transfer protein large subunit. *Dev Dyn* **232**, 506-18.

McFarland, K. N., Warga, R. M. and Kane, D. A. (2005). Genetic locus half baked is necessary for morphogenesis of the ectoderm. *Dev Dyn* **233**, 390-406.

Miyagi, C., Yamashita, S., Ohba, Y., Yoshizaki, H., Matsuda, M. and Hirano, T. (2004). STAT3 noncell-autonomously controls planar cell polarity during zebrafish convergence and extension. *J Cell Biol* **166**, 975-81.

Miyamoto, D. M. and Crowther, R. J. (1985). Formation of the notochord in living ascidian embryos. *J Embryol Exp Morphol* **86**, 1-17.

Mizuno, T., Yamaha, E., Kuroiwa, A. and Takeda, H. (1999). Removal of vegetal yolk causes dorsal deficencies and impairs dorsal-inducing ability of the yolk cell in zebrafish. *Mech Dev* **81**, 51-63.

Mizuno, T., Yamaha, E., Wakahara, M., Kuroiwa, A. and Takeda, H. (1996). Mesoderm induction in zebrafish. *Nature* **383**, 131-132.

Montero, J. A., Carvalho, L., Wilsch-Brauninger, M., Kilian, B., Mustafa, C. and Heisenberg, C. P. (2005). Shield formation at the onset of zebrafish gastrulation. *Development* **132**, 1187-98.

Montero, J. A. and Heisenberg, C. P. (2004). Gastrulation dynamics: cells move into focus. *Trends Cell Biol* **14**, 620-7.

Montero, J. A., Kilian, B., Chan, J., Bayliss, P. E. and Heisenberg, C. P. (2003). Phosphoinositide 3-kinase is required for process outgrowth and cell polarization of gastrulating mesendodermal cells. *Curr Biol* **13**, 1279-89.

Moon, R. T. (1993). In pursuit of the functions of the Wnt family of developmental regulators: insights from Xenopus laevis. *Bioessays* **15**, 91-7.

Morris, N. R. (2003). Nuclear positioning: the means is at the ends. *Curr Opin Cell Biol* **15**, 54-9.

Morris, N. R., Efimov, V. P. and Xiang, X. (1998). Nuclear migration, nucleokinesis and lissencephaly. *Trends Cell Biol* **8**, 467-70.

Mudumana, S. P., Wan, H., Singh, M., Korzh, V. and Gong, Z. (2004). Expression analyses of zebrafish transferrin, ifabp, and elastaseB mRNAs as differentiation markers for the three major endodermal organs: liver, intestine, and exocrine pancreas. *Dev Dyn* **230**, 165-73.

Myers, D. C., Sepich, D. S. and Solnica-Krezel, L. (2002a). Bmp activity gradient regulates convergent extension during zebrafish gastrulation. *Dev Biol* **243**, 81-98.

Myers, D. C., Sepich, D. S. and Solnica-Krezel, L. (2002b). Convergence and extension in vertebrate gastrulae: cell movements according to or in search of identity? *Trends Genet* **18**, 447-55.

Nakagawa, H., Koyama, K., Murata, Y., Morito, M., Akiyama, T. and Nakamura, Y. (2000). EB3, a novel member of the EB1 family preferentially expressed in the central nervous system, binds to a CNS-specific APC homologue. *Oncogene* **19**, 210-6.

Newport, J. and Kirschner, M. (1982). A major developmental transition in early Xenopus embryos: II. Control of the onset of transcription. *Cell* **30**, 687-96.

Nodder, S. and Martin, P. (1997). Wound healing in embryos: a review. *Anat Embryol (Berl)* **195**, 215-28.

Nogales, E. (2001). Structural insight into microtubule function. *Annu Rev Biophys Biomol Struct* **30**, 397-420.

Ober, E. A. and Schulte-Merker, S. (1999). Signals from the yolk cell induce mesoderm, neuroectoderm, the trunk organizer, and the notochord in zebrafish. *Dev Biol* **215**, 167-81.

Oheim, M., Michael, D. J., Geisbauer, M., Madsen, D. and Chow, R. H. (2006). Principles of two-photon excitation fluorescence microscopy and other nonlinear imaging approaches. *Adv Drug Deliv Rev* **58**, 788-808.

Okada, A., Lansford, R., Weimann, J. M., Fraser, S. E. and McConnell, S. K. (1999). Imaging cells in the developing nervous system with retrovirus expressing modified green fluorescent protein. *Exp Neurol* **156**, 394-406.

Oppenheimer, J. M. (1936). Processes of localization in developing *Fundulus*. *Journal Experimental Zoology* **73**, 405-44.

Osmani, A. H., Osmani, S. A. and Morris, N. R. (1990). The molecular cloning and identification of a gene product specifically required for nuclear movement in Aspergillus nidulans. *J Cell Biol* **111**, 543-51.

Pagano, R. E., Martin, O. C., Kang, H. C. and Haugland, R. P. (1991). A novel fluorescent ceramide analogue for studying membrane traffic in animal cells: accumulation at the Golgi apparatus results in altered spectral properties of the sphingolipid precursor. *J Cell Biol* **113**, 1267-79.

Parsons, M. J., Pollard, S. M., Saude, L., Feldman, B., Coutinho, P., Hirst, E. M. and Stemple, D. L. (2002). Zebrafish mutants identify an essential role for laminins in notochord formation. *Development* **129**, 3137-46.

Peters, K. G., Rao, P. S., Bell, B. S. and Kindman, L. A. (1995). Green fluorescent fusion proteins: powerful tools for monitoring protein expression in live zebrafish embryos. *Dev Biol* **171**, 252-7.

Raff, J. W. and Glover, D. M. (1989). Centrosomes, and not nuclei, initiate pole cell formation in Drosophila embryos. *Cell* **57**, 611-9.

Ragsdale, G. K., Phelps, J. and Luby-Phelps, K. (1997). Viscoelastic response of fibroblasts to tension transmitted through adherens junctions. *Biophys J* **73**, 2798-808.

Rauch, G. J., Hammerschmidt, M., Blader, P., Schauerte, H. E., Strahle, U., Ingham, P. W., McMahon, A. P. and Haffter, P. (1997). Wnt5 is required for tail formation in the zebrafish embryo. *Cold Spring Harb Symp Quant Biol* **62**, 227-34.

Rebagliati, M. R., Toyama, R., Haffter, P. and Dawid, I. B. (1998). cyclops encodes a nodal-related factor involved in midline signaling. *Proc Natl Acad Sci U S A* **95**, 9932-7.

Reim, G. and Brand, M. (2006). Maternal control of vertebrate dorsoventral axis formation and epiboly by the POU domain protein Spg/Pou2/Oct4. *Development* **133**, 2757-70.

Reim, G., Mizoguchi, T., Stainier, D. Y., Kikuchi, Y. and Brand, M. (2004). The POU domain protein spg (pou2/Oct4) is essential for endoderm formation in cooperation with the HMG domain protein casanova. *Dev Cell* **6**, 91-101.

Reinsch, S. and Gonczy, P. (1998). Mechanisms of nuclear positioning. *J Cell Sci* **111 (Pt 16)**, 2283-95.

Renucci, A., Lemarchandel, V. and Rosa, F. (1996). An activated form of type I serine/threonine

kinase receptor TARAM-A reveals a specific signalling pathway involved in fish head organiser formation. *Development* **122**, 3735-43.

Rink, J., Ghigo, E., Kalaidzidis, Y. and Zerial, M. (2005). Rab conversion as a mechanism of progression from early to late endosomes. *Cell* **122**, 735-49.

Rodaway, A., Takeda, H., Koshida, S., Broadbent, J., Price, B., Smith, J. C., Patient, R. and Holder, N. (1999). Induction of the mesendoderm in the zebrafish germ ring by yolk cell-derived TGF-beta family signals and discrimination of mesoderm and endoderm by FGF. *Development* **126**, 3067-78.

Sakaguchi, T., Kikuchi, Y., Kuroiwa, A., Takeda, H. and Stainier, D. Y. (2006). The yolk syncytial layer regulates myocardial migration by influencing extracellular matrix assembly in zebrafish. *Development* **133**, 4063-72.

Sakaguchi, T., Mizuno, T. and Takeda, H. (2002). Formation and patterning roles of the yolk syncytial layer. *Results Probl Cell Differ* **40**, 1-14.

Sambrook, J., Russell, D. W. and Cold Spring Harbor Laboratory. (2001). Molecular cloning: a laboratory manual. Cold Spring Harbor, N.Y.: Cold Spring Harbor Laboratory.

Sanes, J. R. and Lichtman, J. W. (2001). Induction, assembly, maturation and maintenance of a postsynaptic apparatus. *Nat Rev Neurosci* **2**, 791-805.

Sausedo, R. A. and Schoenwolf, G. C. (1994). Quantitative analyses of cell behaviors underlying notochord formation and extension in mouse embryos. *Anat Rec* **239**, 103-12.

Schier, A. F. and Talbot, W. S. (2005). Molecular genetics of axis formation in zebrafish. *Annu Rev Genet* **39**, 561-613.

Schiff, P. B., Fant, J. and Horwitz, S. B. (1979). Promotion of microtubule assembly in vitro by taxol. *Nature* **277**, 665-7.

Schoenwolf, G. C. and Alvarez, I. S. (1989). Roles of neuroepithelial cell rearrangement and division in shaping of the avian neural plate. *Development* **106**, 427-39.

Schulte-Merker, S., Hammerschmidt, M., Beuchle, D., Cho, K. W., De Robertis, E. M. and Nusslein-Volhard, C. (1994). Expression of zebrafish goosecoid and no tail gene products in wild-type and mutant no tail embryos. *Development* **120**, 843-52.

Schuyler, S. C. and Pellman, D. (2001). Microtubule "plus-end-tracking proteins": The end is just the beginning. *Cell* **105**, 421-4.

Seifert, J. R. and Mlodzik, M. (2007). Frizzled/PCP signalling: a conserved mechanism regulating cell polarity and directed motility. *Nat Rev Genet* **8**, 126-38.

Sepich, D. S., Calmelet, C., Kiskowski, M. and Solnica-Krezel, L. (2005). Initiation of convergence and extension movements of lateral mesoderm during zebrafish gastrulation. *Dev Dyn* **234**, 279-92.

Sepich, D. S., Myers, D. C., Short, R., Topczewski, J., Marlow, F. and Solnica-Krezel, L. (2000). Role of the zebrafish trilobite locus in gastrulation movements of convergence and extension. *Genesis* **27**, 159-73.

Shimizu, T., Yabe, T., Muraoka, O., Yonemura, S., Aramaki, S., Hatta, K., Bae, Y. K., Nojima, H. and Hibi, M. (2005). E-cadherin is required for gastrulation cell movements in zebrafish. *Mech Dev* **122**, 747-63.

Shimmen, T. (2007). The sliding theory of cytoplasmic streaming: fifty years of progress. *J Plant Res*

120, 31-43.

Shimmen, T. and Yokota, E. (2004). Cytoplasmic streaming in plants. *Curr Opin Cell Biol* **16**, 68-72.

Sire, M.-F., Babin, P. J. and Vernier, J.-M. (1994). Involvement of the lysosomal system in yolk protein deposit and degradation during vitellogenesis and embryonic development in trout. *Journal Experimental Zoology* **269**, 69-83.

Smith, M. L., Bruhn, J. N. and Anderson, J. B. (1992). The fungus *Armillaria bulbosa* is among the largest and oldest living organisms. **256**, 428-31.

Solnica-Krezel, L. (2005). Conserved patterns of cell movements during vertebrate gastrulation. *Curr Biol* **15**, R213-28.

Solnica-Krezel, L. (2006). Gastrulation in zebrafish -- all just about adhesion? *Curr Opin Genet Dev* **16**, 433-41.

Solnica-Krezel, L. and Cooper, M. S. (2002). Cellular and genetic mechanisms of convergence and extension. *Results Probl Cell Differ* **40**, 136-65.

Solnica-Krezel, L. and Driever, W. (1994). Microtubule arrays of the zebrafish yolk cell: organization and function during epiboly. *Development* **120**, 2443-55.

Solnica-Krezel, L., Stemple, D. L., Mountcastle-Shah, E., Rangini, Z., Neuhauss, S. C., Malicki, J., Schier, A. F., Stainier, D. Y., Zwartkruis, F., Abdelilah, S. et al. (1996). Mutations affecting cell fates and cellular rearrangements during gastrulation in zebrafish. *Development* **123**, 67-80.

Stepanova, T., Slemmer, J., Hoogenraad, C. C., Lansbergen, G., Dortland, B., De Zeeuw, C. I., Grosveld, F., van Cappellen, G., Akhmanova, A. and Galjart, N. (2003). Visualization of microtubule growth in cultured neurons via the use of EB3-GFP (end-binding protein 3-green fluorescent protein). *J Neurosci* **23**, 2655-64.

Strahle, U., Blader, P., Henrique, D. and Ingham, P. W. (1993). Axial, a zebrafish gene expressed along the developing body axis, shows altered expression in cyclops mutant embryos. *Genes Dev* **7**, 1436-46.

Strahle, U. and Jesuthasan, S. (1993). Ultraviolet irradiation impairs epiboly in zebrafish embryos: evidence for a microtubule-dependent mechanism of epiboly. *Development* **119**, 909-19.

Streisinger, G., Walker, C., Dower, N., Knauber, D. and Singer, F. (1981). Production of clones of homozygous diploid zebra fish (Brachydanio rerio). *Nature* **291**, 293-6.

Suelmann, R., Sievers, N. and Fischer, R. (1997). Nuclear traffic in fungal hyphae: in vivo study of nuclear migration and positioning in Aspergillus nidulans. *Mol Microbiol* **25**, 757-69.

Sun, L., Zou, Z., Collodi, P., Xu, F., Xu, X. and Zhao, Q. (2005). Identification and characterization of a second fibronectin gene in zebrafish. *Matrix Biol* **24**, 69-77.

Swindell, C. S., Krauss, N. E., Horwitz, S. B. and Ringel, I. (1991). Biologically active taxol analogues with deleted A-ring side chain substituents and variable C-2' configurations. *J Med Chem* **34**, 1176-84.

Tada, M., Concha, M. L. and Heisenberg, C. P. (2002). Non-canonical Wnt signalling and regulation of gastrulation movements. *Semin Cell Dev Biol* **13**, 251-60.

Theurkauf, W. E. (1994). Microtubules and cytoplasm organization during Drosophila oogenesis. *Dev Biol* **165**, 352-60.

Theurkauf, W. E., Smiley, S., Wong, M. L. and Alberts, B. M. (1992). Reorganization of the cytoskeleton during Drosophila oogenesis: implications for axis specification and intercellular transport. *Development* **115**, 923-36.

Thisse, B., Heyer, V., Lux, A., Alunni, V., Degrave, A., Seiliez, I., Kirchner, J., Parkhill, J. P. and Thisse, C. (2004). Spatial and temporal expression of the zebrafish genome by large-scale in situ hybridization screening. *Methods Cell Biol* **77**, 505-19.

Thisse, C., Thisse, B., Halpern, M. E. and Postlethwait, J. H. (1994). Goosecoid expression in neurectoderm and mesendoderm is disrupted in zebrafish cyclops gastrulas. *Dev Biol* **164**, 420-9.

Thomas, P. Q., Brown, A. and Beddington, R. S. (1998). Hex: a homeobox gene revealing peri-implantation asymmetry in the mouse embryo and an early transient marker of endothelial cell precursors. *Development* **125**, 85-94.

Tokunaka, S., Friedman, T. M., Toyama, Y., Pacifici, M. and Holtzer, H. (1983). Taxol induces microtubule-rough endoplasmic reticulum complexes and microtubule-bundles in cultured chondroblasts. *Differentiation* **24**, 39-47.

Trinh, L. A. and Stainier, D. Y. (2004). Fibronectin regulates epithelial organization during myocardial migration in zebrafish. *Dev Cell* **6**, 371-82.

Trinkaus, J. P. (1951). A study of mechanism of epiboly in the egg of *Fundulus heteroclitus*. *Journal Experimental Zoology* **118**, 269-320.

Trinkaus, J. P. (1984). Mechanism of *Fundulus* epiboly - a current view. *American Zoologist* **24**, 673-88.

Trinkaus, J. P. (1992). The midblastula transition, the YSL transition and the onset of gastrulation in Fundulus. *Dev Suppl*, 75-80.

Trinkaus, J. P. (1993). The yolk syncytial layer of Fundulus: its origin and history and its significance for early embryogenesis. *J Exp Zool* **265**, 258-84.

Trinkaus, J. P. (1996). Ingression during early gastrulation of fundulus. *Dev Biol* **177**, 356-70.

Trinkaus, J. P. (1998). Gradient in convergent cell movement during Fundulus gastrulation. *J Exp Zool* **281**, 328-35.

Trinkaus, J. P. and Drake, J. W. (1956). Exogenous control of morphogenesis in isolated *Fundulus* blastoderms by nutrient chemical factors. *Journal Experimental Zoology* **132**, 311-47.

Trinkaus, J. P. and Erickson, C. A. (1983). Protrusive activity, mode and rate of locomotion, and pattern of adhesion of *Fundulus* deep cells during gastrulation. *Journal Experimental Zoology* **228**, 41-70.

Trinkaus, J. P., Trinkaus, M. and Fink, R. D. (1992). On the convergent cell movements of gastrulation in Fundulus. *J Exp Zool* **261**, 40-61.

Ulrich, F., Concha, M. L., Heid, P. J., Voss, E., Witzel, S., Roehl, H., Tada, M., Wilson, S. W., Adams, R. J., Soll, D. R. et al. (2003). Slb/Wnt11 controls hypoblast cell migration and morphogenesis at the onset of zebrafish gastrulation. *Development* **130**, 5375-84.

Ulrich, F., Krieg, M., Schotz, E. M., Link, V., Castanon, I., Schnabel, V., Taubenberger, A., Mueller, D., Puech, P. H. and Heisenberg, C. P. (2005). Wnt11 functions in gastrulation by controlling cell cohesion through Rab5c and E-cadherin. *Dev Cell* **9**, 555-64.

Van der Ghinst, M. (1935). Mise en evidence de ferments dans le syncytium vitellin de la truite (*Salmo*

irideus). *Bull. Histol. Appl.* **12**, 257-259.

Veith, D., Scherr, N., Efimov, V. P. and Fischer, R. (2005). Role of the spindle-pole-body protein ApsB and the cortex protein ApsA in microtubule organization and nuclear migration in Aspergillus nidulans. *J Cell Sci* **118**, 3705-16.

Viebahn, C. (1999). The anterior margin of the mammalian gastrula: comparative and phylogenetic aspects of its role in axis formation and head induction. *Curr Top Dev Biol* **46**, 63-103.

von Dassow, G. and Schubiger, G. (1994). How an actin network might cause fountain streaming and nuclear migration in the syncytial Drosophila embryo. *J Cell Biol* **127**, 1637-53.

von der Hardt, S., Bakkers, J., Inbal, A., Carvalho, L., Solnica-Krezel, L., Heisenberg, C. P. and Hammerschmidt, M. (2007). The Bmp gradient of the zebrafish gastrula guides migrating lateral cells by regulating cell-cell adhesion. *Curr Biol* **17**, 475-87.

Wagner, D. S., Dosch, R., Mintzer, K. A., Wiemelt, A. P. and Mullins, M. C. (2004). Maternal control of development at the midblastula transition and beyond: mutants from the zebrafish II. *Dev Cell* **6**, 781-90.

Wallace, K. N., Yusuff, S., Sonntag, J. M., Chin, A. J. and Pack, M. (2001). Zebrafish hhex regulates liver development and digestive organ chirality. *Genesis* **30**, 141-3.

Walzer, C. and Schonenberger, N. (1979). Ultrastructure and cytochemistry study of the yolk syncytial layer in the alevin of trout (Salmo fario trutta L.) after hatching. I. The vitellolysis zone. *Cell Tissue Res* **196**, 59-73.

Wang, L., Zhang, Y., Shao, M. and Zhang, H. (2007). Spatiotemporal expression of the creatine metabolism related genes agat, gamt and ct1 during zebrafish embryogenesis. *Int J Dev Biol* **51**, 247-53.

Warga, R. M. and Kimmel, C. B. (1990). Cell movements during epiboly and gastrulation in zebrafish. *Development* **108**, 569-80.

Warga, R. M. and Nusslein-Volhard, C. (1999). Origin and development of the zebrafish endoderm. *Development* **126**, 827-38.

Wehland, J., Henkart, M., Klausner, R. and Sandoval, I. V. (1983). Role of microtubules in the distribution of the Golgi apparatus: effect of taxol and microinjected anti-alpha-tubulin antibodies. *Proc Natl Acad Sci U S A* **80**, 4286-90.

Westerfield, M. (2000). The zebrafish book. A guide for the laboratory use of zebrafish (*Danio rerio*). Eugene: University of Oregon Press.

Wheatley, S., Kulkarni, S. and Karess, R. (1995). Drosophila nonmuscle myosin II is required for rapid cytoplasmic transport during oogenesis and for axial nuclear migration in early embryos. *Development* **121**, 1937-46.

Williams, D. W., Muller, F., Lavender, F. L., Orban, L. and Maclean, N. (1996). High transgene activity in the yolk syncytial layer affects quantitative transient expression assays in zebrafish Danio rerio) embryos. *Transgenic Res* **5**, 433-42.

Williams-Masson, E. M., Malik, A. N. and Hardin, J. (1997). An actin-mediated two-step mechanism is required for ventral enclosure of the C. elegans hypodermis. *Development* **124**, 2889-901.

Wilson, E. T., Cretekos, C. J. and Helde, K. A. (1995). Cell mixing during early epiboly in the zebrafish embryo. *Dev Genet* **17**, 6-15.

Wilson, E. T., Helde, K. A. and Grunwald, D. J. (1993). Something's fishy here--rethinking cell movements and cell fate in the zebrafish embryo. *Trends Genet* **9**, 348-52.

Wilson, H. V. (1889). The embryology of the sea bass (*Serranus atrarius*). *Bull. U. S. Fish Commision* **9**, 209-278.

Winklbauer, R. and Keller, R. E. (1996). Fibronectin, mesoderm migration, and gastrulation in Xenopus. *Dev Biol* **177**, 413-26.

Winklbauer, R., Nagel, M., Selchow, A. and Wacker, S. (1996). Mesoderm migration in the Xenopus gastrula. *Int J Dev Biol* **40**, 305-11.

Witzel, S., Zimyanin, V., Carreira-Barbosa, F., Tada, M. and Heisenberg, C. P. (2006). Wnt11 controls cell contact persistence by local accumulation of Frizzled 7 at the plasma membrane. *J Cell Biol* **175**, 791-802.

Wolke, U., Jezuit, E. A. and Priess, J. R. (2007). Actin-dependent cytoplasmic streaming in C. elegans oogenesis. *Development* **134**, 2227-36.

Woo, K., Shih, J. and Fraser, S. E. (1995). Fate maps of the zebrafish embryo. *Curr Opin Genet Dev* **5**, 439-43.

Wood, A. and Timmermans, L. P. M. (1988). Teleost epiboly: a reassessment of deep cell movement in the germ ring. *Development* **102**, 575-585.

Xiang, X., Beckwith, S. M. and Morris, N. R. (1994). Cytoplasmic dynein is involved in nuclear migration in Aspergillus nidulans. *Proc Natl Acad Sci U S A* **91**, 2100-4.

Xiang, X. and Fischer, R. (2004). Nuclear migration and positioning in filamentous fungi. *Fungal Genet Biol* **41**, 411-9.

Xiang, X., Roghi, C. and Morris, N. R. (1995). Characterization and localization of the cytoplasmic dynein heavy chain in Aspergillus nidulans. *Proc Natl Acad Sci U S A* **92**, 9890-4.

Yamanaka, Y., Mizuno, T., Sasai, Y., Kishi, M., Takeda, H., Kim, C. H., Hibi, M. and Hirano, T. (1998). A novel homeobox gene, dharma, can induce the organizer in a non-cell-autonomous manner. *Genes Dev* **12**, 2345-53.

Yamashita, S., Miyagi, C., Carmany-Rampey, A., Shimizu, T., Fujii, R., Schier, A. F. and Hirano, T. (2002). Stat3 Controls Cell Movements during Zebrafish Gastrulation. *Dev Cell* **2**, 363-75.

Yamashita, S., Miyagi, C., Fukada, T., Kagara, N., Che, Y. S. and Hirano, T. (2004). Zinc transporter LIVI controls epithelial-mesenchymal transition in zebrafish gastrula organizer. *Nature* **429**, 298-302.

Zalik, S. E., Lewandowski, E., Kam, Z. and Geiger, B. (1999). Cell adhesion and the actin cytoskeleton of the enveloping layer in the zebrafish embryo during epiboly. *Biochem Cell Biol* **77**, 527-42.

Zhang, J., Talbot, W. S. and Schier, A. F. (1998). Positional cloning identifies zebrafish one-eyed pinhead as a permissive EGF-related ligand required during gastrulation. *Cell* **92**, 241-51.

6. Appendix

6.1 Expression of dorsal and mesendodermal markers in hypoblast-like cells transplanted into MZ*oep* embryos

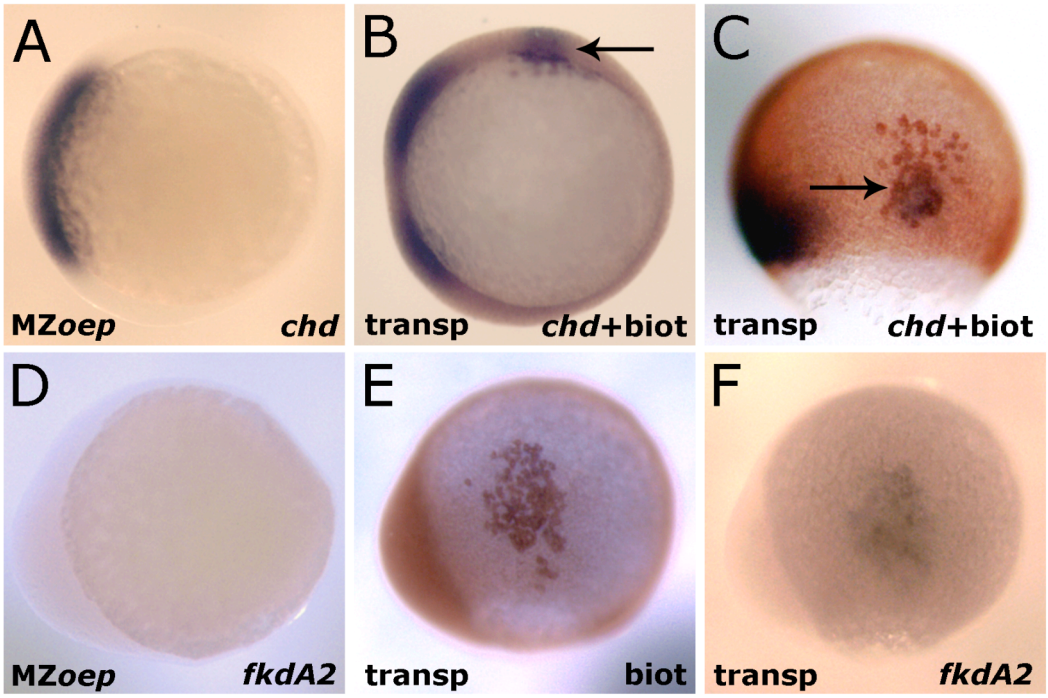

Figure 6.1 – Expression of dorsal and mesendodermal markers in MZ*oep* and MZ*oep* mutant embryos transplanted with hypoblast-like cells. (A-C) Expression of *chd*, a dorsal-organizer marker. (A) Animal pole view of an MZ*oep* mutant embryo showing *chd* expression on the dorsal side (blue). (B) Animal pole view of a transplanted MZ*oep* mutant embryo showing *chd* expression on the dorsal side (blue) and also on laterally-located transplanted cells simultaneously marked with biotin (arrow; blue and brown). (C) Lateral view of same embryo as in (B) showing transplanted cells expressing *chd* (arrow; blue and brown). (D-E) Expression of *fkdA2*, a mesendodermal marker. (D) Lateral view of an MZ*oep* mutant embryo showing no expression of *fkdA2*. (E) Lateral view of a transplanted MZ*oep* mutant embryo showing biotin staining on the transplanted cells (brown). (F) Same embryo as in (E) showing *fkdA2* expression in the transplanted cells (blue). Animal pole is on top in (C-E); dorsal is always on the left; (A,B) are animal pole views. Abbreviations: biot, biotin; transp, MZ*oep* mutant embryos transplanted with hypoblast-like cells.

6.2 Expression of several patterning genes in *cdh1* YSL-morphants compared to wild-type control embryos

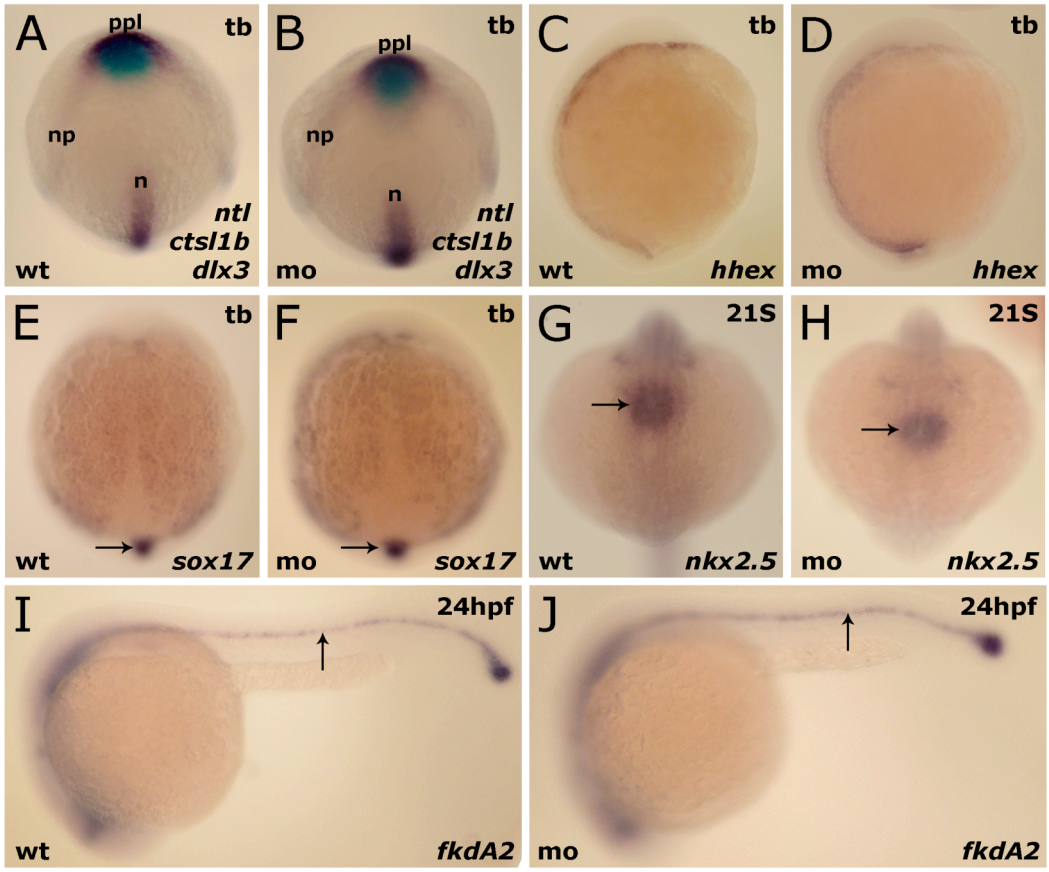

Figure 6.2 – Expression of several patterning genes in *cdh1* YSL-morphants compared to wild-type control embryos. (A,B) Dorsal view of wild-type (A) and morphant (B) embryos at tailbud stage showing expression of notochord (*ntl*), prechordal plate (*ctsl1b*) and neural plate (*dlx3*) markers. Morphant embryos have a regular shaped notochord (n), a prechordal plate (ppl) with a normal degree of elongation, and a neural plate (np) with a normal width. (C,D) Lateral view of wild-type (C) and morphant (D) embryos showing similar pattern of *hhex*, a transcription factor specifically expressed in the dorsal region of the YSL. (E,F) Dorsal view of wild-type (E) and morphant (F) embryos showing similar distribution of endodermal progenitors and Kupfer's vesicle (arrows). (G,H) Anterior view of wild-type (G) and morphant (H) embryos stained for a heart marker, showing that heart progenitor cells migrate to normally to the midline (arrows). (I,J) Lateral view of wild-type (I) and morphant (J) embryos showing that both normally specify the gut (arrows). Animal pole is on top in (A-F); dorsal is on the left in (C,D,G,H) and on top in (G-J); anterior is on the left in (I,J). Abbreviations: 21S, 21-somite stage; mo, *cdh1* YSL-morphant embryo; n, notochord; np, neural plate; ppl, prechordal plate; tb, tailbud stage; wt, wild-type embryo.

6.3 Movie legends

All the movies listed here are included in the attached Compact Disc.

Movie 1 – Nomarski time-lapse of the paraxial region of a wild-type embryo from 65% until 90% epiboly. Dorsal side is on the left, animal pole on top. The time between frames is 2 minutes. Scale bar, 50 µm.

Movie 2 - Two-photon confocal time-lapse imaging of YSL nuclei during gastrulation in a wild-type embryo. Dorsal view, animal pole is on top. Each frame is a projection of 35 slices. The time between frames is 2.5 minutes. Some of the trajectories obtained with Motion Tracking Software are shown. The circles mark the end-point of each track. Scale bar, 50 µm.

Movie 3 – Two-photon confocal time-lapse imaging of Tau-GFP-labeled microtubules in dorsal and paraxial I-YSL during gastrulation in a wild-type embryo. Dorsal and paraxial view, animal pole is on top. Each frame is a projection of 16 slices. The time between frames is 3 minutes. I-YSL nuclei are the non-stained circles. Scale bar, 10 µm.

Movie 4 – Two-photon confocal time-lapse imaging of Tau-GFP-labeled microtubules in ventral I-YSL during gastrulation in a wild-type embryo. Ventral view, animal pole is on top. Each frame is a projection of 14 slices. The time between frames is 3 minutes. I-YSL nuclei are the non-stained circles. Scale bar, 10 µm.

Movie 5 – Two-photon confocal time-lapse imaging of Tau-GFP-labeled microtubules at the leading of E-YSL epiboly in a wild-type embryo. Dorsal view, animal pole is on top. Each frame is a projection of 21 slices. The time between frames is 1.5 minutes. E-YSL nuclei are the non-stained circles. The leading edge of epiboly is marked by an arrowhead. Scale bar, 10 µm.

Movie 6 - Two-photon confocal time-lapse imaging of EB3-GFP-labeled microtubule plus-ends in blastodermal cells during gastrulation. Arrows indicate examples of EB3-GFP positive dots moving towards the cortex of the cell. Animal pole is on top. Each frame is a single slice. The time between frames is 3 seconds. Scale bar, 5 µm.

Movie 7 - Two-photon confocal time-lapse imaging of EB3-GFP-labeled microtubule plus-ends in the I-YSL during gastrulation. Animal pole is on top. Each frame is a single slice. The time between frames is 3 seconds. Abbreviations: n, nucleus. Scale bar, 5 µm.

Movie 8 - Two-photon confocal time-lapse imaging of EB3-GFP-labeled microtubule plus-ends in the E-YSL during gastrulation. Animal pole is on top. Each frame is a single slice. The time between frames is 3 seconds. Abbreviations: n, nucleus. Scale bar, 5 µm.

Movie 9 - Two-photon confocal time-lapse imaging of histone-labeled YSL nuclei and a 20 µm-diameter polystyrene bead during gastrulation. Lateral view; animal pole is on top; dorsal side is on the right. Each frame is a projection of 35 slices. The time between frames is 5 minutes. Some of the nuclear trajectories obtained with Motion Tracking Software are shown. The circles mark the end-point of each track. The arrow indicates the position of the inserted bead. Scale bar, 50 µm.

Movie 10 - Two-photon confocal time-lapse imaging of histone-labeled YSL nuclei and 0.5 µm-diameter fluorescent polystyrene beads during gastrulation. Lateral view; animal pole is on top; dorsal side is on the right. Each frame is a projection of 35 slices. The time between frames is 2.5 minutes. Some of the trajectories of both nuclei and beads obtained with Motion Tracking Software are shown. The circles mark the end-point of each track. The white arrows indicate the position of some of the injected beads; the pink arrows indicate the position of some of the YSL nuclei. The beads look larger than 0.5 µm because they are overexposed. Scale bar, 50 µm.

Movie 11 - Two-photon confocal time-lapse imaging of histone-labeled YSL nuclei at the end of gastrulation in paclitaxel control embryo. Dorsal view, animal pole is on top. Each frame is a projection of 35 slices. The time between frames is 5 minutes. Some of the trajectories obtained with Motion Tracking Software are shown. The circles mark the end-point of each track. Time-lapse was performed at room temperature. Scale bar, 50 µm.

Movie 12 - Two-photon confocal time-lapse imaging of histone-labeled YSL nuclei at the end of gastrulation in 75% epiboly-paclitaxel treated embryo. The embryo was incubated in paclitaxel from 75% epiboly and the time-lapse starts at 85% epiboly (ca. 1 hour and half later), and was performed in the presence of the drug. Dorsal view, animal pole is on top. Each frame is a projection of 35 slices. The time between frames is 5 minutes. Some of the trajectories obtained with Motion Tracking Software are shown. The circles mark the end-point of each track. Time-lapse was performed at room temperature, therefore respective control is shown in Movie 11. Scale bar, 50 µm.

Movie 13 - Two-photon confocal time-lapse imaging of histone-labeled YSL nuclei at the end of gastrulation in 60% epiboly-paclitaxel treated embryo. The embryo was incubated in paclitaxel from 60% epiboly onwards and the time-lapse starts at 80% epiboly (ca. 2 hours and half later), and was performed in the presence of the drug. Dorsal view, animal pole is on top. Each frame is a projection of 35 slices. The time between frames is 5 minutes. Some of the trajectories obtained with Motion Tracking Software are shown. The circles mark the end-point of each track. Time-lapse was performed at room temperature, therefore respective control is shown in Movie 11. Scale bar, 50 µm.

Movie 14 - Nomarski time-lapse of the paraxial region of an MZ*oep* mutant embryo from 65% until 90% epiboly. Dorsal side is on the left, animal pole on top. The time between frames is 2 minutes. Scale bar, 50 µm.

Movie 15 - Two-photon confocal time-lapse imaging of YSL nuclei during gastrulation in an MZ*oep* mutant embryo. Dorsal view, animal pole is on top. Each frame is a projection of 35 slices. The time between frames is 2.5 minutes. Some of the trajectories obtained with Motion Tracking Software are shown. The circles mark the end-point of each track. Scale bar, 50 µm.

Movie 16 - Nomarski time-lapse of the paraxial region of an MZ*oep* mutant embryo injected with 100 pg of *oep* mRNA in the YSL from 65% until 90% epiboly. Dorsal side is on the left, animal pole on top. The time between frames is 2 minutes. Scale bar, 50 µm.

Movie 17 - Two-photon confocal time-lapse imaging of YSL nuclei during gastrulation in an MZ*oep* mutant embryo transplanted with hypoblast-like cells on the left side. Dorsal view, animal pole is on top. Each frame is a projection of 35 slices. The time between frames is 2.5 minutes. Some of the trajectories obtained with Motion Tracking Software are shown. The circles mark the end-point of each track. Scale bar, 50 µm.

Movie 18 - Two-photon confocal time-lapse imaging of YSL nuclei and transplanted hypoblast-like cells in an MZ*oep* mutant embryo. Dorsal is on the right, animal pole is on top. Each frame is a projection of 35 slices. The time between frames is 5 minutes. Cells are labeled with membrane-bound GAP43-GFP. One cell is artificially marked in red; two I-YSL nuclei are artificially marked in blue. Transplanted cells and I-YSL nuclei directly underneath them move toward the dorsal side. Scale bar, 50 µm.

Movie 19 - Two-photon confocal time-lapse imaging of YSL nuclei and transplanted wild type cells in an MZ*oep* mutant embryo. Dorsal is on the right, animal pole is on top. Each frame is a projection of 35 slices. The time between frames is 3 minutes. Cells are labeled with membrane-bound GAP43-GFP but the fluorescence is weak, thus some of the cells are marked with an arrow. Transplanted cells and I-YSL nuclei directly underneath them move toward the dorsal side. Scale bar, 50 µm.

Movie 20 - Two-photon confocal time-lapse imaging of YSL nuclei and transplanted tar* over-expressing cells in an MZ*oep* mutant embryo. Dorsal is on the right, animal pole is on top. Each frame is a projection of 35 slices. The time between frames is 3 minutes. Cells are labeled with membrane-

bound GAP43-GFP. Transplanted cells and I-YSL nuclei directly underneath them move toward the dorsal side. Scale bar, 50 µm.

Movie 21 - Two-photon confocal time-lapse imaging of YSL nuclei during gastrulation in a *slb/ppt* mutant embryo. Dorsal view, animal pole is on top. Each frame is a projection of 35 slices. The time between frames is 2.5 minutes. Some of the trajectories obtained with Motion Tracking Software are shown. The circles mark the end-point of each track. Scale bar, 50 µm.

Movie 22 – Nomarski time-lapse of the paraxial region of a *slb/ppt* mutant embryo from 65% until 90% epiboly. Dorsal side is on the left, animal pole on top. The time between frames is 2 minutes. Scale bar, 50 µm.

Movie 23 - Two-photon confocal time-lapse imaging of YSL nuclei during gastrulation in a *cdh1* YSL-morphant embryo. Dorsal view, animal pole is on top. Each frame is a projection of 35 slices. The time between frames is 5 minutes. Some of the trajectories obtained with Motion Tracking Software are shown. The circles mark the end-point of each track. Time-lapse was performed at room temperature, and a respective control is shown in Movie 11. Scale bar, 50 µm.

Movie 24 - Two-photon confocal time-lapse imaging of YSL nuclei during gastrulation in a *cdh1/hab* mutant embryo. Dorsal view, animal pole is on top. Each frame is a projection of 35 slices. The time between frames is 2.5 minutes. Some of the trajectories obtained with Motion Tracking Software are shown. The circles mark the end-point of each track. Scale bar, 50 µm.

Movie 25 - Two-photon confocal time-lapse imaging of YSL nuclei during gastrulation in a *cdh1/hab* mild mutant embryo ("hab-mild"). Dorsal view, animal pole is on top. Each frame is a projection of 35 slices. The time between frames is 2.5 minutes. Some of the trajectories obtained with Motion Tracking Software are shown. The circles mark the end-point of each track. Scale bar, 50 µm.

Movie 26 – Nomarski time-lapse of the paraxial region of a *cdh1/hab* mutant embryo from 65% until 90% epiboly. Dorsal side is on the left, animal pole on top. The time between frames is 2 minutes. Scale bar, 50 µm.

Movie 27 – Nomarski time-lapse of the paraxial region of a *cdh1/hab* mild mutant embryo ("hab-mild") from 65% until 90% epiboly. Dorsal side is on the left, animal pole on top. The time between frames is 2 minutes. Scale bar, 50 µm.

Movie 28 – Nomarski time-lapse of the paraxial region of a *cdh* YSL-morphant embryo from 65% until 90% epiboly. Dorsal side is on the left, animal pole on top. The time between frames is 2 minutes. Scale bar, 50 µm.

Acknowledgements

In first place, I would like to express my gratitude to Dr. Carl-Philipp Heisenberg, my PhD thesis supervisor, for accepting me in his lab (even though I could not play kicker…) and giving me the opportunity to work at the MPI-CBG. His constant support, presence, and positive thinking, as well as his scientific insight and knowledge, were definitely very encouraging and helpful during these years.

I would also like to thank the other members of my thesis advisory committee, Prof. Michael Brand, Prof. Kai Simons, and Dr. Andy Oates, for their useful discussions and scientific advices. In addition, I am grateful to Prof. Michael Brand, Prof. António Jacinto and CP Heisenberg for reviewing this thesis.

I am very grateful to the people with whom I collaborated in various parts of this thesis. I thank Prof. Yannis Kalaidzidis for sharing his brilliant Motion Tracking Software, which has been so important for the quantitative analysis, and also for statistical advice. A special word goes to Michaela Wilsch-Bräuninger, for the friendly collaboration, for her time in teaching me how to work with the electron microscope, and for many helpful discussions. I would also like to thank Dr. Darren Gilmour for sharing the EB3-GFP construct prior to publication and many colleagues from the fish community for providing other reagents and technical advices.

I am also thankful to the members of the light microscopy facility and fish facility, who were always very helpful and without whom would have been difficult to obtain such confocal images and to have good eggs for injection! I am especially grateful to Jan Peychl, for his patience and assistance with the 2-photon microscope.

I would also like to thank all present and past members of the Heisenberg lab, for the friendly and lively atmosphere, for the scientific discussions and technical help. It is very difficult to imagine working in a different lab other than this one...;-) In particular, I would thank Mathias and Jan, who were closer to

different aspects of this project, and Sabine, Irinka, and Petra. Scientific discussions were also very fruitful with members of neighboring labs, such as the Brand and Oates lab: Muriel, Andy, and many others.

I will always be grateful to Prof. Sólveig Thorsteinsdóttir, the person who introduced me to Developmental Biology and whose enthusiasm for science was a major motivation for me to take this path.

I am truly indebted to Mathias, for the careful and thorough corrections he made of this thesis: obrigada Dr. Köppen! Thanks to CP, Hristio, Marta and Florian for also taking time in proof reading this thesis.

I would also like to thank all my friends here in Dresden, who made me enjoy things other than the lab (e.g. bier&wurst!). In particular, Marta with whom I shared the rent… and all my thoughts! Thanks for being there Martinha.

I thank Hristio for his care and continuous support.

Finally, and most importantly, I want to thank my "little" sister and my parents, who always supported my choices throughout the years and believed I could do it! Obrigada por tudo.

Declaration according to §5.5

I herewith declare that I have produced this thesis without the prohibited assistance of third parties and without making use of aids other than those specified and acknowledged; notions taken over directly or indirectly from other sources have been identified as such. This paper has not been previously presented in identical or similar form to other German or foreign examination board.

The thesis work was conducted from September 2003 until August 2007, under the supervision of Dr. Carl-Philipp Heisenberg at the Max Planck Institute of Molecular Cell Biology and Genetics in Dresden, Germany.

Dresden, August 2007

Lara Cristina de Jesus Carvalho